REVIEWS OF GEOPHYSICS AND SPACE PHYSICS, VOL. 21, NO. 7, PAGES 1567–1606, AUGUST 1983

Models of the Oceanic Internal Wave Field

DIRK J. OLBERS

Max-Planck-Institut für Meteorologie, Hamburg, Federal Republic of Germany

In recent years, considerable progress has been made in internal wave research by a fruitful combination of experiment and theory. Kinematical models of the wave field appear to be well established, and dynamical models are evolving toward a stage of understanding the energetics and the interrelations of the waves within the oceanic field of motion. This review presents kinematical models of the wave field in terms of vertically progressive waves (WKB waves) as well as standing modes. Some emphasis is attributed to critical layer effects. Spectral models have been successfully developed for the wave field in the main thermocline. This appears to be in a stationary universal state with respect to spectral shape and level, whereas the upper ocean wave field shows considerable temporal and regional variability. Several approaches for separating the internal wave contribution from turbulence and other contaminations in observations have been proposed. This problem is of particular relevance in the transition region between waves and small-scale turbulence at small vertical wavelengths. An accurate identification of reversible (wave induced) fine structure and irreversible fine structure is needed to determine the dissipation rate of the wave field and the mixing rates of the ocean. The search for dynamical relations of the wave field to environmental conditions has been extensive. The lack of dynamical correspondences between the wave spectrum and possible forcing fields in observations suggests that forcing is weak. Theoretical models of wave generation show that many mechanisms may contribute with equal efficiency. In concert with the observed low dissipation rates in the deep ocean, these results point toward the conclusion that there is no dominant source of energy but weak forcing by many different sources and weak dissipation. Under such conditions the interrelation between forcing and dissipation as well as the spectral form is controlled by internal transfer by wave-wave interactions which are very efficient in relaxing spectral distortions to the observed universal form.

CONTENTS

1. INTRODUCTION

Internal waves arise in a stably stratified fluid through the restoring force of gravity on water particles displaced from their equilibrium levels. Interfacial waves occurring between two superposed layers of different density are a familiar phenomenon, in particular at the upper free surface of the ocean in the form of surface waves. In the continuously stratified interior of the ocean the restoring force of gravity is much weaker (by a factor $\delta\rho/\rho$), and the periods and wavelengths of internal waves are much larger than those of surface gravity waves. Internal waves have periods between the inertial period ($2\pi/f$, where f is the Coriolis parameter) and the local buoyancy period ($2\pi/N$, where N is the buoyancy frequency). This interval of about 10 octaves is precisely fixed by kinematical reasons. Spatial scales range from a few meters to a few tens of kilometers. In the spectrum of oceanic motions, internal waves are thus embedded between small-scale three-dimensional turbulence and the geostrophic turbulence of the oceanic eddy field.

The first scientific observations of oceanic internal waves were reported by the Norwegian explorer Fridtjof Nansen in the last decade of the nineteenth century. During his passage across the Barents Sea he noted that the forward motion of his ship *Fram* was considerably reduced when sailing on a thin layer of fresh water overlying saltier water. This phenomenon, which he called 'dead water,' was later explained by Ekman as being due to the drag by ship-generated interfacial internal waves. A historical discussion of observations of internal waves in the first half of this century can be found in *Defant*'s [1961] book. Theoretical investigations of internal waves had preceded the observations by half a century. Interfacial waves were studied by *Stokes* [1847], and the extension to continuous stratification was done by *Rayleigh* [1883]. However, the important role of internal waves in the spectrum of oceanic variability has been recognized only for a few decades, and we may look back on a period of intense research on this subject. The time has definitely passed when oceanographers merely considered internal waves as a passive contaminant, as unwanted noise (lumped together with any other kind of 'turbulence') in the measurements. The ascent from 'noise' to 'signal' took place when by the combined improvement of measuring and data interpretation techniques and the guidance of theoretical ideas it became obvious that internal waves play an active dynamical part in the energetics of the oceanic circulation.

1.1. *A Survey of Recent Observation Techniques*

The present state of knowledge about the structure and importance of the oceanic internal wave field is strongly based on experimental evidence of the wave motion. A brief survey of experimental techniques and observations therefore may help the reader to get acquainted with the interplay of measurements and theory presented in this paper.

Paper number 3R0297.
0034-6853/83/003R-0297$15.00

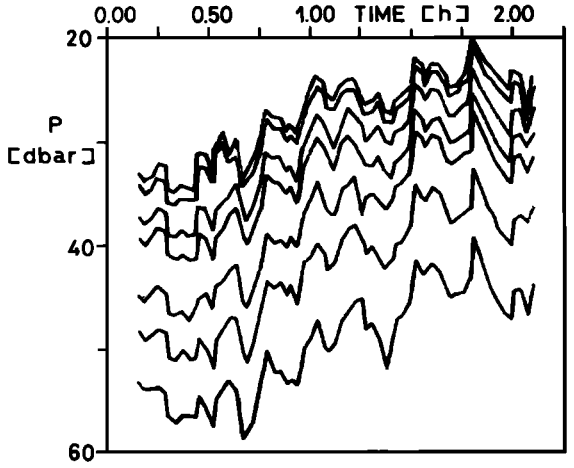

Fig. 1. Depth of selected isopycnals (23.75–25.25) interpolated from rapid successive CTD casts [*Käse and Clarke*, 1978].

Most early measurements of internal waves are records of temperature variations from thermometers at a fixed depth. The measurements of today are more sophisticated in adapting to the formidable task of obtaining a view of the highly complex space-time structure of the internal wave field. A great variety of devices have been designed to measure either the velocity associated with the wave motion or the temperature and salinity fluctuations which are due to the vertical displacements of the stratified fluid induced by the waves.

Moored current observations constitute the main data base for constructing internal wave models. The common current meter measures the speed of the horizontal flow by a rotor and the direction by a vane. Other devices with acoustic or propeller sensors are also coming into use. The technique of mooring these instruments in the deep ocean was mainly developed by members of the Woods Hole Oceanographic Institution [e.g., *Fofonoff and Webster*, 1971]. Temperature sensors are frequently used in connection with moored current meters to obtain the vertical component of the current velocity through the what might be called slightly 'mutilated' heat equation $w = -\partial_t T/\partial_z \bar{T}$, where $\partial_z \bar{T}$ is the mean vertical temperature gradient [*Briscoe*, 1975*b*]. Sensors which move through the wave field with speeds much larger than the phase speed of the waves yield a spatial snapshot of the wave fluctuations. Towed and dropped devices have been designed to collect data on the spatial structure of the motion. There are many kinds of dropped instruments measuring profiles of temperature, for example, the rapidly repeated sounding system on the platform Flip [*Pinkel*, 1975]. Thermistors arranged in a chain which is lowered from a ship and towed through the upper layers of the ocean have been used by, for example, *LaFond* [1962] and *Charnock* [1965] to document the evidence of internal wave motion. This technique maps a two-dimensional section of the thermal structure down to about 200 m depth. A towed depth-controlled 'fish' was used by *Katz* [1975] to follow particular isotherms at greater depths (700–800 m) and thereby to measure vertical displacements. The Batfish is another, more sophisticated towed device measuring pressure, temperature, and salinity on an undulating track through the water (down to about 400 m) and thus mapping a two-dimensional section of the density field [*Woods and Minnett*, 1979].

There are many other instruments and measuring techniques which reflect the effort required to collect reliable information on the wave motion. Noteworthy examples are displayed in Figures 1–5. Figure 1 shows the time history of displacements of selected isopycnals in the upper ocean extracted by interpolation from a time series of 66 successive conductivity-temperature-depth (CTD) casts [*Käse and Clarke*, 1978]. The associated motion appears to be well correlated over the complete depth range, which apparently is a characteristic feature of internal waves in the upper ocean. *Brekhovskikh et al.* [1975] have designed a sensor with the specific aim of filtering out such low-mode motion. They used an insulated vertically stretched wire whose resistance is proportional to the average temperature of the layer in which it is immersed. Therefore it is sensitive mainly to low-mode oscillations. Figure 2 shows such measurements from the Black Sea obtained with 20-m sensors spanning the thermocline. Measurements of the velocity field in the upper ocean using a Doppler sonar have been made by *Pinkel* [1979, 1981]. The sound beam is scattered off drifting organisms in the sea; the velocity parallel to the beam is obtained from the Doppler shift of the returning signal. Figure 3 displays perturbations of the velocity field dominated by inertial motions. An ingenious instrument measuring vertical displacements of isotherms in the deeper ocean is the yo-yo capsule of *Cairns* [1975]. This capsule freely drifts with the mean current, yo-yoing up and down approximately 15 m about a selected isotherm while sensing temperature and pressure. The data segment given in Figure 4 shows a couple of high-frequency waves riding on a large-amplitude wave with a period of about half a day. Profiles of relative horizontal current have been obtained by the electromagnetic velocity profiler of *Sanford* [1975], which measures the electric potential in the sea induced by the motion of the salty seawater in the magnetic field of the earth. Figure 5 shows two vertical profiles of each of the horizontal current components taken about half an inertial period apart at the same location. This picture is a simple but convincing illustration of the internal wave variability of the oceanic motion at all depths.

Internal waves are a three-dimensional phenomenon (the four-dimensional space-time continuum is constrained by the dispersion relation), but any of the commonly used sensors gets only one- or two-dimensional cuts of the three-dimensional variability: moored sensors record the time history of the fluctuations at a fixed point; towed and dropped sensors record a mixture of temporal and spatial structure. Single point or section measurements thus get only a limited amount of information, and quantitative interpretation of these data is ex-

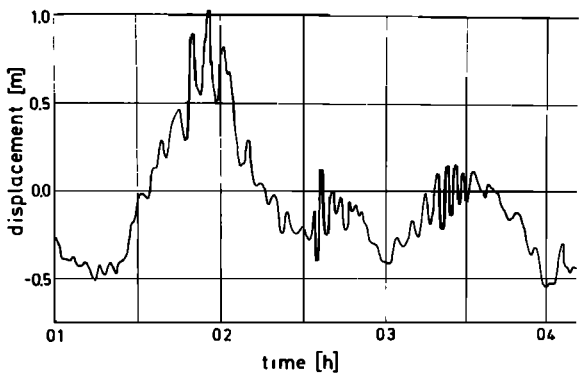

Fig. 2. Vertical displacement of the thermocline for groups of short-period internal waves on crests of long-period waves (Black Sea, 500 m from the coast, water depth 50 m, length of sensors 20 m, depth of sensors 25–44 m, thermocline depth 30–40 m, temperature changes in the thermocline from 22°C to 9°C) [*Brekhovskikh et al.*, 1975].

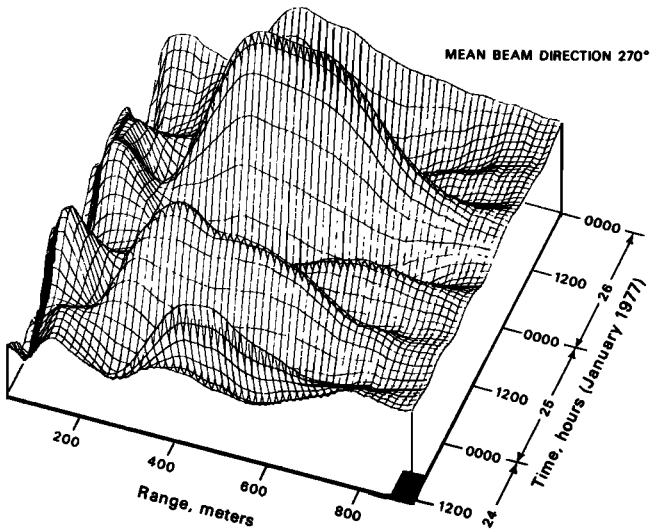

Fig. 3. Low-frequency velocity variations taken with a sonar at 50 m depth slanted 7° down from the horizontal. Profiles are low-pass filtered in range and time as indicated by the black square. The greatest range corresponds to approximately 225 m depth [*Pinkel*, 1981].

tremely difficult. Further, most of the more conventional observation techniques may yield a severely disturbed picture of the true fluctuations. Moored measurements suffer from a substantial unknown Doppler shift if the phase speed of the waves is not large compared to the velocity of lower-frequency currents. In this instance, moreover, the estimation of vertical displacement from temperature fluctuation and mean gradient becomes invalid [*Ruddick and Joyce*, 1979]. Freely drifting devices such as Cairn's capsule avoid this problem. Moored temperature records may also be contaminated by the vertical migration past the sensor of layered temperature fine structure induced by the wave motion [e.g., *Phillips*, 1971]. Decontamination of data from such effects (i.e., filtering out the true wave fluctuations) is only possible if experiments collect separable information about time and space structure and if certain knowledge about the contaminating fields is available. Many recent experiments have indeed proceeded in this direction. The step from single moorings to complex arrays of moored instruments was taken some years ago [*Webster*, 1972]. The most ambitious attempts were pursued with the IWEX experiment [*Briscoe*, 1975*b*] and the H mooring of the GATE experiment [*Käse and Siedler*, 1980]. Analysis and results of these experiments will be presented later.

1.2. *The Impetus of Spectral Modeling*

The first attempt to provide a unified picture of the internal wave field was made by *Garrett and Munk* [1972*a*], who synthesized a model of the complete wave number–frequency spectrum of the motion on the basis of linear theory and the available observations. Except for inertial-internal waves and tides this model is believed to reflect the spectral features of the internal wave climate in the deep ocean and to possess a certain global validity. The model, which since its inception has been slowly changing with the accumulation of new data, may be viewed as a milestone in internal wave research. It may be said without overstating that it has influenced (if not originated) nearly all recent activities in experimental as well as in theoretical investigations on internal waves.

To the experimeter the model served as a guide as to what type of measurements would yield new information about the motion and what space-time scales could be expected in a specific part of the oceanic water column and should be covered by experimental strategy. Many of the instruments and experiments described above have been designed to measure specific properties of the spectrum. Most data were in good agreement with the model or could be incorporated by slight modifications [*Garrett and Munk*, 1975; *Müller et al.*, 1978]. Apparent deviations from the model could only be found in the proximity of possible source regions of wave energy such as topographic

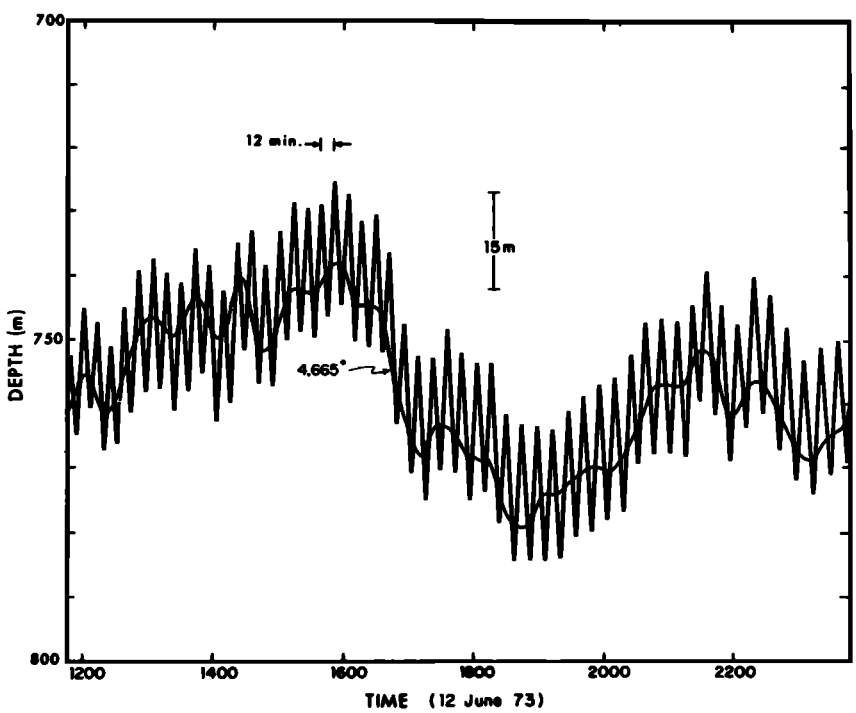

Fig. 4. A segment of yo-yo data. The light zigzag line is the depth of the 4.665°C isotherm [*Cairns*, 1975].

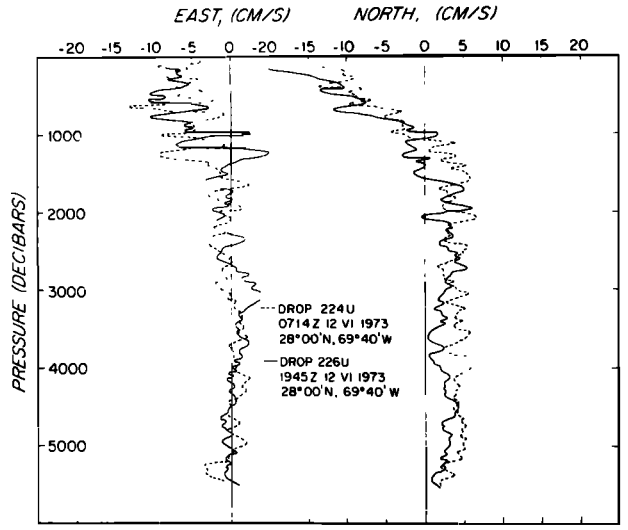

Fig. 5. Vertical profiles of eastward and northward velocity taken 12.5 hours apart at the same location [*Sanford*, 1975].

features [*Wunsch*, 1976] and regions of large mean flow [*Ruddick and Joyce*, 1979] and in the upper thermocline [e.g., *Brekhovskikh et al.*, 1975; *Käse and Siedler*, 1980; *Roth et al.*, 1981; *Pinkel*, 1981]. Here, under the direct influence of the atmospheric variability and with waveguide properties differing strongly from those in the deep ocean, the universal model turned out to be inappropriate.

To the theoretican the canonical model of Garrett and Munk posed the problem of explaining its universality and specific spectral shape on a dynamical basis. At the same time he was enabled to study these questions by using the form and the scale parameters of the model in the evaluation of generation and dissipation mechanisms of internal wave energy [e.g., *Müller and Olbers*, 1975]. A fundamental role in shaping the deep ocean spectrum could be attributed to nonlinear resonant wave-wave interactions within the wave field [*Olbers*, 1976; *McComas and Bretherton*, 1977; *McComas and Müller*, 1981*a*] which transfer energy across the spectrum but conserve its total amount. However, interactions with external fields were also studied extensively. As the universality of the spectrum strongly suggests universality of at least some of the dominant dynamical processes, the interactions of the wave field may also reveal some results about the external fields which possess global relevance.

It has frequently been conjectured that not all of the variance observed by the many kinds of measuring devices can be attributed to internal waves, but quantitative results could hardly be obtained. Also in this difficult problem of separating the internal wave part from nonwave contributions in observations the spectral modeling approach originated by Garrett and Munk made a crucial impetus. The knowledge of the approximate shape of the internal wave spectrum allows one to formulate the separation problem as a linearized inverse problem which is solved by linear matrix algebra. The great variety of different model classes for interpretation of the wave turbulence data may be narrowed a priori by application of appropriate consistency tests [*Müller and Siedler*, 1976]. A carefully tuned combination of these methods may be used to arrive at a statistically consistent interpretation of wave turbulence data [cf. *Olbers et al.*, 1976; *Müller et al.*, 1978].

This paper attempts a survey on the line of research which has started with the spectral modeling of oceanic internal waves. The time for such a review seems to be due, since after a productive decade the internal wave research has come to a stagnant phase, partly because many problems are solved whereas others turned out to be rather entangled.

The kinematics of internal waves will be considered in some detail in section 2, which covers the theoretical properties of linear free waves, in particular their propagation characteristics and critical layers. Spectral models will be considered in section 3. The separation problem of waves and turbulence in observations is discussed in section 4. Dynamical models will be presented in section 5, which gives a discussion of interaction processes affecting the oceanic internal wave field and, based on these, some aspects of the energy balance and the universality of the internal wave spectrum.

This paper supplements recent reviews by *Garrett and Munk* [1979] on internal waves in the ocean and by *Munk* [1981] on the interrelation of internal waves and smaller-scale structures. Some of the theoretical framework can be found in the textbooks by *LeBlond and Mysak* [1978], *Phillips* [1977], and *Lighthill* [1978] and in the papers by *Müller and Olbers* [1975] and *Thorpe* [1975]. A comprehensive bibliography of the internal wave research in recent years has been given and discussed in the IUGG reviews by *Briscoe* [1975*a*] and *Gregg and Briscoe* [1979].

2. Kinematical Models

Waves are by definition an essentially linear disturbance of the wave-carrying medium: once they are generated, they propagate almost freely along their rays, slowly changing by nonlinear effects and coupling to their supporting background, thereby slowly losing attributes acquired during their particular generation process. Strongly nonlinear effects such as breaking occur only as very localized events in space and time. This picture is certainly true for surface gravity waves [e.g., *Hasselmann et al.*, 1973] and is generally accepted for internal waves as a working hypothesis. Indeed, linear kinematics work surprisingly well despite evidence for strong nonlinearities over some part of the spectral range (see section 5).

A linear wave is characterized by an amplitude $a(\mathbf{k})$, a wave vector $\mathbf{k}$, and frequency ω, which are related by a dispersion relation $\omega = \Omega(\mathbf{k})$. Large-scale inhomogeneities (compared to period and wavelength) of the wave-carrying background can be treated by WKB methods. Waves then appear in the form of slowly varying wave trains which may be represented locally by wave groups characterized by a local dispersion relation

$$\omega = \Omega(\mathbf{k}, \mathbf{x}, t) \tag{1}$$

A mean current $\mathbf{U}$ is included in Ω as a Doppler shift $\mathbf{kU}$ so that $\omega - \mathbf{kU}$ represents the intrinsic frequency. A wave group propagates with the group velocity

$$\dot{\mathbf{x}} = \partial_{\mathbf{k}}\Omega \tag{2}$$

On the trajectory (ray), wave vector and frequency change according to

$$\dot{\mathbf{k}} = -\partial_{\mathbf{x}}\Omega \tag{3}$$

$$\dot{\omega} = \partial_t\Omega \tag{4}$$

while changes in amplitude are conveniently expressed in the form of action conservation [*Whitham*, 1970; *Bretherton and Garrett*, 1968]

$$\partial_t\left(\frac{\varepsilon}{\omega - \mathbf{kU}}\right) + \partial_{\mathbf{x}}\left(\dot{\mathbf{x}}\,\frac{\varepsilon}{\omega - \mathbf{kU}}\right) = 0 \tag{5}$$

The wave energy density $\varepsilon \sim |a(\mathbf{k})|^2$ is a quadratic functional of the amplitude. Equation (5) states that the wave action $\int [\varepsilon/(\omega - \mathbf{kU})]\, d^3x$ is an adiabatic invariant (see, for example, *Landau and Lifschitz* [1970]) for slowly varying linear wave groups. The application of this general framework of wave kinematics to internal waves is the aim of this section.

The kinematical structure of internal waves is determined by the mean buoyancy and current fields and the bottom topography. Only variations of these mean oceanic fields have an essential influence: the reflection properties of a flat horizontal bottom are fairly simple, a constant current merely implies a Doppler shift, and the waves feel the buoyancy field only through its gradients. Horizontal gradients of buoyancy and currents generally are small compared to the vertical gradients and therefore are neglected in the traditional kinematical models based on a horizontally homogeneous buoyancy (or Brunt-Väisälä) frequency $N(z) = (g/\rho_0)^{1/2}(-d\rho/dz)^{1/2}$ and shear current $\mathbf{U}(z)$. A typical profile of the mean current may be extracted from Figure 5 by averaging by eye the fluctuations of the internal wave motion. The buoyancy frequency usually has maxima below the upper mixed layer and in the deeper ocean where strong gradients of temperature and thus density exist. Typical peak values of N are 10^{-2} s^{-1} (period 10 min) in the upper (seasonal) thermocline and 10^{-3} s^{-1} (period 1.5 hours) in the lower (main) thermocline (see Figures 8 and 12).

A further external parameter which is essential for the kinematic description of internal waves, in particular for waves of low frequency and larger wavelength, is the local Coriolis frequency $f = 2\Omega$ sin (latitude) associated with the earth's angular velocity Ω. In most kinematical models, f is assigned a constant local value (the f plane approximation). However, if a wave group travels substantial distances on the globe, the variation of f with latitude must be taken into account.

Horizontal variations of N and $\mathbf{U}$ of large scale (in a WKB sense) may be considered in horizontal refraction models, while variations with scales comparable to (or smaller than) those of the waves define scattering problems discussed in the section on dynamical models. Latitudinal variations of the Coriolis frequency may also be treated by a WKB theory or by more sophisticated theories. Two basic concepts are used to describe the vertical structure of internal waves: vertically progressive waves and vertically standing waves (generally denoted 'modes'). The first concept is somewhat more general, though applicable only if the vertical wavelength is small compared to the vertical scales of N and $\mathbf{U}$, since it allows independent upward and downward propagating waves. Vertically standing waves represent the vertical eigenmodes of the complete water column (the ocean acts as a wave duct) and propagate only horizontally. Which of these concepts is more adequate for describing the real ocean must be determined by experiments. This will be discussed in section 3. Here the basic ingredients of the kinematical models will be presented.

2.1. *Vertically Progressive Waves*

In a geostrophic mean flow the horizontal density gradient affects the WKB approximation only in higher orders [*Olbers*, 1981*b*]. Thus the kinematics are determined by the slowly varying buoyancy frequency $N(\mathbf{x})$ and current $\mathbf{U}(\mathbf{x})$, where $\mathbf{x} = (x_1, x_2, x_3 = z)$ denotes the three-dimensional position vector. A wave with a phase factor $\exp\{i(\mathbf{kx} - \omega t)\}$ then obeys the local dispersion relation

$$\omega = \Omega(\mathbf{k}, \mathbf{x}) = \omega_0 + \mathbf{kU}(\mathbf{x}) \tag{6a}$$

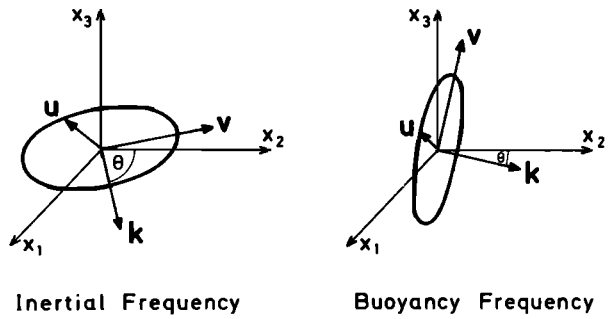

Fig. 6. The wave number vector $\mathbf{k}$, the group velocity $\mathbf{v}$, and the hodograph of the particle velocity $\mathbf{u}(t)$ near the inertial frequency and the buoyancy frequency, respectively; $\mathbf{k}$ is normal to both $\mathbf{v}$ and $\mathbf{u}$ and $\mathbf{k}$ lies here in the (x_2, x_3) plane; θ is the inclination with respect to the horizontal plane (adapted from *Garrett and Munk* [1979]).

where the intrinsic frequency is given by

$$\omega_0 = \Omega_0(\mathbf{k}, \mathbf{x}) = \left\{N^2(\mathbf{x})\frac{k_h^2}{k^2} + f^2\frac{k_3^2}{k^2}\right\}^{1/2} = \{N^2(\mathbf{x})\cos^2\theta + f^2\sin\theta\}^{1/2} \tag{6b}$$

Equivalently,

$$(k_3/k_h)^2 = \frac{N^2(\mathbf{x}) - \omega_0^2}{\omega_0^2 - f^2} = \tan^2\theta \tag{6c}$$

which relates the inclination θ of the three-dimensional wave vector $\mathbf{k} = (k_1, k_2, k_3)$ to the intrinsic frequency ω_0 (cf. Figure 6). In these expressions, k is the modulus of $\mathbf{k}$, and k_h is the modulus of the horizontal wave vector $\mathbf{k}_h = (k_1, k_2)$. The intrinsic frequency ω_0 is restricted to $f < \omega_0 < N$ and is independent of the magnitude of $\mathbf{k}$. The ray equations (2), (3), and (4) take the form

$$\begin{aligned} \dot{x}_i &= \partial\Omega/\partial k_i = v_i + U_i \\ \dot{k}_i &= -\partial\Omega/\partial x_i = r_i - k_j\,\partial U_j/\partial x_i \qquad i = 1, 2, 3 \\ \omega &= \text{const} \end{aligned} \tag{7}$$

where $\mathbf{v}$ and $\mathbf{r}$ are the intrinsic group velocity and rate of refraction:

$$\begin{aligned} \mathbf{v} &= \partial_{\mathbf{k}}\Omega_0 = \frac{N^2 - \omega_0^2}{\omega_0 k_h^2}\frac{\omega_0^2 - f^2}{N^2 - f^2}\left(k_1, k_2, -\frac{\omega_0^2 - f^2}{N^2 - \omega_0^2}k_3\right) \\ \mathbf{r} &= -\partial_{\mathbf{x}}\Omega_0 = -\frac{N}{\omega_0}\frac{N^2 - \omega_0^2}{N^2 - f^2}\partial_{\mathbf{x}}N \end{aligned} \tag{8}$$

Well-known properties of the wave group propagation are that the intrinsic stretching or shrinking of the wave vector occurs always along the gradient of the buoyancy frequency and that phase and group propagation of a wave are orthogonal ($\mathbf{v} \cdot \mathbf{k} = 0$), nicely demonstrated in tank experiments by *Mowbray and Rarity* [1967]. Also, the local particle motion takes place in the plane orthogonal to $\mathbf{k}$ because of incompressibility. The polarization vector

$$\begin{aligned} U_1(\mathbf{k}) &= C(\omega_0 k_1 + if k_2) \\ U_2(\mathbf{k}) &= C(\omega_0 k_2 - if k_1) \\ U_3(\mathbf{k}) &= C\left(-\omega_0\frac{\omega_0^2 - f^2}{N^2 - \omega_0^2}k_3\right) \end{aligned} \tag{9}$$

of the wave velocity field indicates elliptical polarization (Figure 6): at near-inertial frequencies $\omega \gtrsim f$ (where $k_h^2 \gg k_3^2$)

the particle motion is almost horizontal and circular; at higher frequencies the ellipse tends toward the vertical and becomes more eccentric with almost up-and-down motion at $\omega_0 \lesssim N$ (where $k_3^2 \gg k_h^2$). The normalization factor C is conveniently chosen as $(\omega_0 k_h)^{-1}\{(N^2 - \omega_0^2)/(N^2 - f^2)\}^{1/2}$. Then the total local energy density of the wave component (averaged over a wave period)

$$\varepsilon = \tfrac{1}{2}(\overline{u_j u_j} + N^2\overline{\zeta^2}) = 2|a(\mathbf{k})|^2 \tag{10a}$$

and its energy flux vector

$$\boldsymbol{\phi} = \overline{p\mathbf{u}} = 2|a(\mathbf{k})|^2\mathbf{v} = \varepsilon\mathbf{v} \tag{10b}$$

take a simple form in terms of the current amplitude $a(\mathbf{k})$ defined by

$$\begin{aligned} \mathbf{u}(\mathbf{x}, t) &= a(\mathbf{k})\mathbf{U}(\mathbf{k}) \exp\{i(\mathbf{kx} - \omega t)\} + \text{c.c.} \\ \zeta(\mathbf{x}, t) &= a(\mathbf{k})iU_3(\mathbf{k})/\omega_0) \exp\{i(\mathbf{kx} - \omega t)\} + \text{c.c.} \\ p(\mathbf{x}, t) &= a(\mathbf{k})C(\omega_0^2 - f^2) \exp\{i(\mathbf{kx} - \omega t)\} + \text{c.c.} \end{aligned} \tag{11}$$

These expressions also give the vertical displacement ζ and the pressure field p of the wave. Equation (10*b*) shows that the wave energy flux becomes the product of the energy density and the group velocity, a relation which is true for many wave types.

The WKB theory is completed by reflection conditions for the rays at the sea surface and at the bottom. These are given, for example, in the textbooks by *Phillips* [1977] and *LeBlond and Mysak* [1978]. For a rigid boundary sloping at an angle α with respect to the horizontal (i.e., $x_3 = x_1 \tan\alpha$) the reflected wave vector (l_1, l_2, l_3) is given by

$$\begin{aligned} l_1 &= \frac{(1 + \tan^2\alpha \sin^2\theta)k_1 + 2k_3 \tan\alpha}{1 - \tan^2\alpha \sin^2\theta} \\ l_2 &= k_2 \\ l_3 &= -\frac{(1 + \tan^2\alpha \sin^2\theta)k_3 + 2k_1 \tan\alpha \sin^2\theta}{1 - \tan^2\alpha \sin^2\theta} \end{aligned} \tag{12a}$$

where (k_1, k_2, k_3) is the incident wave vector with the inclination angle θ given by (6*c*). If $\tan^2\alpha \sin^2\theta < 1$, that is, $\omega^2 < \omega_s^2$ with

$$\omega_s^2 = N^2 \sin^2\alpha + f^2 \cos^2\alpha \tag{12b}$$

the reflection process is horizontally transmissive in the sense that the group velocities of the incident and the relfected wave point in the seme horizontal direction. For $\omega^2 > \omega_s^2$ the horizontal group velocities are opposite to each other, and the reflection process is said to be horizontally reflective. The frequency ω_s thus is an important parameter of the wave field close to sloping bottoms. Waves with a frequency below ω_s will be reflected backward if they impinge on a sloping bottom. Waves with $\omega > \omega_s$ must proceed up the slope, which may lead to accumulation of wave energy at topographic features. Consequences of this process will be considered in section 5.1.

For a single monochromatic wave the wave pattern at a fixed position is stationary, and the action conservation (5) takes the form

$$\partial_x\{(\mathbf{v} + \mathbf{U})(\varepsilon/\omega_0)\} = 0 \tag{13}$$

stating that wave action flux through any cross section of a ray tube is constant. This equation and the ray equations (7) determine global changes of the wave parameters along the ray. Solutions of the ray equations (7) and the action conservation (13) are discussed below.

In a horizontally homogeneous ocean with a constant horizontal mean current (the traditional kinematical model), integration of (7) and (13) yields the constancy of the horizontal wave vector $\mathbf{k}_h$ and the intrinsic frequency ω_0, whereas the vertical wave number and energy change according to

$$\begin{aligned} k_3(z) &\sim [N^2(z) - \omega_0^2]^{1/2} \\ \varepsilon(z) &\sim 1/v_3 \sim \frac{N^2(z) - f^2}{[N^2(z) - \omega_0^2]^{1/2}} \end{aligned} \tag{14a}$$

The velocity components and the displacement then scale as (the 'WKB scaling')

$$\begin{aligned} u_1, u_2 &\sim a(\mathbf{k}) \cdot C \sim [N^2(z) - \omega_0^2]^{1/4} \\ u_3, \zeta &\sim a(\mathbf{k}) \cdot C[N^2(z) - \omega_0^2]^{-1/2} \sim [N^2(z) - \omega_0^2]^{-1/4} \end{aligned} \tag{14b}$$

which may be inferred from (10), (11), and (14*a*). Thus when a wave group propagates toward a region of lower $N(z)$, the vertical wave number and the group velocity tend to zero, but the group still reaches the depth where $N(z) = \omega_0$ (turning depth) in a finite time, and internal reflection occurs. Near this depth the WKB solution becomes invalid and should be replaced by solutions in terms of Airy functions [*Desaubies*, 1973, 1975]. These show that the energy $\varepsilon(z)$ possesses a finite maximum at the turning depth rather than the weak singularity given by (14).

By allowing the current to have a vertical shear (i.e., $\mathbf{U} = \mathbf{U}(z)$), another important kinematical feature is introduced. Here still $(k_1, k_2) = \text{const}$, but the intrinsic frequency $\omega_0(z) = \omega - \mathbf{kU}(z)$ now varies with depth, and (6) and (13) yield

$$\begin{aligned} k_3(z) &\sim \left(\frac{N^2(z) - \omega_0^2(z)}{\omega_0^2(z) - f^2}\right)^{1/2} \\ \varepsilon(z) &\sim \omega_0/v_3 \sim \frac{\omega_0^2(z)[N^2(z) - f^2]}{[\omega_0^2(z) - f^2]^{3/2}[N^2(z) - \omega_0^2(z)]^{1/2}} \end{aligned} \tag{15}$$

A wave group propagating toward increasing $\mathbf{k} \cdot \mathbf{U}(z)$ and thus decreasing ω_0 may encounter a level where ω_0 approaches f. Here k_3 and ε tend to infinity, the wave group shrinks, its vertical shear increases, and the group velocity tends toward the horizontal. However, in contrast to the turning depth behavior, the group never reaches the level where $\omega_0 = f$ [*Bretherton*, 1966]. Dynamical considerations suggest that near this critical layer where the wave shear becomes very large there will be substantial dissipation and the wave will be absorbed by the mean flow [*Booker and Bretherton*, 1967].

Horizontally homogeneous models are of limited value, in particular when discussing internal waves in the upper ocean, where N and $\mathbf{U}$ are known to vary in the horizontal direction on a broad range of scales. The effect of horizontal inhomogeneities of large scale on the oceanic internal wave field has been investigated only for very special cases. *Samodurov* [1974], *Miropol'skiy* [1974], and *Miropol'skiy et al.* [1976] studied the propagation effects in a density front with a vertically constant but horizontally varying buoyancy frequency. These authors found critical layer properties of the wave at the point on the ray where the intrinsic frequency equals the local buoyancy frequency, that is, at $\omega_0 = N$. The interaction with a shear current is taken into account in the work of *Magaard* [1968] and *Mooers* [1975*a*], who considered normal incidence of waves onto a geostrophic current, and *Jones* [1969] and *Mooers* [1975*b*], who investigated the propagation in a geostrophic flow with constant buoyancy frequency and constant

current shears. In this latter work, critical layer conditions are found at a frequency between $\omega_0 = f$ and $\omega_0 = N$.

The propagation of internal waves in geostrophic current with straight, sloping isopycnals was analyzed by *Olbers* [1981*b*]. For this configuration, which covers the cases discussed above, the refraction equations can still be integrated analytically. Taking the current into the x_2 direction, it is found that the frequency of encounter ω, the wave number component k_2 along the current U_2, and the wave number component $k_\parallel$ parallel to the isopycnals remain constant, whereas the normal component changes along the ray. The waveguide is the region defined by

$$\omega_c^2(x_1, x_3) \le \omega_0^2 = [\omega - k_2 U_2(x_1, x_3)]^2 \le N^2(x_1, x_3) \quad (16a)$$

with

$$\omega_c^2 = \frac{L^2(x_1, x_3)k_2^2 + f^2 k_\parallel^2}{k_2^2 + k_\parallel^2}$$
$$L^2(x_1, x_3) = N^2(x_1, x_3)\rho_1^2 + f^2\rho_3^2 \quad (16b)$$

where $\boldsymbol{\rho} = (\rho_1, \rho_3)$ is the normal to the isopycnals in the (x_1, x_3) plane. At $\omega_0 = \pm\omega_c$ and $\omega_0 = \pm N$, waves are reflected, and at $\omega_0 = \pm L$ (which is inside the waveguide), waves encounter a critical layer with a valve type behavior: these surfaces can be penetrated from one side, while incidence from the other side results in absorption. A sketch of this behavior is shown in Figure 7. For a horizontally homogeneous ocean ($\rho_1 = 0$) one recovers the critical layer at $\omega_c^2 = L^2 = f^2$, and for a vertically homogeneous ocean ($\rho_3 = 0$) the critical layer shifts to $\omega_0^2 = L^2 = N^2$, the case treated by *Miropol'skiy* [1974] and others. The conservation of action takes the form

$$v_\perp(\varepsilon/\omega_0) = \text{const} \quad (17)$$

where $v_\perp$ is the component of the intrinsic group velocity normal to the isopycnals. It is then shown, in agreement with the conception of internal reflection and critical layer absorption, that the energy possesses an integrable singularity at the reflecting surfaces $\omega_0 = \pm\omega_c$ and $\omega_0 = \pm N$, while at $\omega_0 = \pm L$ a nonintegrable singularity appears for waves arriving from the nonpenetrative side.

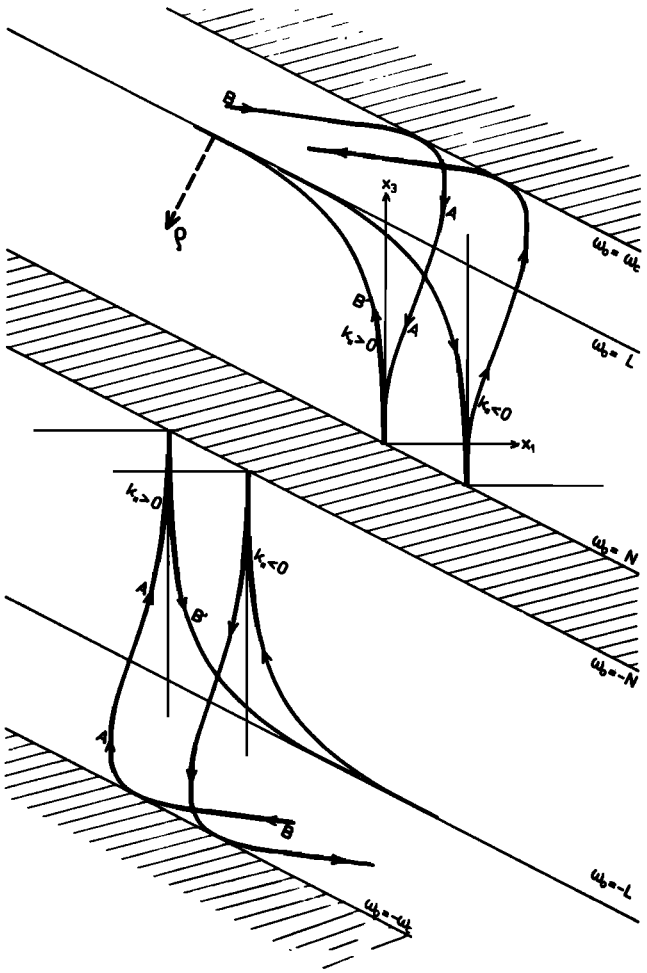

Fig. 7. Sketch of rays for a wave $(\omega, k_2, k_\parallel)$ for different $k_\parallel$, projected onto the (x_1, x_3) plane. The current is normal to this plane, and the vector $\boldsymbol{\rho}$ is normal to the sloping isopycnals. The forbidden region for wave propagation is hatched. Reflection occurs at $\omega_0 = \pm\omega_c$ and $\omega_0 = \pm N$. At $\omega_0 = \pm L$, wave A is allowed to penetrate, whereas B' runs into a critical layer.

The WKB approximation presented so far is valid for large values of the Richardson number $Ri = N^2/(\partial U/\partial z)^2$. The behavior at critical layers is quite different for small Richardson numbers. For wave propagation in a horizontally homogeneous shear flow, *Booker and Bretherton* [1967] found that very little energy and momentum is transmitted or reflected. The wave energy flux is attenuated by a factor $\exp\{2\pi(Ri - \frac{1}{4})\}$ across the critical layer, which in the limit of large Ri recovers the WKB prediction of complete absorption. *Jones* [1968] extended the theory to Richardson numbers in the range $0 < Ri < \frac{1}{4}$ and found that here substantial reflection may occur. At any given wave number and intrinsic frequency there is a critical value of Ri below which the wave is able to extract energy and momentum from the mean flow, so that the reflected wave is actually larger than the incident wave. The intimate relation of such an 'overreflection' process to the instability of the ambient shear flow at $Ri < \frac{1}{4}$ was analyzed by, for example, *Lindzen and Rosenthal* [1976].

2.2. *Vertically Standing Waves*

Vertically standing waves are formed if long coherent wave trains make many reflections at top and bottom or at turning points and if fixed phase relations between upward and downward reflected parts of the wave pattern are established. From a mathematical point of view a representation of an internal wave field in terms of standing modes is always possible (since the vertical modes constitute a complete set of eigenfunctions), but physically, it may be inappropriate. A well-developed standing mode for the full water column appears a priori rather questionable, at least for high mode numbers (i.e., small vertical wavelengths), since typical vertical propagation times are comparable to typical relaxation times of nonlinear interactions [*Olbers*, 1976; *McComas and Bretherton*, 1977]. Phases then will be randomized, and energy will be exchanged among the waves before a mode can be formed. Moreover, the basic state of the wave duct is often oversimplified, since modal wave models almost exclusively neglect the mean current shear and use modes computed from $N(z)$ alone. But even a weak mean shear current may have significant influence on the wave structure, since phase speeds of internal waves are comparable with typical changes in the current profile and critical layers may appear. Interpretation of internal waves in an ocean with shear in terms of 'shearless' modes will yield time-varying mode amplitudes even if the wave field is strictly stationary. In the

following discussion some features of shearless and shear modes will be discussed.

Consider waves with phases exp $\{i(\mathbf{k}_h \cdot \mathbf{x}_h - \omega t)\}$ in a horizontally homogeneous wave duct. Standing modes based on the density stratification alone are defined by the eigenvalue problem (appropriate to the Boussinesq approximation with upper free surface)

$$\frac{d^2\varphi}{dz^2} + k_h^2 \frac{N^2(z) - \omega^2}{\omega^2 - f^2}\varphi = 0$$

$$\frac{d\varphi}{dz} - \frac{gk_h^2}{\omega^2 - f^2}\varphi = 0 \qquad \text{at } z = 0 \tag{18}$$

$$\varphi = 0 \qquad \text{at } z = -H$$

Solution of this Sturm-Liouville type problem yields an infinite complete and orthogonal set of modes $\varphi_\nu(z)$, $\nu = 0, 1, 2, \cdots$, with eigenvalues ω_ν^2 if k_h is prescribed, or vice versa. The numbering may be arranged such that the mode $\varphi_\nu(z)$ has $\nu - 1$ zero crossings in the interior $0 < z < -H$. Then ω_ν is a monotonically decreasing sequence. The barotropic or surface mode $\varphi_0(z)$ has $\omega_0 \gg \omega_1$ and vanishes only at the bottom. It is associated with the displacement of the free surface and represents surface waves. The baroclinic or internal modes $\varphi_\nu(z)$, $\nu \geq 1$, exists only in the range $f < \omega_\nu < N_{max}$, where N_{max} is the maximum buoyancy frequency in the water column. These modes represent internal waves. The modes $\varphi_\nu(z)$ describe the structure of the vertical current and buoyancy field, whereas $d\varphi_\nu/dz$ applies to the horizontal current and pressure field.

In the presence of a horizontal mean current $[U(z), V(z)]$ the vertical eigenvalue problem (18) must be replaced by the Taylor-Goldstein equation [e.g., *LeBlond and Mysak*, 1978]

$$\frac{d^2\varphi}{dz^2} + \left(\frac{N^2}{(\hat{U} - c)^2} - \frac{d^2\hat{U}/dz^2}{\hat{U} - c} - k_h^2\right)\varphi = 0$$

$$\frac{d\varphi}{dz} - \frac{g + (\hat{U} - c)\, d\hat{U}/dz}{(\hat{U} - c)^2}\varphi = 0 \qquad \text{at } z = 0 \tag{19}$$

$$\varphi = 0 \qquad \text{at } z = -H$$

where $c = \omega/k_h$ is the phase speed and

$$\hat{U}(z) = \mathbf{k}_h \mathbf{U}(z)/k_h = U(z) \cos\alpha + V(z) \sin\alpha \tag{20}$$

which is the component of the mean current in the direction of the wave vector $\mathbf{k}_h = k_h(\cos\alpha, \sin\alpha)$. Again, φ determines the vertical structure of the vertical velocity of the wave. Rotational effects have been neglected in (19); that is, $\omega^2 \gg f^2$ is assumed. The Taylor-Goldstein equation is usually formulated for a parallel mean flow (i.e., $V \equiv 0$), but its form is retained for a spiraling current by the definition of $\hat{U}(z)$. Note that (18) with $f = 0$ is recovered from (19) with $\hat{U} = 0$. However, the character of the eigenvalue problem is severely changed by the inclusion of the shear current. Not only does this lead to shear modification of the internal wave modes, but the singularity of (19) at depths where $\hat{U}(z) = c$ (the critical levels) is responsible for additional modes. These are either unstable or damped (i.e., the eigenvalue $c = c_r + ic_i$ is complex) or have real eigenvalues but, in contrast to the internal wave modes, have discontinuous eigenfunctions at the critical levels. Unstable modes are confined to $\hat{U}_{min} < c_r < \hat{U}_{max}$, with c_i bounded by Howard's semicircle theorem, and do not occur if the Richardson number (based on $\hat{U}$) is above $\frac{1}{4}$ everywhere in the water column (Miles' theorem) [c.f. *LeBlond and Mysak*, 1978]. A complete classification of the modes of the Taylor-Goldstein equation has been given by *Banks et al.* [1976]. The class of unstable modes is finite. Stable modes include (1) a finite set of damped modes (those conjugate to the unstable modes), (2) a discrete set of modes which essentially are internal waves modified by the shear (these have $c > \hat{U}_{max}$ or $c < \hat{U}_{min}$), (3) a finite set of modes with c inside the range of the velocity distribution (these have branch points at the critical levels), and (4) a continuous set of modes which also have c inside the range of $\hat{U}(z)$ (these have discontinuities at the critical levels).

Figure 8 illustrates the behavior of shearless and shear modes calculated from the eigenvalue problems (18) and (19), respectively [*Peters*, 1980, 1983]. The mean profiles (Figure 8*a*) of $N(z)$ and $\mathbf{U}(z)$ are from the JASIN experiment. The profile of the stability frequency consists of a high-frequency waveguide in the upper ocean and a low-frequency waveguide at greater depths extending to the bottom. These are separated by a broad minimum of intermediate depths with N around 1 cph. The current decreases almost monotonically toward the bottom and is approximately unidirectional toward the northwest.

The dispersion curves of the first five shearless modes are shown in Figure 8*b*, and some low-frequency and high-frequency modes in Figure 8*c*. The latter modes illustrate the trapping of energy in the region $\omega < N(z)$: here the modes have a sinusoidal appearance, whereas they fade away exponentially beyond the turning points. Notice the distortion of the dispersion curves close to the minimum of $N(z)$ separating the upper and lower thermoclines [c.f. *Eckart*, 1961]. Here the wavelength suddenly decreases for a slight increase of frequency (this causes reduction of the waveguide to the extent of the seasonal thermocline). The phase velocity drops and the group velocity attains low values in this frequency range. Also, the dispersion curves come very close to each other by pairs. These features may lead to distortions in observed spectra and coherences [e.g., *Katz and Briscoe*, 1979] either because of the kinematical reasons or because of enhanced nonlinear coupling for the small separation of the eigenfrequencies.

Shear modes are discussed in Figures 8*d*–8*f*. The Richardson number for the profiles in Figure 8*a* is above $\frac{1}{4}$ at all depths, so that only stable modes exist. The phase speed c_ν and hence the eigenfrequency $\omega_\nu = k_h c_\nu$ of the mode ν now depend on the magnitude k_h of the wave vector as well as its direction α. Apparently, the discussion may be restricted to positive frequencies, since as in the case of the shearless modes, $\omega_\nu(k_h, \alpha) = -\omega_\nu(k_h, \alpha + \pi)$. The mean flow is almost parallel with a mean direction of $\alpha = 135°$ counted from east. The deviations from this angle introduce small asymmetries in the dispersion curves with respect to the direction. These will be disregarded in the following discussion. Since $\hat{U}_{min} = 0$, critical levels may occur in the $\omega - k_h$ plane in the sector between $\omega = k_h\hat{U}_{max}$ and $\omega = 0$. This sector is present if $\mathbf{k}_h$ has a component into the direction of the mean current $\mathbf{U}$. The internal wave modes lie above this sector (Figure 8*d*, upper panel). Compared to the shearless modes, these waves which travel downstream undergo an increase of frequency and may even be observed above the maximum stability frequency. For $\mathbf{k}_h$ perpendicular to $\mathbf{U}$ (again neglecting the small deviation from a parallel flow) the critical layer sector vanishes, and the shearless modes are recovered. If $\mathbf{k}_h$ points opposite to $\mathbf{U}$, the frequencies are decreased (Figure 8*d*, lower panel). These waves are traveling upstream. At low wave numbers the group velocity still points into the direction of $\mathbf{k}_h$, and thus also, energy propagates upstream. At larger wave numbers the group velocity reverses, and energy thus propagates downstream, that is, opposite to the phase propaga-

tion. A more detailed view of the dispersion curves for mode 1 is given in Figure 8*e*. Here the asymmetries caused by the nonparallelism of the flow are revealed in the difference between the curves for $\alpha = 90°$ and $\alpha = 180°$ as well as $\alpha = 0°$ and $\alpha = -90°$. Figure 8*f* displays the first mode at $\omega = 1.5 \times 10^{-3}\ s^{-1}$ (0.86 cph). It is fairly obvious that the shear current has profound influences on the structure of the modes. In particular, the upstream modes are significantly different. Note that the frequency of the modes considered here is close to the intermediate minimum in the N profile. Here the modes are strongly modified by the shear, while low-frequency modes undergo only minor changes.

2.3. *The Planetary Waveguide*

The kinematical models presented so far have neglected the latitudinal dependence of the Coriolis frequency. This may be incorporated and leads to latitudinal bounds of the waveguide. Waves of a frequency ω traveling poleward encounter reflection at the latitudes given by $\omega = 2\Omega \sin \varphi$. As demonstrated by *Munk* [1980], the behavior at these turning latitudes is closely analogous to the reflection process of vertically progressive waves in an ocean with a variable $N(z)$ profile. *Kroll* [1975] presented a WKB theory of internal waves on a β plane (i.e., taking $\beta = df/dx_2$ constant). *Munk* [1980] considers a β plane with turning point solutions in terms of Airy functions, and *Munk and Phillips* [1968] consider Airy function solutions on a sphere. A slightly more complete analysis is provided by *Fu* [1981]. Again, as in the vertical direction, the problem of propagating versus standing waves appears. Preference for the latter case seems the more appropriate the narrower the latitudinal extent of the waveguide.

3. SPECTRAL MODELS

Oceanic internal waves are a phenomenon best treated statistically. Because of broadband forcing by a great variety of generation mechanisms and because of nonlinear coupling, the wave field generally consists of a large ensemble of wave groups. The wave motion may be represented by a continuous superposition of linear waves with random amplitudes and phases each of which moves in (x, k) space subject to the kinematical constraints discussed in the last section and weakly affected by dynamical processes which will be discussed in section 5. It will be shown that a superposition of vertically progressive waves

$$\mathbf{u}(\mathbf{x}, t) = \int d^3k\, a(\mathbf{k})\mathbf{U}(\mathbf{k}) \exp\,[i(\mathbf{k} \cdot \mathbf{x} - \omega t)] + \text{complex conjugate} \qquad (21)$$

adequately describes the state of the wave field away from turning points in the deep ocean. For high-frequency waves in the upper ocean a modal representation seems to be more appropriate. The basic difference lies in the statistical conception associated with these representations. It is reasonable to assume statistical independence of WKB waves with different wave vectors far from reflecting boundaries, that is,

$$\begin{aligned} \langle a(\mathbf{k})a(\mathbf{k}')\rangle &= 0 \\ \langle a(\mathbf{k})a^*(\mathbf{k}')\rangle &= \tfrac{1}{2}E(\mathbf{k})\delta(\mathbf{k} - \mathbf{k}') \end{aligned} \qquad (22)$$

while a modal field of upward and downward propagating waves with the same frequency and horizontal wave vector must have equal amplitude and deterministic phase relation to form the standing mode.

The statistical properties of the wave field are then condensed in the spectrum $E(\mathbf{k})$, which is the density in k space of the total local energy density. The spectrum represents a complete description of the statistical state if the wave field is Gaussian. For the deep-ocean wave field observed during IWEX this was shown by *Briscoe* [1977] to be so 'most of the time, but not always.'

Measurements yield series of data points. The adequate tool for interpretation is spectral analysis, which converts the data to autospectra and cross spectra of frequency or wave number. The modeling of the energy spectrum $E(\mathbf{k})$ from such one-dimensional data spectra is the subject of this section, where the basic relations are inferred by simple reasoning, and the next section, where a more formal approach is introduced which allows a quantitative separation of waves and turbulence in the data. The state of the wave field in the deep ocean (which is defined here as the main thermocline and region below) and the upper ocean (which is defined here as the region above the main thermocline, in particular the seasonal thermocline) will be considered separately.

3.1. *The Wave Field in the Deep Ocean*

Illustrative examples of moored, towed, and dropped autospectra are displayed in Figure 9. Moored spectra generally show significant drops below f and N (Figure 9*a* [from *Cairns and Williams*, 1976]) which suggest some relations of the fluctuations with internal wave kinematics. The energy at the inertial period dominates, followed by a steep decrease with a spectral power law slope of about -2. Dropped spectra (Figure 9*b* [from *Hayes*, 1975]) and towed spectra (Figure 9*c* [from *Katz*, 1975]) decrease with slight changes of the spectral slope. However, they reveal no obvious indication of internal wave kinematics, since there are no natural bounds of wave numbers as in the frequency range. Though moored spectra therefore appear more useful for identifying internal waves, they do not allow a unique identification: fluctuations in the frequency range $f < \omega < N$ may have horizontal and vertical wavelengths which are inconsistent with the dispersion relation. The identification of internal waves from purely spatial information as towed and dropped spectra is hindered by the fact that baroclinicity (measured with towed devices) may also be caused by geostrophically balanced flows of lower frequency, and vertical variations in temperature or current (measured with dropped devices) might likewise correspond to the quasistationary layered fine structure of the ocean. Separation of internal waves from such phenomena requires information linking the structure of the fluctuations in the time and the space domains. This kind of information is contained in the cross spectra (or coherences and phases) relating the time histories of measurements at different times. Many of these measurements have been made in recent years following the pioneering work of *Webster* [1972] and *Siedler* [1971, 1974] with moored sensors separated by a vertical distance (yielding the moored vertical coherence) or by a horizontal distance (yielding the moored horizontal coherence). Whereas coherences from sensors supported by moorings are severely contaminated (this will be discussed below), the floating measurements of *Cairns* [1975] and *Cairns and Williams* [1976] are not (Figure 10). Measurements with time-lagged pairs of dropped devices allowed estimation of the dropped lagged coherence [*Hayes*, 1975]. Also, cross spectra relating simultaneous spatial sections have been published, for example, the towed vertical coherence [*Katz*, 1975] and the dropped horizontal coherence [*Stegen et al.*, 1975].

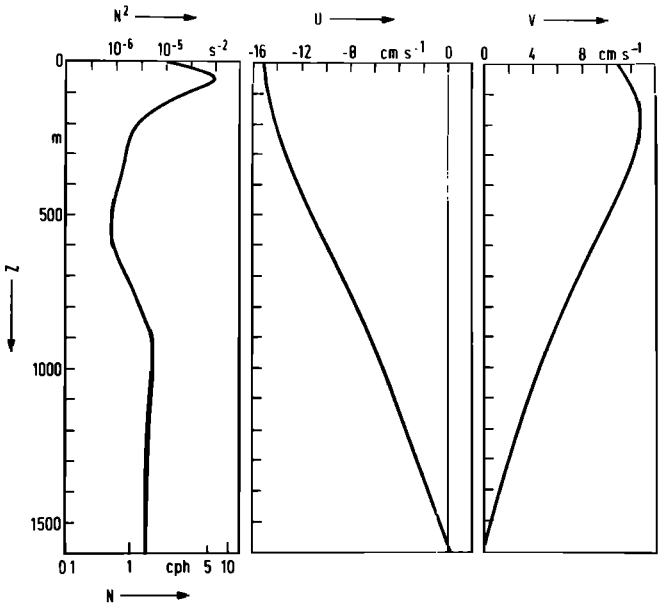

Fig. 8*a*

Fig. 8. Shearless modes and shear modes computed for the mean buoyancy and mean current profiles shown in Figure 8*a*. The dispersion curves (Figure 8*b*) and modes (Figure 8*c*) are computed without the shear current. The dispersion curves of shear modes are shown in Figure 8*d* (upper panel shows downstream waves; lower panel shows upstream waves). The angular dependence of the first mode is displayed in more detail in Figure 8*e*, and the vertical structure in Figure 8*f* [*Peters*, 1980].

Provided that the observed fluctuations are caused merely by internal waves, the relation of all these cross spectra and the energy spectrum $E(\mathbf{k})$ is fairly simple and may be computed from the representation (21) and the statistical properties (22). Thus, for example, the one-sided cross spectrum between moored sensors with separation $\mathbf{r}$ becomes

$$A_{ij}(\mathbf{r}, \omega) = \frac{1}{\pi}\int_{-\infty}^{\infty} d\tau \langle u_i(\mathbf{x}, t) u_j(\mathbf{x} + \mathbf{r}, t + \tau)\rangle \exp(-i\omega\tau)$$

$$= \int d^3k U_i U_j^* E(\mathbf{k}) \delta[\omega - \Omega(\mathbf{k})] \exp(-i\mathbf{k}\cdot\mathbf{r}) \qquad (23)$$

which represents a weighted projection of the spectral density $E(\mathbf{k})$ onto the dispersion surface $\omega = \Omega(\mathbf{k})$. Cross spectra of towed and dropped sensor pairs may be expressed as similar one-dimensional projections. Recovering the complete spectrum $E(\mathbf{k})$ by direct methods (e.g., by Fourier transformation of (23)) appears to be impossible in view of the sparse (in space) data base, so that indirect methods must be employed. The most extensive and far-reaching attempt has been undertaken by Garrett and Munk and published in a series of papers [*Garrett and Munk*, 1972*a*, 1975, 1979] describing the carving of the first coarse model and its subsequent streamlining, which was made possible by the increasing feedback with the experimental endeavor reported above. On the basis of such spectral data obtained at different locations, depths, and times and by different instruments (but nevertheless showing surprising similarities) they proposed a spectral model with the following basic features [*Garrett and Munk*, 1975]: (1) horizontal isotropy, (2) vertical symmetry, (3) horizontal scales of the order of some kilometers and vertical scales down to tens of meters, and (4) a -2 slope in frequency domain with a cuspy increase at the inertial frequency and a -2.5 decrease in wave number. Because of horizontal isotropy and vertical symmetry (which originates from the modal approach of Garrett and Munk) the spectrum is completely specified by its density $E(\alpha, \beta)$ in (α, β) space, where α and β are the moduli of horizontal wave vector and vertical wave number, respectively. Likewise, the densities $E(\alpha, \omega)$ or $E(\beta, \omega)$ may be used. These distributions of energy in wave number–frequency space are displayed in Figure 11. The method of construction from the observations will be described briefly.

The spectrum was factorized in the form

$$E(\alpha, \omega) = \varepsilon B(\omega) A(\alpha, \omega) \qquad (24)$$

where the frequency distribution $B(\omega)$ and the wave number distribution $A(\alpha, \omega)$ of each frequency are normalized so that ε represents the total local energy. The wave number distribution $A(\alpha, \omega)$ was chosen from a simple model class: Garrett and Munk assumed that $A(\alpha, \omega)$ has the same shape at each frequency and only one scale parameter $\alpha_*(\omega)$ characterizing its width. Then

$$A(\alpha, \omega) = A[\alpha/\alpha_*(\omega)]/\alpha_*(\omega) \qquad (25)$$

The second restriction concerns the form of the wave number scale $\alpha_*(\omega)$. Guided by their modal approach, the authors assumed that $\alpha_*(\omega)$ corresponds roughly to a constant mode number ν_* which is obtained if the continuum of the (α, ω)

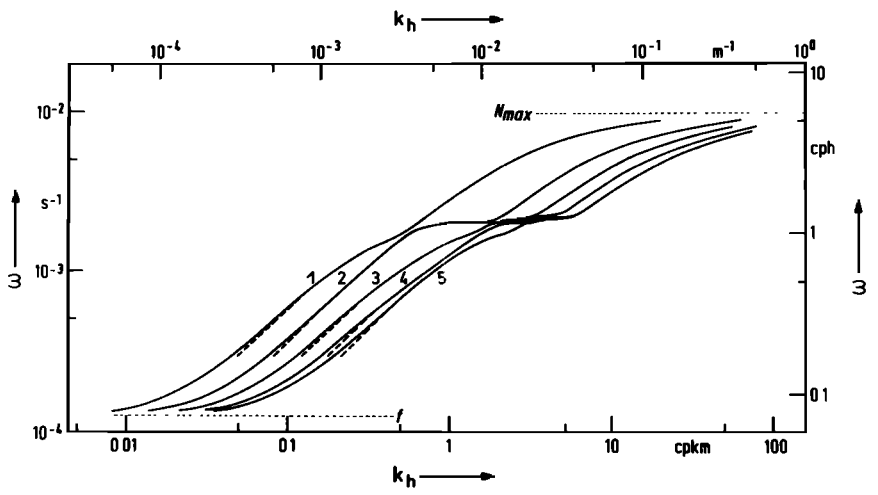

Fig. 8*b*

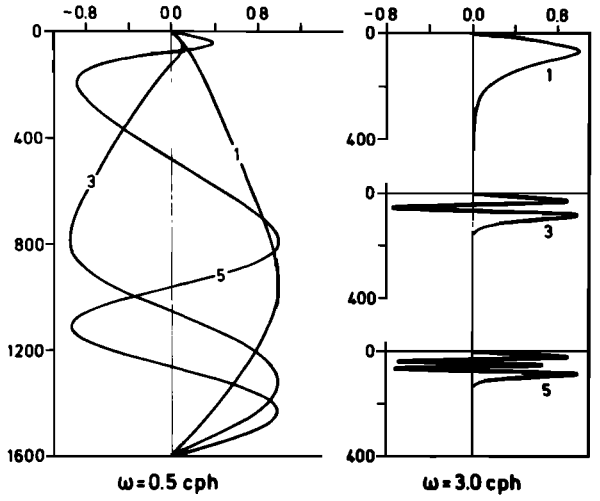

Fig. 8c

domain is resolved in equivalent modes. Solving the modal eigenvalue problem (18) by WKB approximation yields the modal dispersion relation

$$\alpha_\nu \int_{-H}^{0} dz \left(\frac{N^2(z)-\omega^2}{\omega^2-f^2}\right)^{1/2} = \nu\pi \tag{26}$$

relating ω to the discrete wave numbers α_ν, $\nu = 1, 2, \cdots$. Thus a choice

$$\alpha_*(\omega) = (\nu_*\pi/bN_0)(\omega^2 - f^2)^{1/2} \tag{27}$$

corresponds to a constant number ν_* of equivalent modes at low frequencies and therefore also to a scale of the local vertical wave numbers

$$\beta_*(\omega, z) = \frac{\pi}{bN_0}[N^2(z) - \omega^2]^{1/2} \sim \frac{\nu_*\pi N(z)}{bN_0} \tag{28}$$

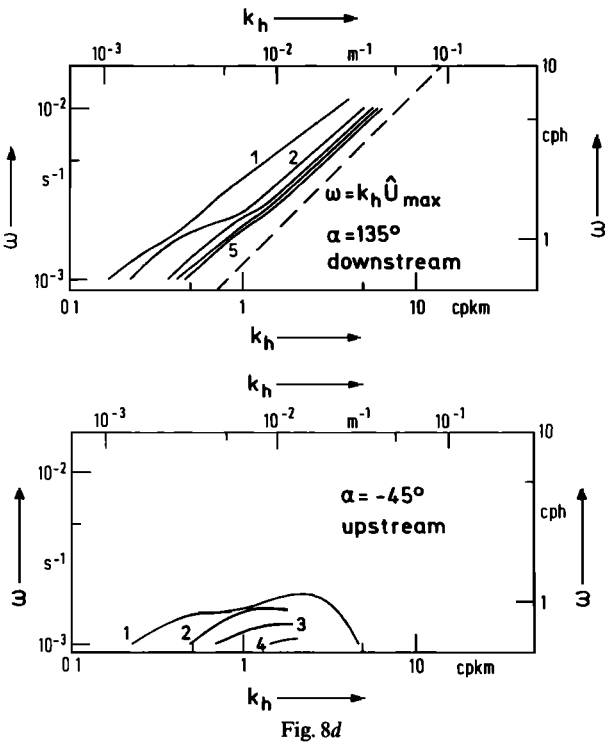

Fig. 8d

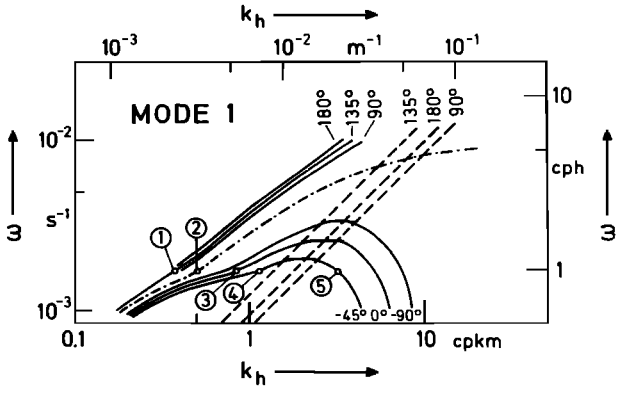

Fig. 8e

which is almost constant for $\omega \ll N$. The scales α_* and β_* are related by the dispersion relation (6) of progressive waves. The parameter

$$bN_0 = \int_{-H}^{0} dz\, N(z)$$

is an integral scale of the stratification. A typical value for the midocean is $bN_0 = 6.5$ m/s with $b = 1300$ m and $N_0 = 5 \times 10^{-3}\,\mathrm{s}^{-1}$.

Though rather restricted, this model proved to embrace the complex structure of the observations. The spectral shape in the frequency domain was inferred from the moored energy spectrum

$$\mathrm{MS}(\omega) = \int_0^\infty d\alpha\, E(\alpha, \omega) = \varepsilon B(\omega) \tag{29}$$

and chosen as

$$B(\omega) = (2/\pi)(f/\omega)(\omega^2 - f^2)^{-1/2} \tag{30}$$

The shape in wave number domain $A(\lambda)$ came from the (one-

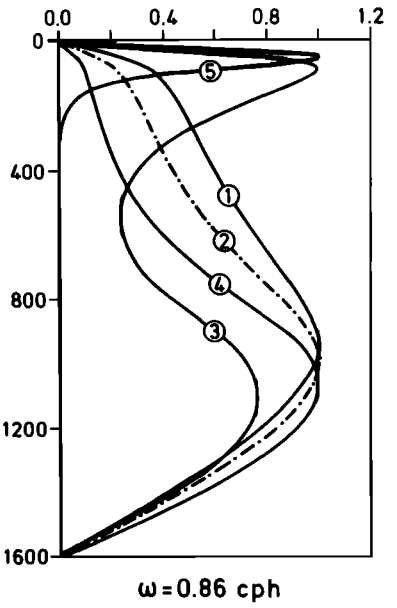

Fig. 8f

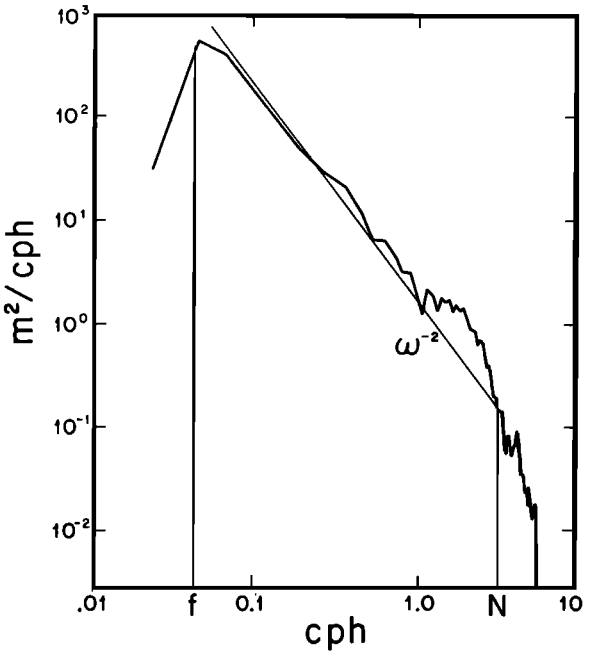

Fig. 9a. Moored vertical displacement spectra [*Cairns*, 1975].

sided) towed and dropped spectra of vertical displacement

$$\mathrm{TS}(k_1) = (2\varepsilon/\pi)\int_f^N d\omega B(\omega)(U_3U_3^*/\omega^2) \cdot \int_{k_1/\alpha_*}^\infty d\lambda\, A(\lambda)(\lambda^2 - k_1^2/\alpha_*^2)^{-1/2} \qquad (31)$$

$$\mathrm{DS}(\beta) = \varepsilon\int_f^N d\omega B(\omega)(U_3U_3^*/\omega^2)A(\beta/\beta_*)$$

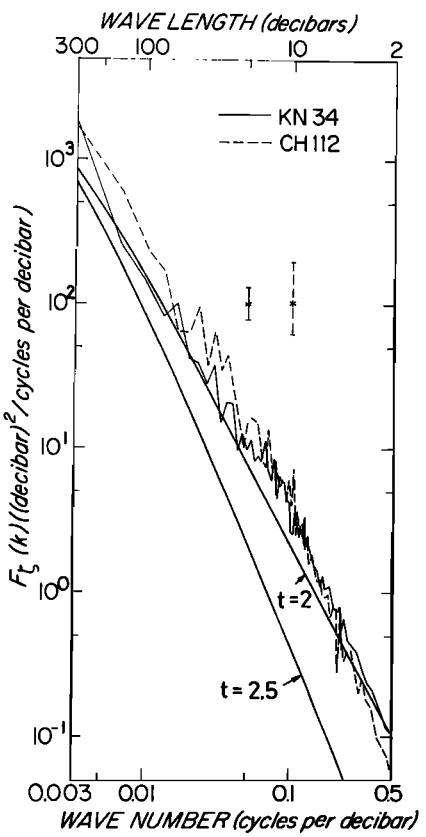

Fig. 9b. Dropped vertical displacement spectra [*Hayes*, 1975].

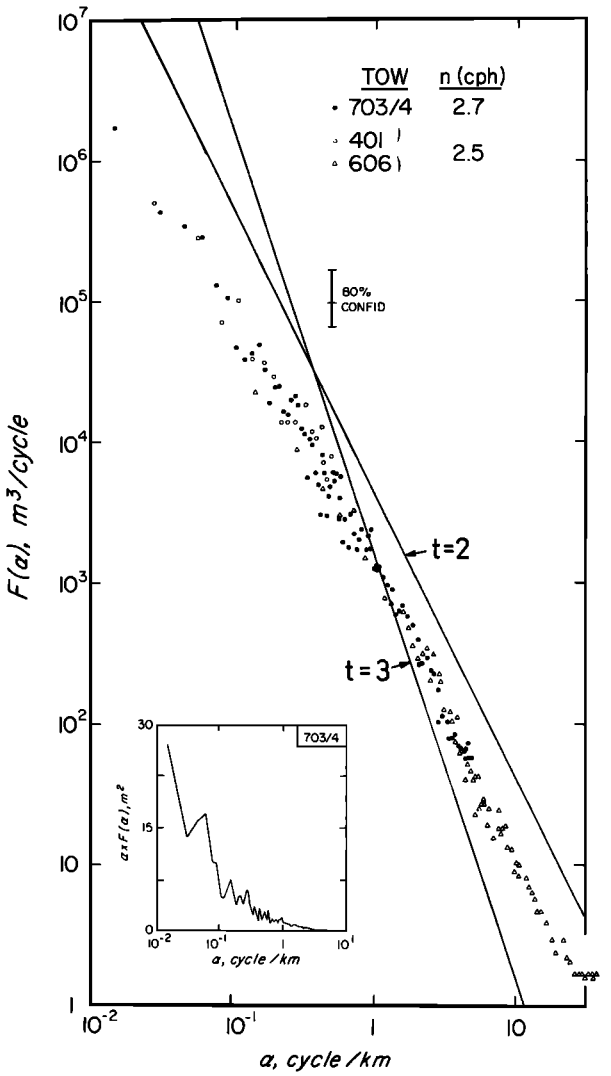

Fig. 9c. Towed vertical displacement spectra [*Katz*, 1975].

If $A(\lambda) \sim \lambda^{-t}$ for $\lambda \gg 1$, then TS $\sim k_1^{-t}$ and DS $\sim \beta^{-t}$ at high wave numbers. A choice

$$A(\lambda) = (t-1)(1+\lambda)^{-t} \qquad (32)$$

with $t = \frac{5}{2}$ thus agrees with observations of TS and DS. The shape of the spectrum is then fixed, and the scale parameters ε and v_* remain to be specified. The form

$$\varepsilon(z) = (\varepsilon_0/N_0)N(z) \qquad (33)$$

with $\varepsilon_0 = 3\ \mathrm{J/m^3}$ agreed with the WKB scaling (14) and (within a factor of 3) with most observed internal wave rms velocities ($\sim$5 cm/s) and rms vertical displacements ($\sim$7 m). The mean square quantities derived from the spectrum are

$$\langle\zeta^2\rangle = \tfrac{1}{2}(\varepsilon_0/N_0)N^{-1}(z)$$
$$\langle u_1^2\rangle = \langle u_2^2\rangle = \tfrac{3}{4}(\varepsilon_0/N_0)N(z) \qquad (34)$$

Integration of (33) yields $b\varepsilon_0$ for the energy per unit surface area, amounting to $4 \times 10^3\ \mathrm{J/m^2}$.

Information on the wave number scale was taken from the moored coherence

$$\mathrm{MC}(\mathbf{r}, \omega) = \int_0^\infty d\lambda\, A(\lambda)J_0(\lambda\alpha_* r_h)\cos(\lambda\beta_*\Delta z) \qquad (35)$$

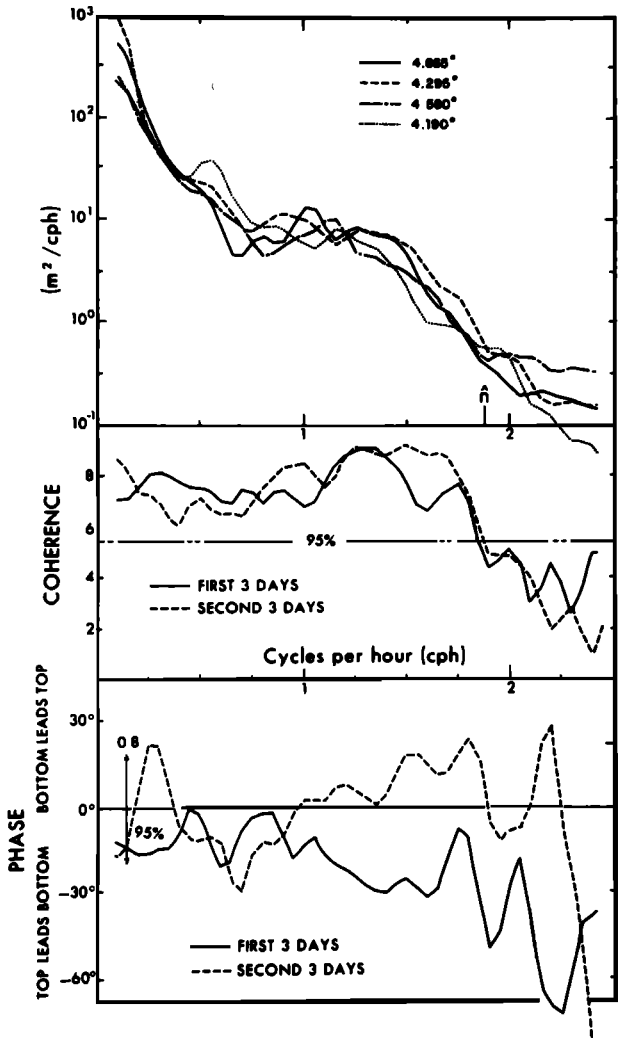

Fig. 10. Spectra and cross spectra of isotherm depth series. Separation of upper and lower isotherm is about 100 m [*Cairns*, 1975].

which reduces to the moored horizontal coherence for pure horizontal separation ($\Delta z = 0$) and to the moored vertical coherence (MVC) for pure vertical separation ($r_h = 0$). In agreement with *Cairn*'s [1975] observation (Figure 10) the moored vertical coherence is independent of frequency for $\omega \ll N$. Estimates of v_* may conveniently be obtained independently from moored vertical and horizontal coherences using relations between v_* and the distance at which the coherences as functions of separation drop below a certain value. Such relations take a simple form if the wave number scale (α_*, β_*, or v_*) is replaced by the bandwidth of the spectral density, which unlike the scale is a parameter characterizing the spectrum independent of its shape. The wave number bandwidth is suitably defined by [*Müller et al.*, 1978]

$$\beta_e(\omega) = \left[\int_0^\infty d\beta\, E(\beta, \omega)\right]^2 \Big/ \int_0^\infty d\beta\, E^2(\beta, \omega) \qquad (36)$$

with the interpretation that a box of width β_e and height $\int E^2\, d\beta / \int E\, d\beta$ (average energy) has the same energy as $E(\beta, \omega)$. For the model (32) one finds

$$\beta_e = \beta_*[2(t-1)]/(t-1)^2$$

The MVC drops below $\frac{1}{2}$ at a separation $\Delta z_{1/2} \sim 2/\beta_e$ rather independently of the shape of $A(\lambda)$. Observations and the slope $t = 2.5$ then yield values for the mode number bandwidth $v_e = \beta_e b N_0/(\pi N)$ of about 10.

Other measurements which did not directly contribute to the construction of the model provided useful checks. Slight modifications were proposed by *Bell* [1976] concerning the shape of the inertial peak and by *Cairns and Williams* [1976] concerning the slope of the wave number density at high wave numbers (they suggest $t = 2$). The wave number distribution (32*a*) was then replaced by

$$A(\lambda) = (2/\pi)(1 + \lambda^2)^{-1} \qquad (37)$$

because of analytical convenience [e.g., *Desaubies*, 1976]. There is an obvious necessity for a spectral cutoff at high wave numbers to avoid an infinite mean shear in the model. Experimental evidence is masked by the presence of fine structure (see section 4). Another modification concerns the behavior of the spectrum in the subbuoyancy range. At frequencies very close to the local turning point $\omega = N(z)$, moored spectra and coherences show a slightly increased level above the expected shape (see, for example, Figures 9 and 10). As demonstrated by *Desaubies* [1975] with solutions in terms of Airy functions this feature can be attributed to local phase coupling between incident and reflected waves near the local buoyancy frequency: here the waves interfere constructively and increase energy and coherence (see also *Munk* [1980]).

This model comprises a considerable amount of internal wave observations, and being able to explain their basic characteristics, it points toward some universality of the spectrum. It has already been noted by *Garrett and Munk* [1972*a*] that measurements of internal waves may be contaminated by Doppler shift, by small-scale turbulence, by mooring motion, and in particular by current and temperature fine structure, which has been studied extensively [*Phillips*, 1971; *Garrett and Munk*, 1971; *McKean*, 1974]. While the use of an inhomogeneous data set and the underlying assumption that all observations may be described by the same universal model allows the determination of the mean wave field and its geophysical variability, the precise local structure and contamination of the measurements cannot be determined. One of the major efforts to overcome this shortcoming of the Garrett and Munk model was the internal wave experiment IWEX performed in 1973 in the Sargasso Sea.

The IWEX experiment consisted of a three-dimensional array of 20 current meter and temperature sensors (to estimate vertical velocity) deployed in the main thermocline with a spatial resolution ranging from 2 m to about 500 m. The array was supported by an extremely stable three-lagged mooring with the form of a tetrahedron (Figure 12). A detailed description of the experiment, the data, and the estimation of cross spectra has been given by *Briscoe* [1975*b*]; the modeling of the spectrum was performed by Müller, Olbers, and Willebrand and presented in a series of papers [*Olbers et al.*, 1976; *Willebrand et al.*, 1977; *Müller et al.*, 1978]. Some features of the IWEX data set will be presented below to illustrate the adequacy and limitations of the conceptions of the Garrett and Munk model about the deep-ocean wave field. A survey of some results of more rigorous modeling follows in the next section.

The discussion will deal with some relations among the components of the moored cross-spectra matrix (23). These relations take a simpler form by transforming from the Cartesian current components (u_1, u_2) to the rotary representation

$$u_\pm = \frac{1}{2^{1/2}}(u_1 \pm i u_2) \qquad (38)$$

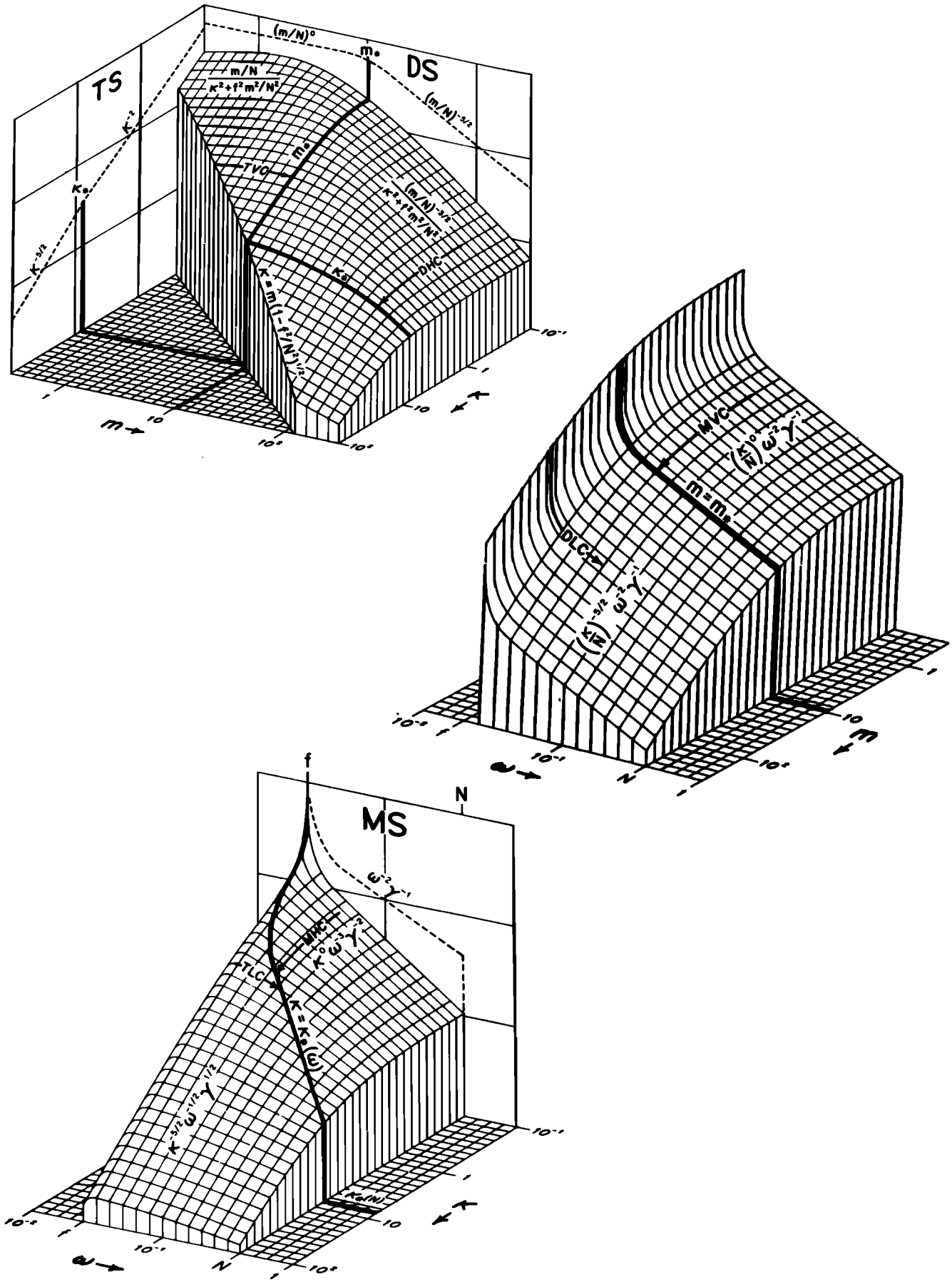

Fig. 11. The Garrett and Munk model for the energy spectrum of internal waves. The upper display is $E(\alpha, \beta)$ in wave number space, the middle and bottom displays are $E(\alpha, \omega)$ and $E(\beta, \omega)$, respectively. Coordinates are dimensionless and plotted logarithmically, so that plane surfaces represent power laws, as designated. The moored spectrum MS is a projection on a vertical plane, as shown in the top right figure, and the towed spectrum TS and dropped spectrum DS are displayed similarly. Coherences (MHC, TLC, $\cdots$) are related to various bandwidths, as indicated [*Garrett and Munk*, 1975]. (In these figures, α is denoted by K and β by m.)

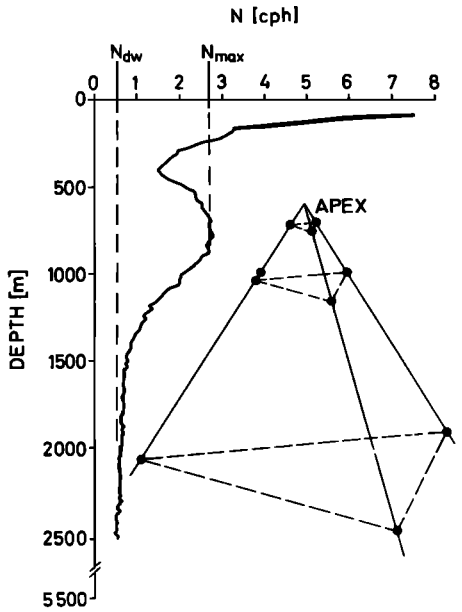

Fig. 12. Profile of buoyancy frequency $N(z)$ at the IWEX site. The geometry of the IWEX array is schematically indicated. Points are instrument positions. Near the apex, 10 more instruments (not shown) are located [*Müller et al.*, 1978].

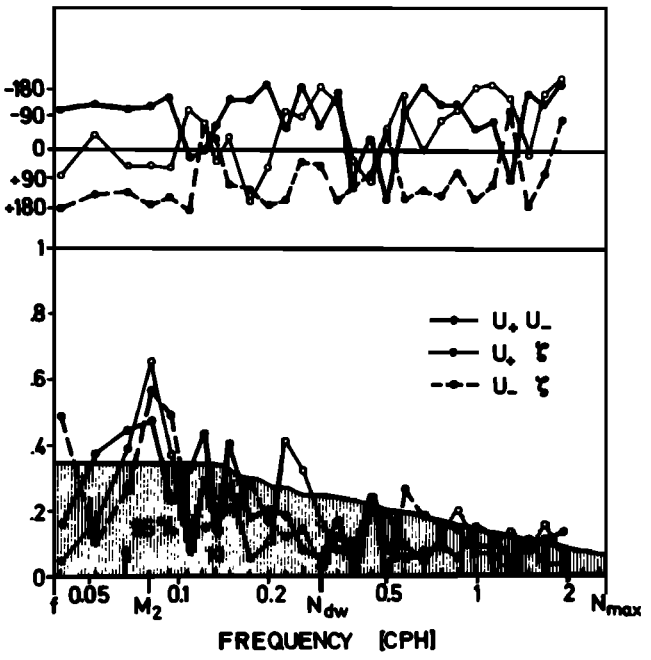

Fig. 13. Coherence and phases between different components of an instrument at 730 m depth [*Müller et al.*, 1978].

The notation of moored rotary spectra will be

$$A_{\mu\nu}(\mathbf{r}, \omega) = P_{\mu\nu}(\mathbf{r}, \omega) - iQ_{\mu\nu}(\mathbf{r}, \omega)$$

$$= \frac{1}{\pi}\int_{-\infty}^{\infty} d\tau \langle u_\mu^*(\mathbf{x}, t) u_\nu(\mathbf{x} + \mathbf{r}; t + \tau)\rangle e^{-i\omega\tau} \qquad (39a)$$

and rotary coherences and phases are defined by

$$\gamma_{\mu\nu}(r, \omega) \exp[i\phi_{\mu\nu}(\mathbf{r}, \omega)] = A_{\mu\nu}(\mathbf{r}, \omega)/\{P_{\mu\mu}(0, \omega)P_{\nu\nu}(0, \omega)\}^{1/2} \qquad (39b)$$

with $\mu, \nu = +, -$ and 3 (occasionally, the vertical displacement will be used). The internal wave model of the moored rotary spectral matrix has the same structure as the Cartesian one. Only the Cartesian polarization vectors must be replaced by the rotary polarizations.

One of the results of the IWEX analysis was that the Garrett and Munk model in fact is basically adequate but gives a rather smoothed picture of the wave field. The local spectrum shows a great deal of variability in wave number–frequency space which is not of statistical origin but must have dynamical reasons. Figure 13 displays the result of a simple test for isotropy and symmetry (both are properties of the Garrett and Munk model) of the wave field. As a property of the cross-spectral matrix (23) of internal waves the coherences γ_{+3} and γ_{-3} vanish at zero separation in the case of symmetry, and γ_{+-} additionally vanishes in the case of isotropy. Indeed, in the wave continuum ($\omega > M_2$, the tidal frequency) all three coherences almost everywhere lie below the 95% confidence limit of zero true coherence. An isotropic and symmetric wave field is here consistent with the data. At low frequencies, however, in particular at the semidiurnal tide M_2, isotropy and symmetry must be rejected. A dominance of downward propagating energy was found. Figure 14 displays the variability of the mode number bandwidth in the frequency domain. Typical values for the 'half coherence separation' $\Delta z_{1/2}$ range from 70 to 140 m for frequencies in the continuum and the inertial frequency, but the tide decreases much more slowly with $\Delta z_{1/2} \sim$ 500 m. Estimates of v_e lie between 10 and 20 in the continuum and at 3 for the tide. Horizontal coherences lead to consistent results. Also, the wave number slope t shows some variability with frequency which, however, is here of the same magnitude as the statistical uncertainty. Moored data are not the appropriate tool for determining t. The procedure is rather indirect and is based on the asymptotic properties of cosine and Hankel transformations which map the wave number spectrum onto

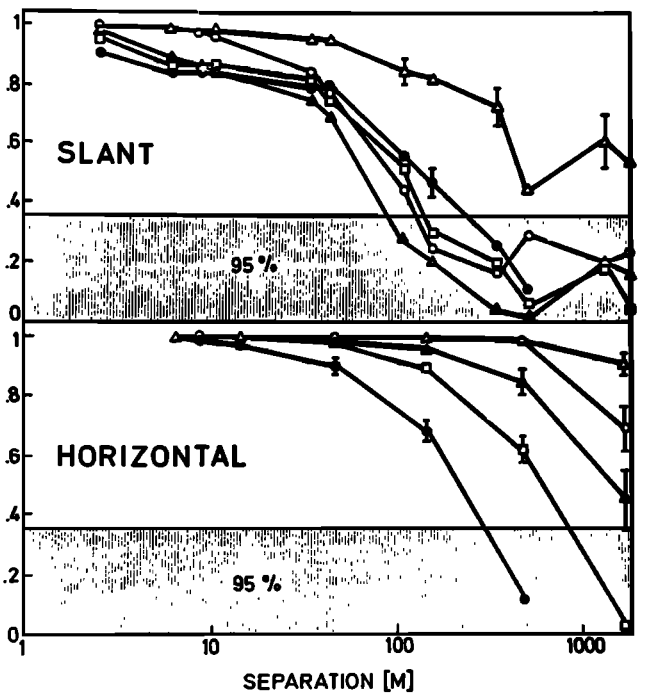

Fig. 14. Slant and horizontal displacement coherences for various frequencies versus separation: inertial (open circles); tidal (open triangles); 5.0 hours (solid triangles); 2.0 hours (open squares); 0.67 hours (solid circles) [*Müller et al.*, 1978].

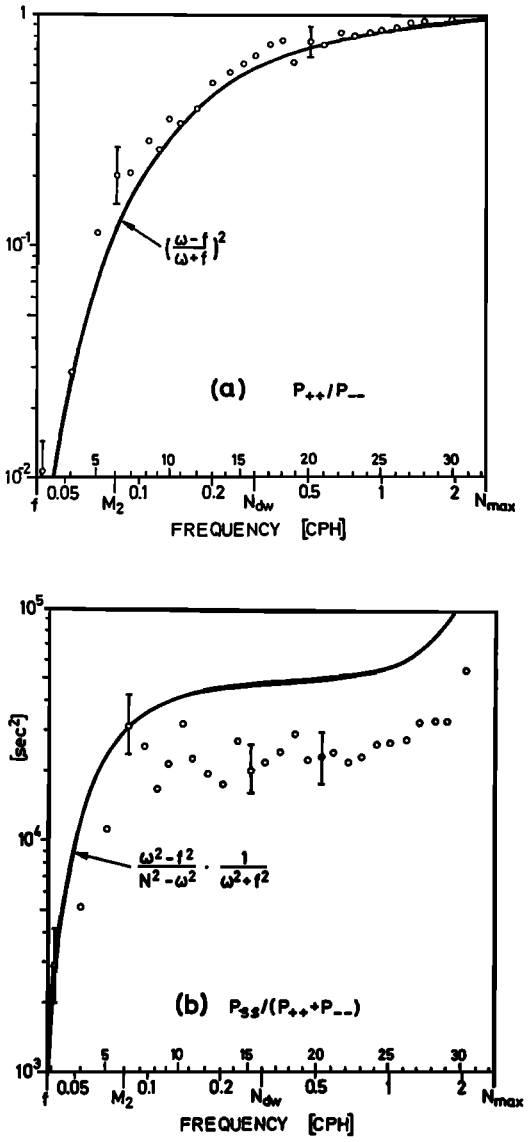

Fig. 15. Internal wave energy tests. (*a*) Observed ratio P_{++}/P_{--} of average rotary spectra and theoretical curve. (*b*) Observed ratio $P_{\zeta\zeta}/(P_{++}+P_{--})$ and theoretical curve [*Müller et al.*, 1978].

the moored coherence (see (35)). If the spectrum behaves as α^{-t} for $\alpha > \alpha_0$, then the moored horizontal coherence becomes

$$\mathrm{MHC}(r_h) = 1 - \text{const}\ (\alpha_0 r_h)^{t-1} + O[(\alpha_0 r_h)^2] \qquad (40)$$

for horizontal separations $r_h \gg \alpha_0^{-1}$. The slope t determined from (40) scatters between 2 and 3, which covers the range obtained from other experiments.

Further disagreements between the IWEX data and the Garrett and Munk model are of a more fundamental nature: the observed fluctuations show small but systematic deviations from internal wave kinematics.

Consider first the question of whether the observed fluctuations are free linear internal waves at all. The simplest way to an answer comes from relations which the autospectra P_{++}, P_{--}, and $P_{\zeta\zeta}$ of the rotary components and vertical displacement must satisfy in the case of internal waves [*Fofonoff*, 1969]. Observed and theoretical ratios (which may be derived from (23)) are shown in Figure 15 for frequencies in the internal wave range. Regarding the ratio P_{++}/P_{--} (Figure 15*a*), the data appear to be consistent with internal waves in the continuum. The violation at $\omega = f$ can be ascribed to the finite frequency resolution of the spectral estimation, while the violation at $\omega = M_2$ points toward a forced or deterministic character of the tidal waves. The observed ratio $\frac{1}{2}N^2P_{\zeta\zeta}/(P_{++}+P_{--})$ of potential to horizontal kinetic energy (Figure 15*b*) lies below the theoretical value almost everywhere in the continuum, and the ratio P_{++}/P_{--} of counterclockwise to clockwise rotating energy lies almost everywhere above. This systematic disparity from internal wave kinematics points toward a complex contamination process.

The coherences also reveal systematic discrepancies. Figure 16 displays some coherences of the same velocity components for slant and horizontal separations. The coherences show a similar monotonic decrease with frequency, but the behavior of horizontal currents and vertical displacements is strikingly different. According to internal wave theory (i.e., the model of the moored cross-spectral matrix) all these coherences should be equal: $\gamma_{++} = \gamma_{--} = \gamma_{33}$, but the last of these equalities is significantly violated. Further details of this coherence disparity may be inferred from Figure 17, showing its spatial structure. Only the horizontal coherences of displacements decrease smoothly; the others show a two-scale behavior: within a few meters they drop rapidly, and for larger separations they decrease similarly to γ_{33} but at a lower level. The simplest model would ascribe the horizontal behavior of γ_{33} to pure internal waves. The other three coherences must then be contaminated by nonwave fluctuations with smaller correlation scales. Since the drop of coherence is larger for slant than for horizontal separations, the contamination is of a rather complex nature. The simplest model bearing physical relevance and leading to

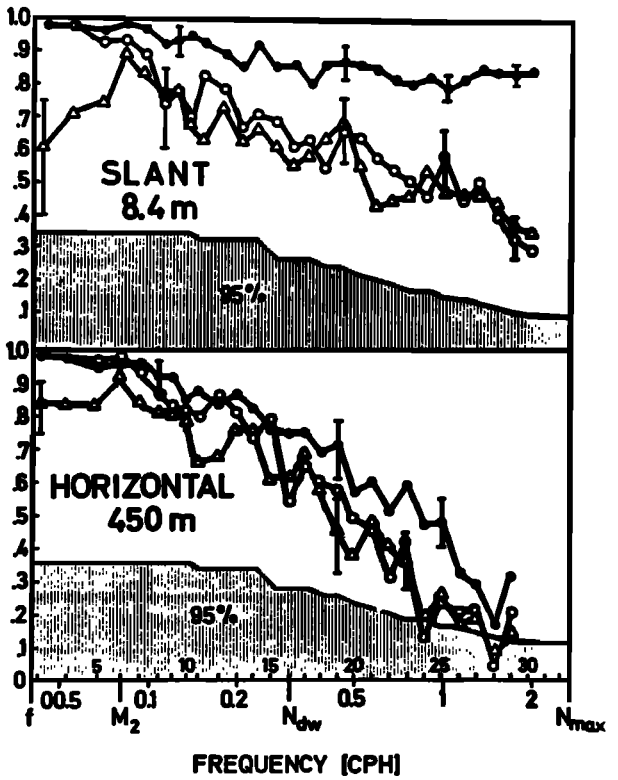

Fig. 16. Observed coherences for a slant and a horizontal separation: γ_{33} (solid circles); γ_{--} (open circles); γ_{++} (triangles). The shaded area indicates the 95% confidence limit for zero coherence. Error bars are rms deviations [*Müller et al.*, 1978].

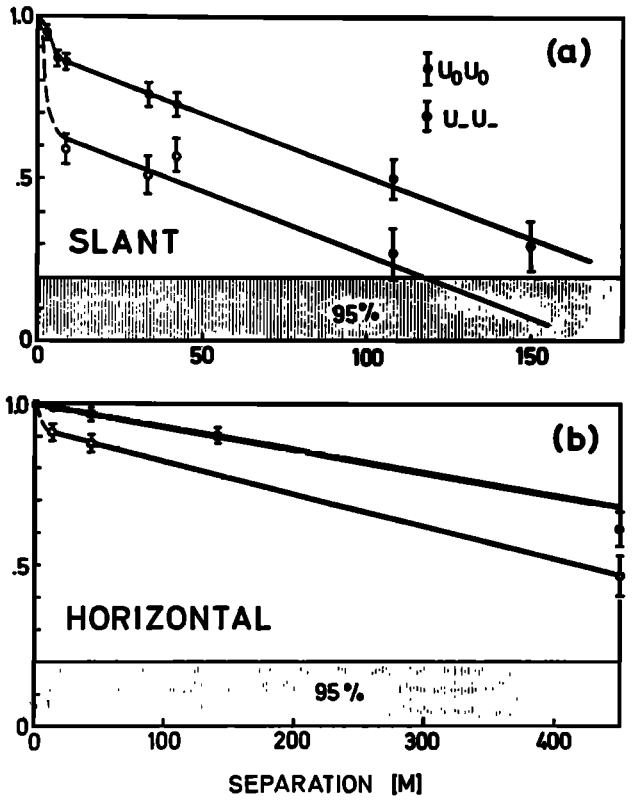

Fig. 17. Observed (*a*) slant and (*b*) horizontal coherence for a period of 1.7 hours versus separation [*Müller et al.*, 1978].

completely consistent data interpretation involves the presence of at least three contaminating fields superimposed on the wave fluctuations. These ideas are discussed in the following paragraphs.

Since vertical displacements are estimated from temperature measurements, the disparity of slant and horizontal displacement coherence is likely to be explained by layered temperature fine structure with small vertical correlation scale (of the order of 2 m) and large (compared to the array dimensions) horizontal correlation scale. Rigorous modeling indeed leads to complete agreement of the fine structure parameters with the contamination model of *McKean* [1974]. Slant and horizontal current coherences are affected differently, and the model proposes a separation of the contaminating agent into a isotropic current field with small correlation scale (less than the smallest separation, ~7 m, actually used) and a layered current field with a correlation pattern similar to the temperature fine structure. This separation allows the interpretation of at least one of these fields as being of a geophysical nature: the layered field may be associated with two-dimensional turbulence advected by a mean current past the current meter. The frequency spectrum obtained by inverse modeling (see section 4) is shown in Figure 29. The isotropic field may be instrumental noise as well as three-dimensional isotropic turbulence confined to homogeneous layers. Neither interpretation is completely convincing: the nonwhite frequency dependence (see Figure 29) does not agree with simple conceptions of instrumental noise; isotropic turbulence would also cause temperature fluctuations, since the layers observed during IWEX are not completely homogeneous [*Hayes et al.*, 1975]. Temperature fluctuations with corresponding magnitude should then contaminate also the displacement coherence at a rate which is not observed.

Apart from some variability in the wave number–frequency domain the mean local IWEX spectrum essentially confirmed (at least for the continuum) the concept of a universal spectrum of deep-ocean internal waves. As *Wunsch* [1975*a*] pointed out, a universal isotropic and symmetric model gives no indication of sources or sinks of energy, 'almost all the physics are ruled out.' To gain insight into the dynamical reasons of the universality, experimenters should look for deviations from this basic state. Observations of temporal and spatial variability of the internal wave spectrum will be considered in section 5.

3.2. *The Wave Field in the Upper Ocean*

A clear picture of upper ocean wave properties has only begun to emerge in recent years. Very few high-quality measurements have been made in the near-surface layers with appropriate space-time resolution. Basic results came from the temperature profiling data of *Pinkel* [1975], collected on the stable platform Flip, and from the line sensor measurements of Soviet scientists [e.g., *Sabinin*, 1973]; a survey has been given by *Brekhovskikh et al.* [1975]. Whereas low-frequency waves seem to agree with the deep-ocean model, both studies suggest that the high-frequency wave field is more intermittent and anisotropic (the waves occur in distinct groups) and has a simpler modal structure. With higher frequency the first mode becomes increasingly prominent. An explanation of these features must include both kinematical and dynamical reasons. Waves of high frequency are trapped in the thin seasonal pycnocline, in which a standing mode structure can be established much more easily than in the diffuse permanent pycnocline. They are in a region of large shear and close to the surface forcing (atmospheric fields and surface waves). The waveguide and the forcing function have substantial space and time variations. Trapping near the surface also may exclude the higher-frequency waves from processes that are responsible for the universal form of the deep-ocean spectrum.

The internal wave experiment performed in 1974 during the GATE field program provided a unique substantiation of the above description of the wave structure in the upper ocean. The experiment consisted of an array of current meters and thermometers covering horizontal scales from a few meters to about 500 m and vertical scales from a few meters down to about 200 m beneath the surface. A summary of the experiment and a discussion of the high-frequency wave field have been given by *Käse and Siedler* [1980]. The variance-conserving plot of the energy spectrum (Figure 18) shows the dominance of waves in three frequency bands: near-inertial waves, tidal waves, and high-frequency waves near 3 cph. The strong deviation of the spectral shape from the deep-ocean universal form is obvious. The peak at 3 cph is far below the local stability frequency (~10 cph) and thus cannot be attributed to constructive interference of waves close to the turning point visible in deep-ocean spectra. These waves of about 20-min period also appear in the isopycnal displacements (Figure 1) measured in the vicinity of the mooring. *Käse and Clarke* [1978] argue that these high-frequency waves trapped in the upper pycnocline are a consequence of the particular stability profile described by a rather narrow pycnocline overlying a thick but weaker stratified layer. In such a waveguide there will appear an accumulation of energy in the pycnocline at the trapped frequencies relative to the 'penetrating' frequencies if the energy input at the surface is smooth in the frequency domain. These trapped waves are highly anisotropic and nonstationary. The latter property is displayed in Figure 19. The first-mode structure has been in-

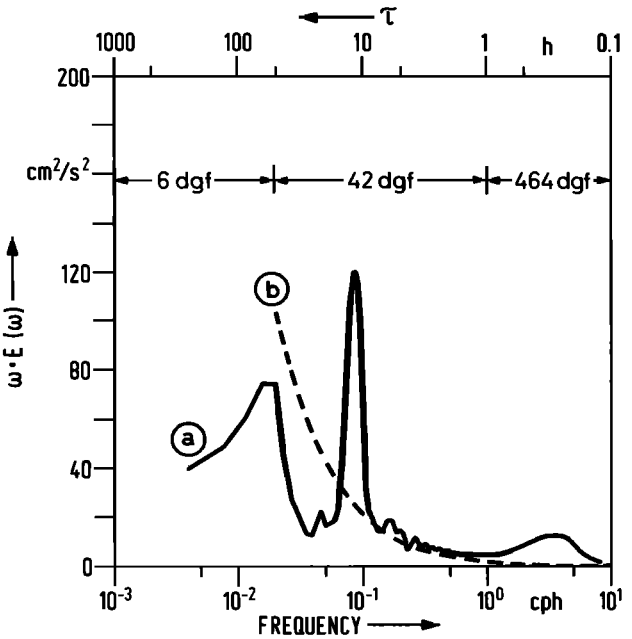

Fig. 18. Variance-preserving presentation of total internal wave energy of the GATE spectrum (curve *a*), and theoretical Garrett-Munk spectrum (curve *b*) with energy in the frequency band 0.1–1 cph equal to that observed in the GATE spectrum (curve *a*) [*Käse and Siedler*, 1980].

ferred from the spatial behavior of normalized displacement cospectra (Figure 20): there is some evidence of an oscillating behavior at higher frequencies which may be attributed to a peak in the wave number distribution at nonzero wave numbers [cf. *Müller et al.*, 1978]. A reciprocal relation similar to that between bandwidth and coherence scale may be used to estimate the peak wave number. Results are inserted in the dispersion curves calculated from the actual N profile at the mooring site (Figure 21). This confirms the presence of first-mode waves with a typical wavelength of 1 km.

Spectral modeling of upper ocean spectra in the spirit of Garrett and Munk is not yet far advanced. *Käse and Clarke*

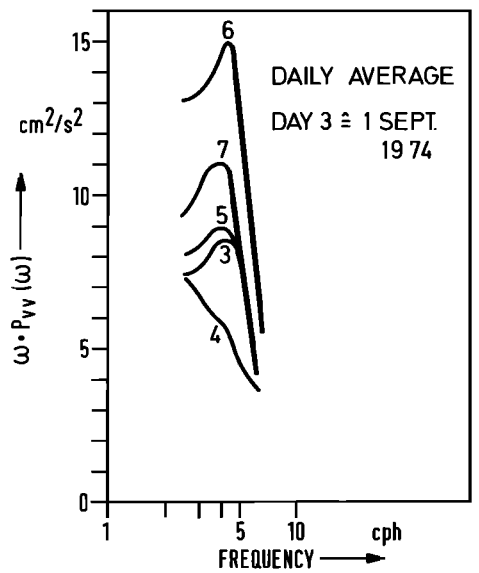

Fig. 19. Variation of high-frequency peak in north component current at 59 m depth [*Käse and Siedler*, 1980].

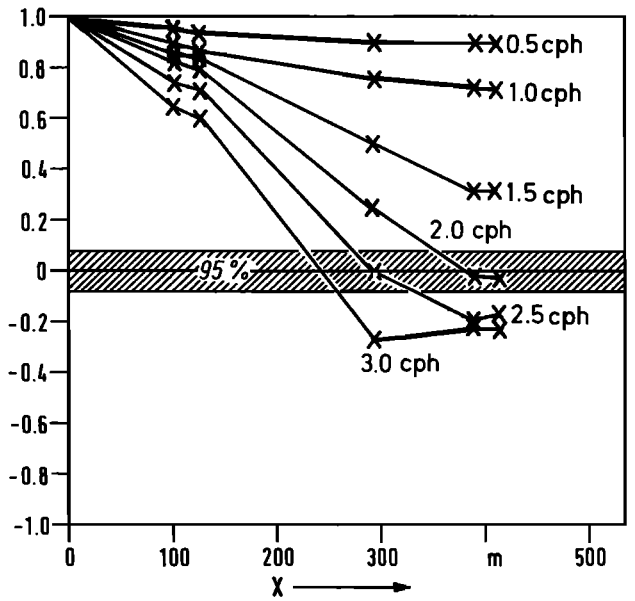

Fig. 20. Normalized temperature cospectrum as a function of separation for different frequencies [*Käse and Siedler*, 1980].

[1978] presented a model of the superenergetic waves at high frequencies which is based on the peculiar response function of the stratification in the upper ocean as described above. *Levine et al.* [1983] applied spectral modeling to temperature and velocity spectra from the Mixed Layer Experiment (MILE), which was performed in the northeast Pacific Ocean. The low-frequency part of the spectra ($0.1 < \omega < 1.0$ cph) could be successfully interpreted by a WKB model, whereas for the high-frequency shoulder in the frequency range $1.0 < \omega < 5.0$

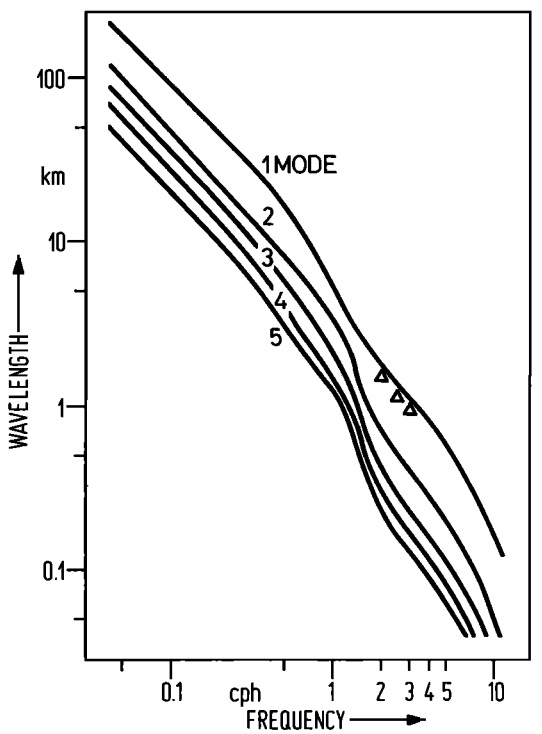

Fig. 21. Dispersion relation of the first five modes. The triangles result from wavelength estimates (4 times the zero crossing distance) of normalized temperature cospectra in Figure 20 [*Käse and Siedler*, 1980].

cph a modal picture was more appropriate. Again the first mode was predominant. *Peters* [1981, 1983] conceived a spectral model based on the shear modes computed from the actual shear current and stratification (c.f. Figure 8). A significant fraction of the observed anisotropy of the wave field could be attributed to the ambient shear. The hump at high frequencies, however, could only be modeled by a corresponding distortion in the wave number distribution. Peters thus concluded that the superenergetic waves are of dynamical origin and are not related to the shear current. *Roth et al.* [1981] attempted by a comparison of various upper ocean spectra to substantiate the idea that the stationary universal Garrett and Munk spectrum is still present in the upper ocean but masked by a variable spectral contribution generated at the surface. Such a concept of separating the spectrum into a locally generated part and a remotely generated part which is in a saturated state was successfully applied by *Fu* [1981] to near-inertial waves (see discussion below).

3.3. *Inertial Waves*

Inertial waves represent a major contribution to the kinetic energy of oceanic motions in the upper and the deep ocean (see, for example, Figure 5). Considerable experimental effort has been spent to establish their basic structure, namely, the clockwise (in the northern hemisphere) rotation of the horizontal current vector with time, a dominant frequency which is slightly larger than the local inertial frequency [e.g., *Day and Webster*, 1965; *Schott*, 1971; *Pollard*, 1980], upward propagation of phase and thus downward energy flux [e.g., *Sanford*, 1975; *Kundu*, 1976; *Leaman*, 1976; *Käse and Olbers*, 1980; *Pollard*, 1980], and clockwise turning of the velocity vector with increasing depth [e.g., *Kundu*, 1976]. These features were also found in the IWEX spectrum [*Müller et al.*, 1978].

An extensive description of the spectral properties of inertial waves away from horizontal and vertical boundaries has recently been presented by *Fu* [1981]. This work uses data from Polymode arrays [*U.S. Polymode Organizing Committee*, 1976], which provided an excellent data base for the study of inertial waves because of the large regional covering (subtropical to temperate latitudes in the western North Atlantic) and the long duration of the observations (at least 9 months at each mooring site). In most of the data there is a prominent peak at frequencies slightly exceeding f, but a universal frequency spectrum close to f does not exist. The parameters characterizing the level and shape of the inertial peak vary substantially with latitude and environmental oceanic conditions. The peak height (measured by the ratio of the peak level to a power law extension from the higher frequencies in the internal wave band) shows large values close to potential sources of inertial waves (near the Mid-Atlantic ridge, at depths less than 2000 m, in the deep ocean over rough topography, and under the Gulf Stream) as compared to regions which are supposed to be dynamically inactive (the deep ocean over smooth topography). The bandwidth of the peak decreases with increasing latitude; the peak frequency seems to be inversely correlated to the peak height. The horizontal coherence scale decreases with depth, and the vertical coherence scale shows an opposite behavior. Further, the vertical structure of the wave field changes from downward energy propagation in the lower thermocline to standing wave properties in the deep water.

Most of these findings could be modeled by a superposition of a remotely generated contribution and a locally generated contribution to the inertial peak. Waves which are generated closer to the equator and propagate poleward approach their turning latitudes to form here part of the inertial wave field. This global wave field is identified with the observations in dynamically inactive regions. A model based on latitudinal Airy solution [*Munk and Phillips*, 1968] and the frequency–wave number model of Garrett and Munk at lower latitudes is able to reproduce the main features of the global part: the magnitude of the peak height, the latitudinal dependence of the bandwidth, and the correlation of the blue shift with the height of the peak. Figure 22 gives an impression of the success of the model. The excess of inertial energy above the spectral level of the global model is interpreted as the result of the local forcing. This contribution then is responsible for the enhanced peaks and the downward propagation of energy in the observations above 2000 m.

4. SEPARATION OF WAVES AND TURBULENCE

A separation of oceanic motions into wavelike modes of motion and nonwavelike modes (generally named turbulence) turned out to be an extremely fruitful concept both from a descriptive and from a theoretical point of view. In a wave field, Fourier components in the wave number–frequency space (wave components) obey a dispersion relation, and therefore wavelike disturbances (and energy) propagate through the background medium relative to the mean flow with the appropriate group velocity. In a turbulent flow there is no unique dispersion relation, and turbulent disturbances are an advected feature rather than a propagating one. Wave components interact in a weakly nonlinear way under the restriction of resonance, while in a turbulent flow all Fourier components are coupled and may interact strongly. This different behavior is a consequence of the relative importance of the nonlinear inertia terms in the governing equations of the motion: the notion of a wave implies an essentially linear phenomenon, and a turbulent flow is a nonlinear one.

In practice, a distinction between internal waves and turbulence may be extremely difficult, since the transition between the wavelike regime and the turbulent regime is continuous and a wide range of graduations may occur in nature. The modes are coupled dynamically and modify each other. Further, both types of motion coexist in the physical space and therefore contribute to the signal recorded by a measuring device. They also overlap in the Fourier space-time domain either through their kinematics or because of aliasing, Doppler shifting, or dynamical coupling. Spectral analysis is thus not sufficient for separating the different modes of motion. Besides contributions of geophysical origin a measured signal may also contain instrumental noise. To identify internal waves in the ocean therefore requires carefully designed experiments and elaborate techniques of data interpretation.

4.1. *Towed and Dropped Measurements*

To decide whether towed or dropped data contain contributions from internal waves is a difficult taks. A very plausible conception was exploited by *Woods and Minnett* [1979] to filter out internal waves from Batfish data: assuming that the waves have only negligible displacements with very small vertical wavelengths, the variability in the separation of two closely neighboring density surfaces must essentially be due to nonwave motion (though each individual isopycnal may be undulated by the long waves).

In recent years, considerable attention has been focused on the interrelation and separation of internal waves and fine

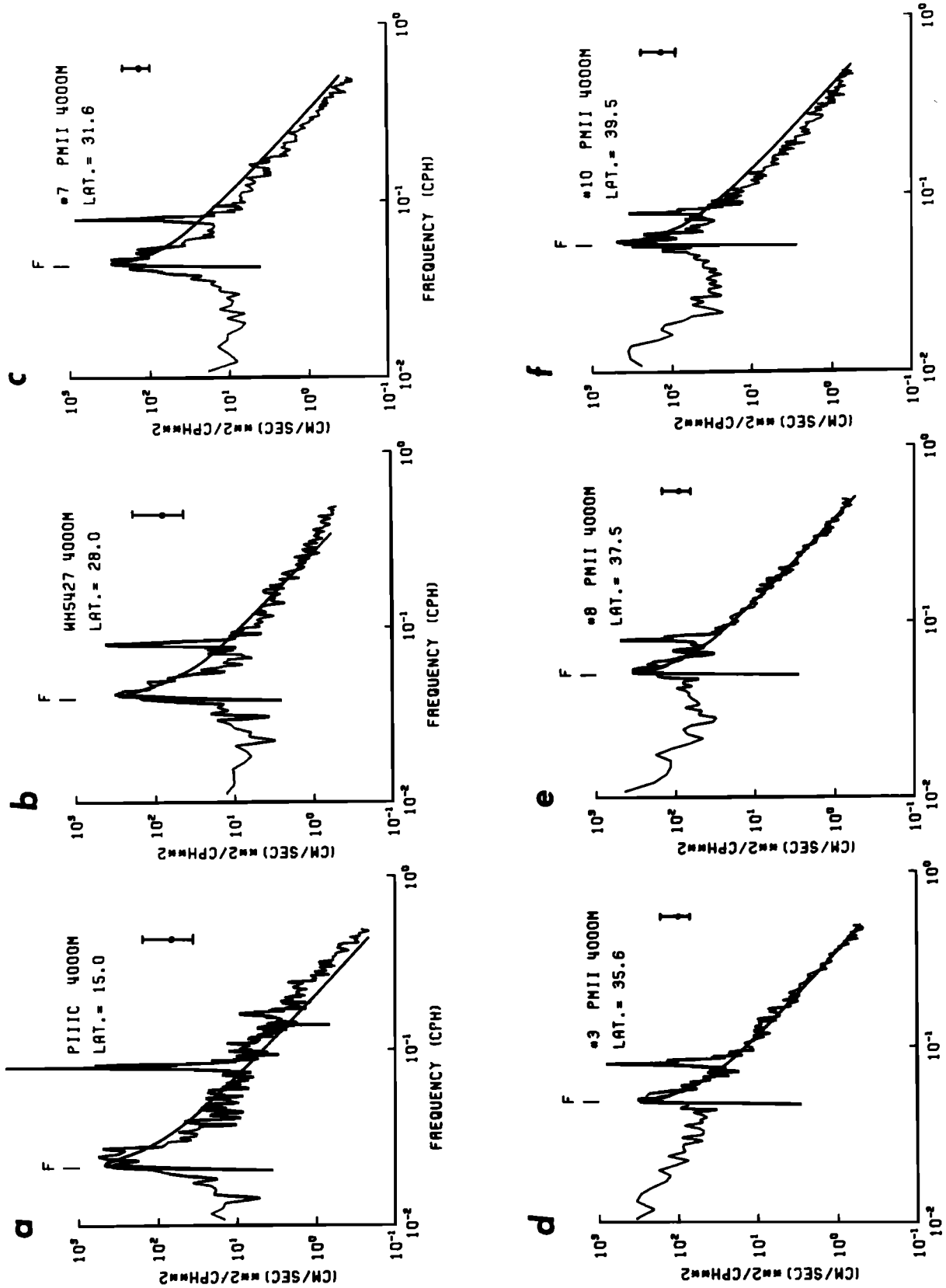

Fig. 22. Observed normalized spectra of the horizontal kinetic energy at 4000 m depth and the global inertial wave model (smooth curve) at various latitudes [*Fu*, 1981].

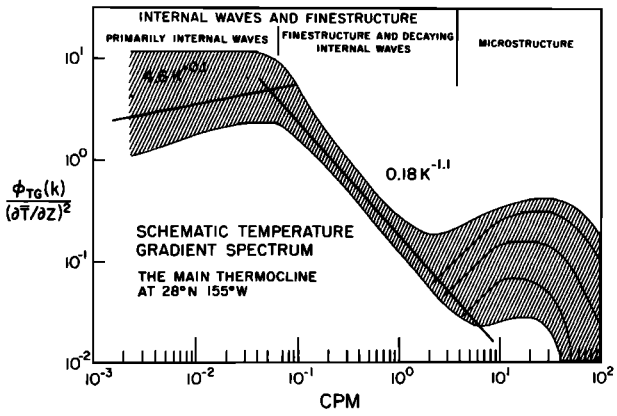

Fig. 23. Schematic temperature gradient spectra. These levels represent spectra that have been averaged vertically over 100 m or more. Spectra averaged over shorter vertical intervals exhibit much more variation in the microstructure range [*Gregg*, 1977].

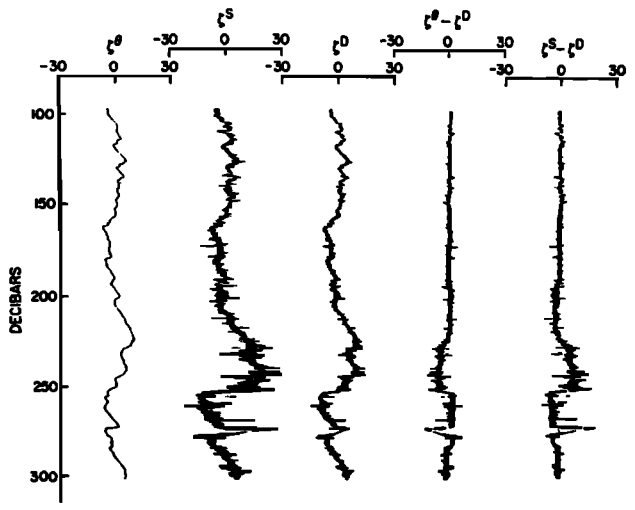

Fig. 24. Displacement profiles from temperature, salinity, and density profiles [*Johnson et al.*, 1978].

structure appearing in any continuous profile of temperature in the ocean. Fine structure may be due to the straining of an otherwise smooth profile $T_0(z)$ by the shear of internal waves with short vertical wavelengths [e.g., *Garrett*, 1973]. If the vertical displacements of internal waves are $\zeta(z)$, the actually observed profile would be

$$T(z) = T_0[z - \zeta(z')] \tag{41a}$$

where z' is implicitly given by

$$z' + \zeta(z') = z \tag{41b}$$

This contribution to the structure at small scales is reversible. An irreversible contribution originates from internal wave breaking which mixes small fractions of the water column [e.g., *Garrett and Munk*, 1972*b*].

Gregg [1977] reported evidence for a change in the spectral slope of vertical temperature profiles at a scale of approximately 10 m. A schematic spectrum of the temperature gradient is given in Figure 23. It is intriguing to ascribe the variance at wave numbers less than 0.1 cpm (where the slope is nearly -2) to internal waves and the variance at higher wave numbers (where the slope is about -3) to irreversible fine structure. Since the wave spectrum must roll off somewhere at high wave numbers faster than -3 to have a finite mean wave shear, the above interpretation is far from being rigorous. Indeed, *Desaubies and Gregg* [1981] presented a model of reversible temperature fine structure down to scales of 2 m. The model is based on the nonlinear heat conservation equation (41) and a Gaussian wave field with a Garrett and Munk spectrum with wave number slope -2. The model reproduces remarkably well the skewed distribution of the observed temperature gradients for scales larger than 2 m. The failure at smaller scales may be due to increasing contribution in the profiles from irreversible processes. Another approach to identify wave-induced fine structure has been reported by *Johnson et al.* [1978], who used conservation of heat, salt, and (in situ) density in the form of (41) to determine from each of these profiles the corresponding displacements (the smooth equilibrium profiles were defined as suitable spatial averages). These are displayed together with their differences in Figure 24. The striking similarity above 230 m supports the concept of wave straining; below, significant differences occur which must be attributed to irreversible effects (the spikes in the profiles at 275 m are due to a data gap).

Spectra of velocity which cover such a broad wave number range as temperature spectra are difficult to obtain. Recently, *Gargett et al.* [1981] have put together a composite velocity shear spectrum from three different velocity profilers (Figure 25). The similarity with the temperature gradient spectrum in Figure 23 is striking. Transition wave numbers as well as slopes agree remarkably. Still, a separation into waves and turbulence according to these transitions is overly simplistic as explained above.

4.2. *Moored Measurements*

A unique identification of internal waves can only be achieved if data allow verification (direct or indirect) of the dispersion relation. Measurements with moored arrays are suited to this purpose. Spectral analysis of moored data naturally filters out much of the nonwave energy because internal waves only exist in a well-defined frequency range (forgetting about Doppler shift). But the analysis of IWEX showed that even spectra of moored data contain significant contributions from other modes of motion. Certainly, the somewhat qualitative arguments about the energy and coherence disparities given in the last section of the basis of a tiny percentage of the data set need to be substantiated by techniques which allow a consistent and concise interpretation of all data. In general, this poses

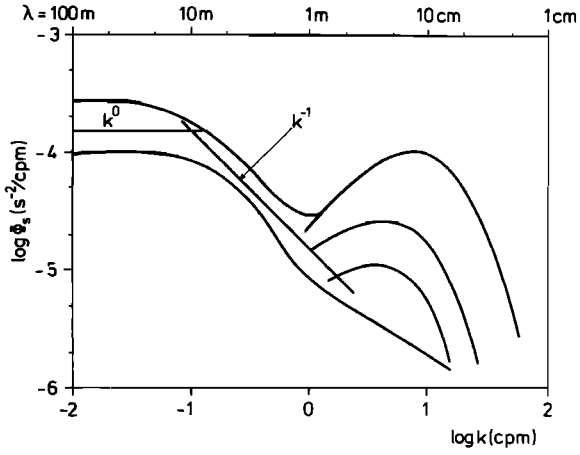

Fig. 25. Schematic vertical wave number spectrum of vertical velocity shear [*Gargett et al.*, 1981].

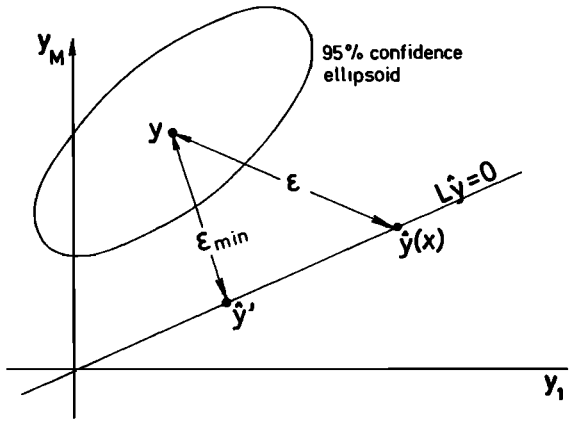

Fig. 26. Schematic graph of data, model point, and model constraints in cross-spectral space [*Müller et al.*, 1978].

computational problems for the large amount of data involved in geophysical experiments. Two methods have shown some success in testing for the presence of a particular mode of motion in field data and possibly extracting the corresponding spectral energy. Consistency tests provide a tool to test a general hypothesis concerning the kinematical structure of the observed fluctuations. Model fitting by a least squares technique is used to construct a parameterized model for the observations. These techniques will be described and illustrated with IWEX results.

The setup of the techniques is displayed in Figure 26. A data set (in our case the set of all cross spectra) consisting of data Y_m ($m = 1, \cdots, M$) may be regarded as a point in an M-dimensional space embedded in its (say) 95% confidence region. A model point ($\hat{Y}_1, \cdots, \hat{Y}_M$) computed by some sort of algorithm will be accepted as being consistent with the data if both points coincide within the confidence limits. An appropriate statistic is the squared distance

$$\varepsilon^2 = \sum_{m,n}(Y_m - \hat{Y}_m)W_{mn}(Y_n - \hat{Y}_n) \qquad (42)$$

where W is a weight matrix (or metric) in the data space. In practice, the data are Gaussian, and ε^2 follows a χ^2 distribution with degrees of freedom depending upon the choice of the metric W_{mn}. Following the maximum likelihood principle, this should be the inverse data covariance matrix. This is impractical because of data correlations or large M. Another choice is discussed by *Müller et al.* [1978] and *Willebrand et al.* [1977]. The rejection (or acceptance) of a model is then reduced to a simple χ^2 test.

The algorithm for computing a model point may require major numerical evaluations as in the case of the internal wave model (23) for the moored cross spectra. Before applying the above χ^2 test to such a model one should look for tests which do not depend on the specific value of the data point but rather on the kinematical structure of the model. For isotropic turbulence, for example, there must be equality of the autospectra of the three current components. Kinematical relations between potential and kinetic energy of internal waves or between the rotary coherences have been mentioned in the last section. A complete set of such consistency relations for vertically progressive or modal internal waves has been worked out by *Müller and Siedler* [1976]. Consistency relations can formally be written as linear constraints

$$\sum_m L_{rm}Y_m = 0 \qquad (r = 1, \cdots, R) \qquad (43)$$

indicating a restriction of the model on an R-dimensional hyperplane in the data space (this restriction may be quite strong: for example, an isotropic and symmetric field of vertically progressive internal waves must satisfy $R = 854$ relations among the $M = 1444$ cross spectra which were used in the analysis). Obviously, the model must be rejected if this hyperplane does not intersect the confidence region. A suitable statistic is the squared minimum distance $\varepsilon_{min}{}^2$ between the data point and the hyperplane, which follows a χ^2 distribution with R degrees of freedom. The distance ε^2 is independent of a specific model value, and thus the consistency tests are computationally simple. Examples of consistency tests applied to the IWEX data are given in Figure 27. The statistic $\varepsilon_{min}{}^2$ (normalized by its expectation value) is displayed versus frequency. The hatched line is the 95% confidence limit.

Consider first the assumptions of the Garrett and Munk model: horizontal homogeneity and isotropy, vertical symmetry, vertically progressive internal waves, and WKB scaling. Figure 27*a* demonstrates that these assumptions cannot be accepted. Strong rejections occur at the tidal and at high frequencies. The model must also be rejected at medium frequencies, since the statistic does not scatter randomly about the expectation value. Tests of particular properties of the model are displayed in the next three figures. Homogeneity and WKB scaling (with the actual N profile) may be accepted with the exception of high frequencies. This presumably is due to the proximity of the turning point. Horizontal isotropy (and vertical symmetry, which is not shown) can be accepted at medium frequencies. The field is strongly anisotropic and asymmetric at low frequencies and slightly so at high frequencies. The consistency relations for propagating waves are strongly violated at the tidal and at high frequencies and slightly so at medium frequencies. The violation is mainly due to the energy and coherence disparities demonstrated in the examples in Figures 15 and 16. This conclusion may be drawn from Figure 27*e*, which shows only those tests for propagating waves which discriminate between these and standing modes. Here the disparities do not enter because standing modes need not satisfy the corresponding tests. The remaining (discriminating) tests are better satisfied by the modes, particularly at high frequencies. To conclude, however, that modes provide an adequate model is overhasty (this shows the limitations of tests which constrain only a fraction of the data), since a modal model cannot remove the energy and coherence disparities and simultaneously reproduce the observed coherence scales: the drop of the vertical coherence within about 100 m requires excitaton of many modes, but such a modal field must satisfy the energy and coherence tests on the average (not strictly, but a systematic violation cannot occur).

Internal waves, either propagating or standing modes, will be unable to model the observations consistently because they cannot cover the disparities. It is informative to compare the pure propagating wave model (Figure 27*d*) with the contamination model inferred by simple reasoning from the disparity structure (see section 3). Addition of temperature fine structure and the layered and isotropic turbulence contributions to the waves still leaves a considerable amount of constraints among the data (there are 224 relations among the 1444 cross spectra). Figure 27*f* shows that this wave turbulence model may provide a consistent description (except for turning point problems).

It must be remembered that consistency tests check only some specific aspects of the data and that there are other (untested) features which decide whether or not the model point

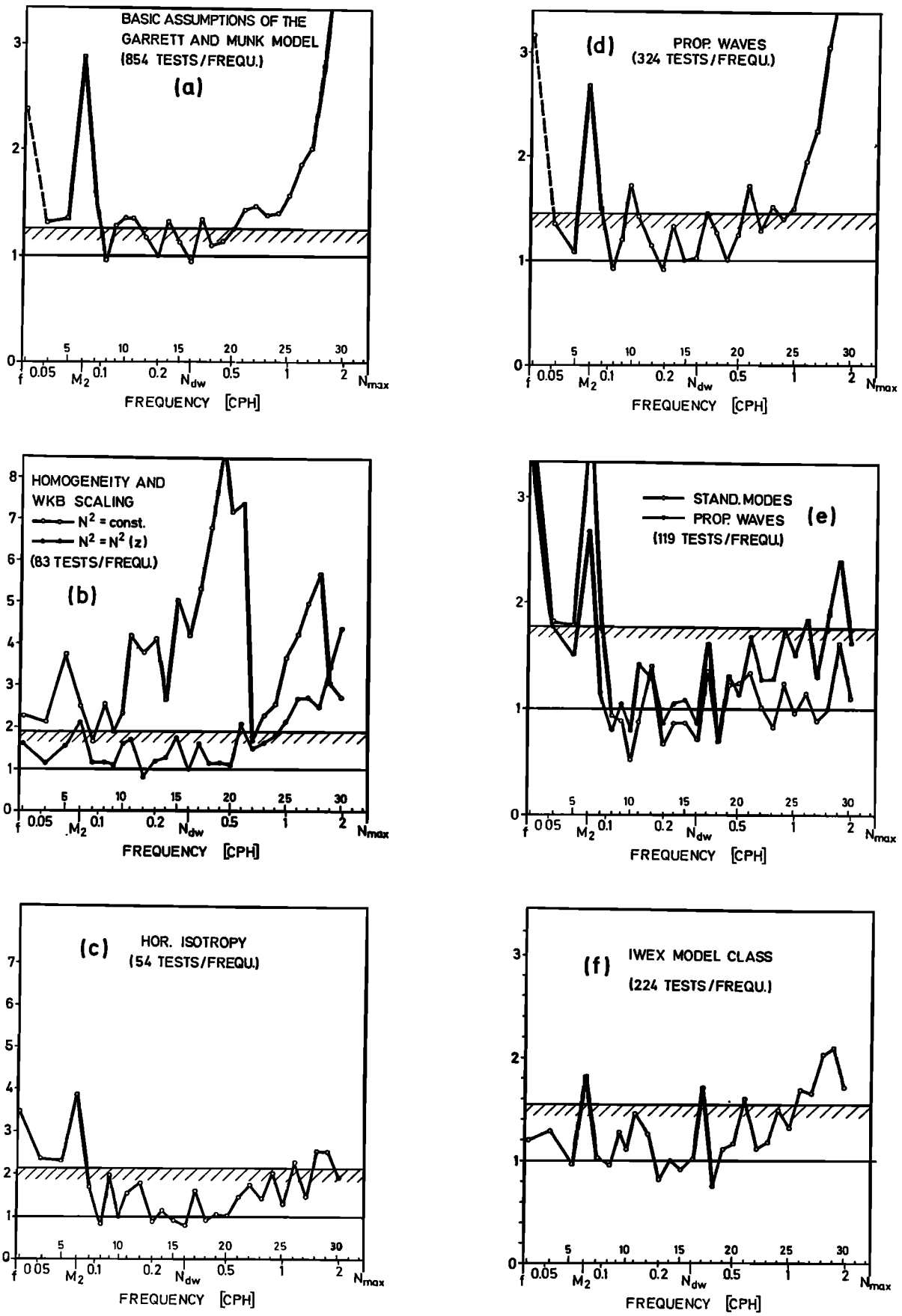

Fig. 27. Consistency tests for the model classes indicated. The normalized statistic ε_{min}^2 is displayed versus frequency (notice the different ordinate scales). If the value exceeds the 95% confidence limit (hatched line), the corresponding model is rejected. Values at the inertial frequency are not always reliable because of finite frequency resolution [*Müller et al.*, 1978].

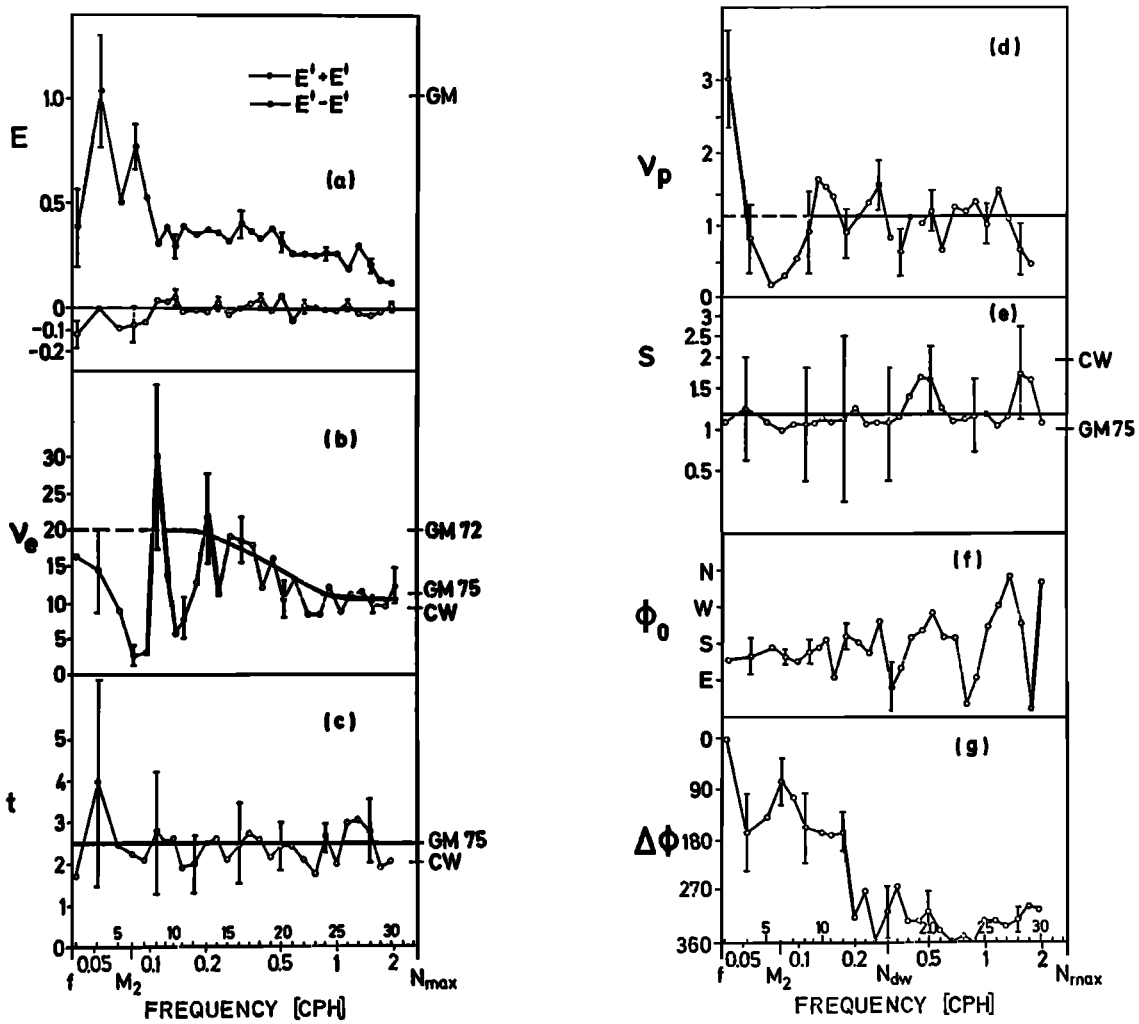

Fig. 28. Parameters of IWEX model versus frequency. Solid curves indicate parameterizations of frequency dependence. The values proposed by *Garrett and Munk* [1972*a*, 1975] and *Cairns and Williams* [1976] are indicated on the right vertical axis (they apply to the entire frequency range). The total wave energy and energy asymmetry are scaled by the frequency distribution $B(\omega)$ [*Müller et al.*, 1978].

on the constraining hyperplane may be chosen within the confidence region. The modeling is conveniently performed by a least squares fit procedure. The model is parameterized in terms of parameters $x_1, \cdots, x_P$ (generally $P \ll M$). The model point which minimizes the squared distance $\varepsilon^2(x_1, \cdots, x_P)$ is the one that most likely lies within the confidence region of the data point. Because the parameterization may be highly nonlinear (for example, as the dependence of the Garrett and Munk model on v_e and t), the condition $\varepsilon^2\ (x_1, \cdots, x_P) = \min$ is conveniently solved by a linearized iteration procedure. The parameters, their variances, and correlations are then computed by linear matrix algebra. The results of the IWEX wave turbulence model are displayed in Figures 28 and 29.

The conception and parameterization of the IWEX model were chosen to be slightly more general than the Garrett and Munk model. Asymmetry between upward ($E\uparrow$) and downward ($E\downarrow$) propagating spectral energy was incorporated as well as horizontal anisotropy. The shape of the wave number distribution allows for a peak at a nonzero wave number. The panels of Figure 28 show the total energy $E\uparrow + E\downarrow$ and the asymmetry $E\uparrow + E\downarrow$ (Figure 28*a*), both scaled by the frequency distribution $\varepsilon B(\omega)$ of the Garrett and Munk model with $\varepsilon = 4 \times 10^3$ J/m^2; the equivalent mode number bandwidth v_e (Figure 28*b*); the slope t at high wave numbers (Figure 28*c*); the mode number v_p of low wave number peak (Figure 28*d*); a peak shape parameter (for $s = 1$ the shape of the Garrett and Munk model (32) is recovered, for $s \sim \infty$ the peak flattens to a plateau) (Figure 28*e*); the dominant propagation direction ϕ_0 (Figure 28*f*); and the beamwidth $\Delta\phi$ of the horizontal directional distribution (Figure 28*g*). In most respects the result confirms the model of Garrett and Munk displayed in Figure 11. Significant deviations occur mainly at low frequencies, in particular at the inertial frequency, the tide, and its harmonics, where the wave field is anisotropic and asymmetric (there is an excess of about 20% of downward propagating energy).

The decontaminated wave spectra of displacement and horizontal kinetic energy are shown in Figure 29 together with the spectra of nonwave contributions. At high frequencies the temperature fine structure contamination agrees fairly well with a theoretical model of *McKean* [1974] which predicts a $-\frac{3}{2}$ decrease below the buoyancy frequency. The parameters determining the level of this model spectrum have been taken from the fine structure analysis of *Joyce and Desaubies* [1977] of IWEX data. The difficulty in interpreting the current contaminations has been discussed in section 3. The interpretation of the three-dimensional contamination as small-scale, over-

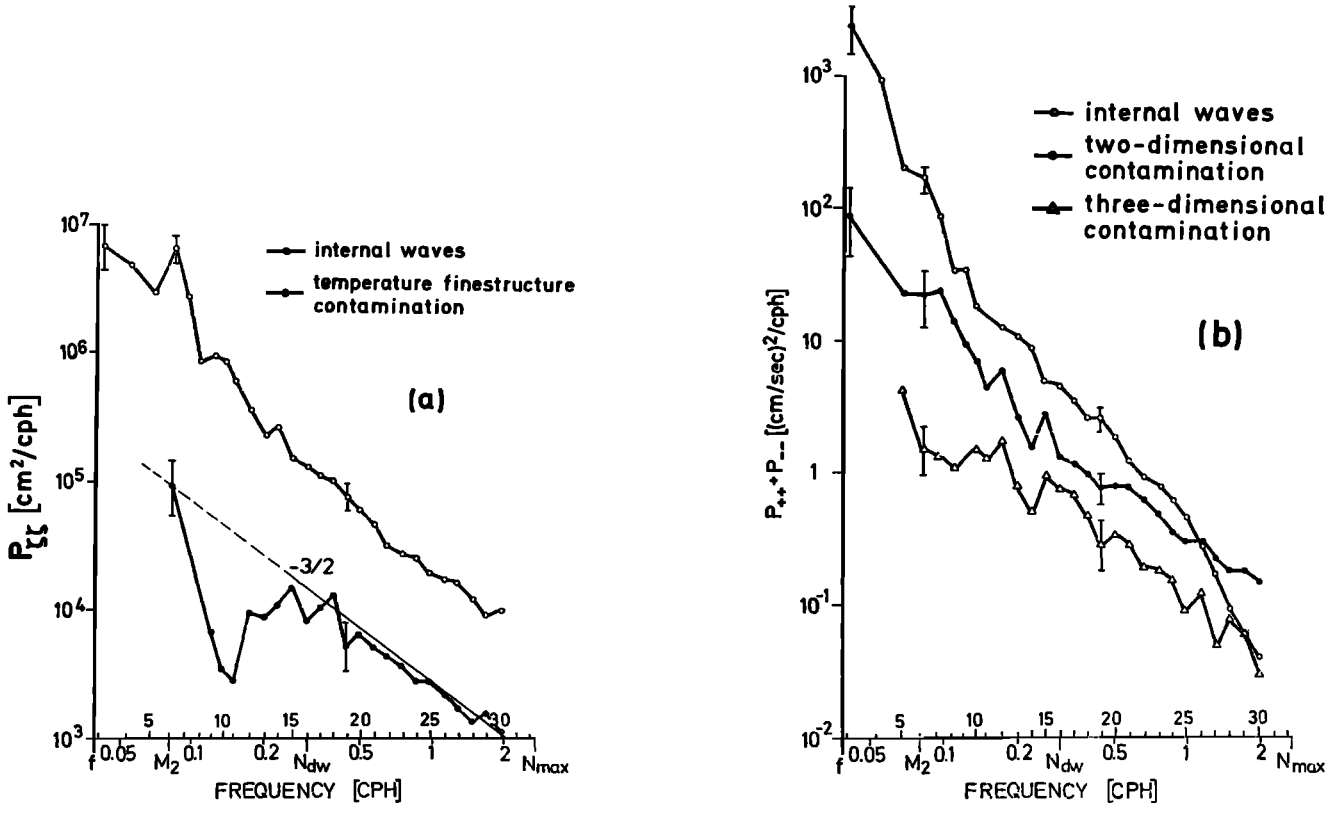

Fig. 29. Partition of the observed spectra into internal waves and contamination. (*a*) The displacement spectra of the internal wave part and the fine structure part. The model of *McKean* [1974] is indicated by the straight line. (*b*) The spectra of horizontal kinetic energy of the internal wave part, the layered and isotropic turbulent contributions [*Müller et al.*, 1978].

turning turbulence is not completely convincing. The two-dimensional field may be associated with flat lenses of two-dimensional turbulent motion. Both these contributions may not have been resolved at their natural frequencies but may rather have advected past the sensors by the mean current and wave field itself. Moreover, it cannot be excluded that the contamination pattern is caused by a single field with a more complicated correlation pattern.

Though there are difficulties in interpreting the result in physical terms, the separation of the observations into wave and nonwave contributions has been achieved within the statistical uncertainties. Figure 30 displays the χ^2 test for the final model: except at the tide and frequencies near the turning point the model and the data coincide within the 95% confidence limit. The similarity of this modeling result, which incorporates all data, with the consistency test (Figure 27*f*) of the wave turbulence model is obvious.

5. Dynamical Models

For many applications, such as passive advection of temperature fine structure by internal waves, it is sufficient to know the state of the wave field. But the waves also actively take part in forming oceanic structures by exchanging energy and momentum with other modes of motion. Besides the phenomenology of the wave state given in section 3 a comprehensive description of internal waves in the ocean therefore must include a treatment of their dynamical role. This is a major oceanographic problem, since the waves interact with many other fields (mesoscale and small-scale turbulence, atmospheric turbulence, surface waves, tides, bottom topography, etc.) with comparable strength and by a wide variety of physical mechanisms. From the point of view of the wave field the ultimate goal is the dynamical balance of the spectrum in terms of generation of energy by external fields, internal transfer of energy within the wave field, and dissipation. The first model of the energy balance [*Olbers*, 1974; *Müller and Olbers*, 1975] was based on the early version of the wave spectrum [*Garrett and Munk*, 1972*a*]. The spectrum was explained as a balance of wave–mean flow interaction, wave-wave interaction, and wave breaking, but this balance did not entirely survive further experimental and theoretical studies. *Käse and Tang* [1976] suggested that the spectrum is balanced by generation of waves by wind stress and dissipation by friction in the bottom boundary

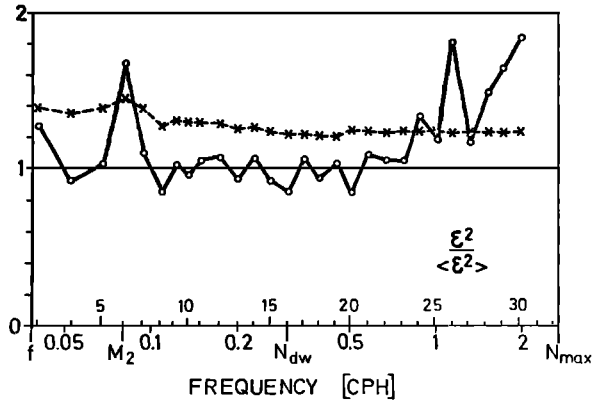

Fig. 30. Consistency of the IWEX model: normalized distance (circles) between data and model point with 95% confidence limit (crosses) versus frequency [*Müller et al.*, 1978].

layer. But this simple model (though being able to reproduce spectra and coherences) also lacks experimental support.

Bell [1975*a*] proposed that topographic generation of internal tides and subsequent spreading of tidal energy across the wave continuum by resonant coupling might be responsible for the wave field in the main thermocline. This model could not be supported by recent detailed analysis of the wave-tidal coupling [*Olbers and Pomphrey*, 1981]. The evolution of the Garrett and Munk spectrum under the influence of resonant wave-wave coupling has been extensively studied by *McComas and Müller* [1981*a*]. Their results, which explain many of the details of the spectral shape, will be presented below. *Fu*'s [1981] conception of the balance of the inertial peak has been discussed in section 3.3.

Though many interaction processes which affect the wave field have been studied with great care, a complete picture of the spectral balance could not be drawn. Rather, extensive investigations in recent years showed that almost no process which was evaluated in detail could be ruled out from possibly taking part in the balance. Thus simple-minded conceptions of the overall balance were refuted, but new conceptions could not yet be introduced. This will surely be attempted in the next few years, and the work of McComas and Müller seems to show the direction. This section reviews some of the basic links which such a model must include.

5.1. *Observational Evidence of Dynamical Relations*

The energy level of deep-sea internal waves varies only very little: a factor of 2–4 as between IWEX and the Garrett and Munk model (with total energy 4×10^3 J/m^2) is typical. The energy in the surface wave field can change by a factor of 10^3 between periods of calm and stormy weather. A relation to the wind as driving agent is quite obvious, and a phenomenology involving wave height and fetch and duration of the wind can be found by rather crude observations even if the generation mechanism remains unknown (see, for example, *Phillips* [1971]). In view of the universal character of the deep-sea wave spectrum and the large number of external fields interacting with the internal wave field it seems difficult to establish such a phenomenology in this case. Indeed, the search by *Wunsch* [1976] and *Wunsch and Webb* [1979] for deviations from the canonical wave spectrum was only moderately successful. These authors investigated the spectral level and slope and the isotropy at medium frequencies of moored measurements in the North Atlantic, the Mediterranean, and the equatorial Indian Ocean. Significant increases of the energy level (see Figure 31) and anisotropy of the spectra were observed near pronounced topographic features (Muir Seamount, canyons), which, however, are lost very rapidly with increasing distance from these regions. If these regions are interpreted as source regions, the dynamics controlling and restoring the spectral shape must be very efficient. But the identification of topographic features as a source is not imperative. As shown by *Eriksen* [1982], linear inviscid theory of wave reflection can account for many of the observations close to a sloping bottom. Indeed, from (6*c*), (12), and (13) we find that an incident wave with total energy E_i and vertical wave number k_3 is reflected into a wave with wave number l_3 and total energy $E_r = E_i l_3/k_3 \sim E_i/(\omega^2 - \omega_s^2)$, where ω_s is the critical frequency (12*b*) associated with the bottom slope. The spectrum of the local energy density will thus be enhanced in the vicinity of the bottom, and as Eriksen also derives, strong anisotropy will develop by the reflection

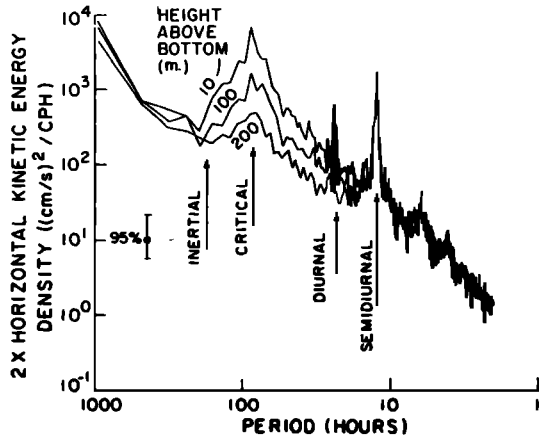

Fig. 31. Spectra of horizontal kinetic energy at 10, 100, and 200 m above the bottom [*Eriksen*, 1982].

process. As is apparent in Figure 31, the perturbation of the spectrum disappears within a few hundred meters, presumably due to redistribution by nonlinear wave interactions and frictional dissipation. If this is true, topographic features would be a sink for wave energy and a source for mixing rather than an energy source.

Below the Gulf Stream and the equator, *Wunsch and Webb* [1979] found a reduction of the coherence scales which may be due to the wave number structure of the spectrum but may also be explained by increased fine structure. Other obvious deviations could not be detected; in particular, no unique relationships were found between the spectral level and shape and tidal or inertial energy. Correlations in the time series of wave energy, the vertical shear of the mean current, and the Cox number (ratio of the variance of the microstructure temperature gradient to the squared mean temperature gradient) have been reported by *Frankignoul and Joyce* [1979], using the very short but highly accurate IWEX data (Figure 32). It is tempting to conclude that this result is an indication of local wave–mean flow interaction and wave breaking which produces microstructure. The authors are rather reserved with this speculation because of large statistical uncertainties. Microstructure activity may also be related directly to the eddy field, as *Hogg et al.* [1978] found near Bermuda. An extensive experimental search for empirical relations between the mean shear and the momentum flux of the wave field [*Frankignoul*, 1947*b*, 1976; *Frankignoul and Joyce*, 1979; *Ruddick and Joyce*, 1979] was devoted to the verification of *Müller*'s [1974, 1976, 1977] concept of wave-induced viscosities, which will be discussed later.

Briscoe [1983] searched for correlations between high-frequency wave energy and various forcing candidates. Integrating the high-frequency energy over frequency (above the tidal frequency) and depth (over the upper 1500 m), this bulk measure of internal wave energy showed time variations of a few milliwatts per square meter. Correlations were found with the deep near-inertial energy with a lag of about 2 days, which makes a transfer of energy from high to low frequencies plausible. This confirms the theoretical prediction [*Olbers*, 1974, 1976; *McComas and Bretherton*, 1977, section 5.2.3] that low frequencies in the deep ocean may draw energy from intermediate frequencies by nonlinear wave coupling. Briscoe also presents correspondences of the time rate of change of the bulk high-frequency energy with the wind energy and large-scale horizontal shear and gives rough estimates in favor of a balance

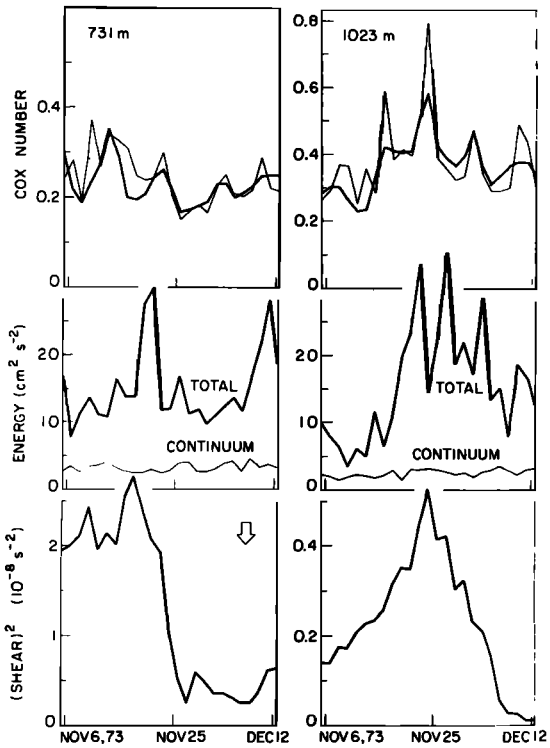

Fig. 32. Time behavior of square mean vertical shear (bottom panels), total energy in the total and continum bands (middle panels), and Cox number (heavy curve in the top panels) and normalized Cox number (light curve in the top panels) at 731 m (left) and 1023 m (right). The arrow indicates a period of observed large vertical shear in the top of the thermocline [*Frankignoul and Joyce*, 1979].

in which the high-frequency energy is generated by the wind (via surface waves?) and large-scale shear and is dissipated by energy transfer to near-inertial waves.

The relation of the upper ocean wave field to surface forcing could be established at low frequencies. Evidence for wind-driven near-inertial waves in the upper thermocline has been reported by, for example, *Käse and Olbers* [1980] and *Weller* [1981]. Correlations between the local wind and inertial currents down to depths of about 200 m were found. The enhancement of the inertial peak in spectra above 2000 m with respect to the global inertial wave field [*Fu*, 1981] was already mentioned above. To interpret this as the consequence of surface forcing seems plausible, in particular in view of the overwhelming evidence of the downward direction energy propagation in the inertial band.

Estimates of the energy flux at near-inertial frequencies by different authors agree roughly within an order of magnitude. *Kundu* [1976] reports a value of 1.5×10^{-3} W/m^2 over the continental shelf; *Perkins and Van Leer* [1977] and *Käse and Olbers* [1980] get values in the range $(0.2–0.7) \times 10^{-3}$ W/m^2 in the near-surface equatorial ocean. In the main thermocline of the Sargasso Sea, *Leaman* [1976] obtains $(0.2–0.6) \times 10^{-3}$ W/m^2, whereas the IWEX parameterization of *Müller et al.* [1978] yields 3×10^{-3} W/m^2. In the bottom boundary layer, *D'Asaro* [1982] found values of $(0.1–0.35) \times 10^{-3}$ W/m^2 for the upward and downward fluxes in the clockwise near-inertial energy. In most cases the downward flux slightly exceeds the upward flux, resulting in a dissipation of wave energy of about 10^{-5} W/m^2 in the benthic boundary layer. A systematic investigation of the inertial wave energy flux has been attempted by *Frankignoul* [1974*a*], searching correlations of the energy in different frequency bands and at different depths. Considering the ambiguity due to the simultaneous presence of propagation and interaction effects, the interpretation of Frankignoul's findings can only be tentative: his 'energy correspondences' also indicate downward flux at low frequencies and a reversal near the bottom. At higher frequencies the correspondences are rather entangled, and a unique picture could not be deduced.

The identification of dominant sources or sinks of the wave energy by experimental means has so far been rather limited. The results confirm the existence of important dynamical processes. The data do, however, indicate that inertial waves may play an important role in the balance of the spectrum. If dissipation in the benthic boundary layer is negligible, as estimated by *D'Asaro* [1982] and also by *Fu* [1981], the energy of near-inertial waves or part of it may be transferred to the wave continuum as they travel from their source into the interior (the travel time of an inertial wave from the top to the bottom of the ocean is of the order of a few days). The observed downward flux of near-inertial energy of about 10^{-3} W/m^2 and the continuum energy of about 10^3 J/m^2 imply a time scale of 10^6 s. Following this speculation the wave field would thus be dissipated and renewed within 10 days. A discussion of possible mechanisms follows. The theoretical treatment of these mechanisms is rather disperse, and a few a priori remarks will help to establish the present status of results.

5.2. *Theoretical Models of Dynamical Processes*

The dynamics of internal waves are governed by the conservation equations for momentum, salt, and mass, which in various stages of approximation are discussed in the literature [e.g., *LeBlond and Mysak*, 1978; *Phillips*, 1977]. External forcing fields enter through the boundary conditions (e.g., wind stress, atmospheric pressure, and buoyancy flux) or are introduced by suitable space-time averaging (e.g., large-scale mean flow, stationary thermal fine structure) or modal decomposition (e.g., surface gravity waves). Coupling between wave components arises from the nonlinearities in the equations. These may be reduced to an equation which describes the evolution of the wave amplitude $a(\mathbf{k})$ in wave number space [*Olbers*, 1979],

$$\frac{d}{dt} a(\mathbf{k}) + i\Omega_0(\mathbf{k})a(\mathbf{k}) = F[a, e; \mathbf{k}] \tag{44}$$

where the source term derives from nonlinearities and external forcing fields denoted here by e. An evolution equation for the spectrum defined by (22) is readily obtained:

$$\frac{d}{dt} \langle a(\mathbf{k})a^*(\mathbf{k}')\rangle = \mathrm{Re}\, \langle a^*(\mathbf{k}')F[a, e; \mathbf{k}]\rangle \tag{45}$$

Slow spatial variations (in the WKB sense) of the spectrum may be included, defining $E(\mathbf{k}, \mathbf{x}, t)$ such that $E(\mathbf{k}, \mathbf{x}, t)\, d^3k$ is the total energy density at the position $\mathbf{x}$ in the wave number band d^3k at $\mathbf{k}$. For some purposes it is more convenient to consider the action spectrum

$$A(\mathbf{k}, \mathbf{x}, t) = E(\mathbf{k}, \mathbf{x}, t)/\Omega_0(\mathbf{k}, \mathbf{x}) \tag{46}$$

which may be loosely interpreted as a number density of waves in the $(\mathbf{k}, \mathbf{x})$ space. Its evolution is governed by a radiative transfer equation

$$\{\partial_t + \dot{\mathbf{x}} \cdot \partial_{\mathbf{x}} + \dot{\mathbf{k}} \cdot \partial_{\mathbf{k}}\} A(\mathbf{k}, \mathbf{x}, t) = S(\mathbf{k}, \mathbf{x}, t) \tag{47a}$$

which is the generalization of the action conservation (5) to a random wave field. Interaction processes described by the

right-hand side of (45) have been accounted for by the source function $S(k, x, t)$, which determines the local change of action of the wave groups due to coupling between them and with external fields as they propagate along their rays. The resemblance between an ensemble of interacting wave groups and an ensemble of interacting particles is apparent: indeed, the ray equations (2) and (3) are the Hamiltonian equations with a Hamiltonian $\Omega(k, x, t)$ for a particle with generalized coordinate $\mathbf{x}$, momentum $\mathbf{k}$, and energy ω. Action conservation is then conservation of particle number, and the radiative transfer equation is the analogue of transport equations governing the particle distribution function.

The radiative transfer equation (47*a*) has to be augmented by radiation conditions at the surface and the bottom stating that the difference of upward and downward flux of action equals the flux through the boundary

$$\dot{x}_3(\mathbf{k}_h, k_3)A(\mathbf{k}_h, k_3) + \dot{x}_3(\mathbf{k}_h, -k_3)A(\mathbf{k}_h, -k_3) = \phi(\mathbf{k}) \qquad (47b)$$

where the boundary source function $\phi(\mathbf{k})$ is the net flux of action through the surface or the bottom of the ocean due to coupling with external fields. In a modal description, volume and boundary forcing appear both in the modal source function $S^\nu(\mathbf{k}_h, \mathbf{x}_h, t)$ and in the radiation balance of the spectrum $E^\nu(\mathbf{k}_h, \mathbf{x}_h, t)$ of the vertical mode ν.

The framework of spectral evolution presented so far is not complete. As a consequence of nonlinearities in the equation of motion the source term $\langle a^*F[a]\rangle$ involves triple correlations of the wave amplitudes. The spectral treatment of wave-wave interactions thus requires a closure hypothesis. This dilemma, which is fundamental in turbulence theory, is much reduced in the theory of random wave fields. Because of the dispersive nature of wave propagation, linear random wave fields are in a Gaussian state. That is a state in which wave amplitudes are mutually statistically independent, so that any wave correlation can be expressed in terms of the spectrum. Weakly nonlinear wave fields never depart much from a Gaussian state. It has been shown by *Prigogine* [1962] that in the limit of infinitely weak nonlinear coupling the correlations $\langle a^*F[a]\rangle$ can be determined under the assumption that the lowest-order amplitudes are elements of a Gaussian ensemble. If, in addition, the free wave amplitudes are uncorrelated with external fields, the radiation balance (47) is a closed equation for the wave spectrum. These ideas form the weak interaction theory, which has found wide applications in geophysical wave problems [e.g., *Hasselmann*, 1966; *Olbers*, 1979].

But is the oceanic internal wave field a weakly nonlinear wave field? Formally, the weak interaction theory requires that the growth time of the amplitude due to wave-wave coupling be small compared to the wave period, that is, $|\dot{a}_{ww}/a| \ll \omega$. The validity of this condition can, however, no longer be assessed from the radiation balance. As was pointed out by *Holloway* [1980, 1982], the condition $|S_{ww}/A| \ll \omega$ on the spectral growth appears to be necessary but not sufficient for the validity of weak coupling between the waves which constitute the spectrum. The source term S_{ww} for wave coupling as derived in the weak interaction limit and evaluated for the Garrett and Munk model is comparable to or even larger than ωA in some part of the spectral domain (see discussion below). For this reason the applicability of weak interaction theory to the oceanic internal wave field has recently been questioned [e.g., *Holloway*, 1980, 1982], and theories for strong interactions have been proposed (a survey can be found in the AIP Conference Proceedings [*West*, 1981]). These approaches have not yet advanced so as to prove consistency or even utility for tackling the energy balance of the oceanic internal wave field. The interested reader is referred to the exhaustive summary by *Holloway* [1980] in the AIP Conference report, which includes further papers on this subject.

Only a few processes have been evaluated in a spectral representation. Many investigations consider the behavior of discrete internal waves forced by a deterministic external field or a Fourier component. Spectral growth rates are inherently smaller than growth rates of deterministically forced waves. Studies of deterministic models are useful for clarifying the dynamics, but they are useless for estimating time scales of a random forcing process and give no information on the form or magnitude of the source function. Studies of deterministic models will not be reviewed here if spectral treatments exist. The reader is referred to the review by *Thorpe* [1975].

The following survey of interaction processes is formally divided into generation processes (i.e., mechanisms which excite waves or enhance those which already exist), dissipation processes (i.e., mechanisms which destroy waves), and transfer processes (i.e., mechanisms which shift energy within the wave spectrum while conserving the total amount). This separation is not a strict one: depending upon wave number and frequency or upon conditions of external fields a process such as wave–mean flow interaction may either enhance or attenuate waves.

5.2.1. *Generation.* Sources of internal waves exist in the interior of the ocean as well as at its boundaries (including the turbulent boundary layers). Energy may be extracted from the mean flow, from the tides, from atmospheric and mixed layer turbulence, and from surface waves.

Atmospheric forcing: At the surface, internal waves can be generated by the atmosphere through resonant coupling to traveling pressure fields and fluctuations of the buoyancy flux and the wind stress. An atmospheric disturbance with wave vector $\mathbf{k}_h$ and frequency ω will generate an internal wave with the same horizontal wave vector and frequency; the mode number (or the vertical wave number) adjusts to satisfy the resonance condition (and the surface radiation condition).

Spectral transfer rates have been considered by *Leonov and Miropol'skiy* [1973] for pressure forcing and by *Käse* [1979] for wind stress forcing. The modal source terms are of the form

$$S_p{}^\nu(\mathbf{k}_h) = \frac{\pi}{2}\frac{\omega_\nu{}^2 + f^2}{\omega_\nu{}^2}|\varphi_\nu(0)|^2 F^p(\mathbf{k}_h, \omega_\nu) \qquad (48a)$$

$$S_\tau{}^\nu(\mathbf{k}_h) = \frac{\pi}{2}\frac{\omega_\nu{}^2 + f^2}{\omega_\nu{}^2}|\varphi_\nu(0)|^2\left(\frac{gk_h}{\omega_\nu{}^2 - f^2}\right)^2 F^\tau(\mathbf{k}_h, \omega_\nu) \qquad (48b)$$

where $F^p(\mathbf{k}_h, \omega)$ and $F^\tau(\mathbf{k}_h, \omega)$ are the spectra of pressure and wind stress, respectively, and $\varphi_\nu(z)$ is the vertical normal mode defined by (18). Insufficient knowledge of the wave number structure of the spectra F^p and F^τ in the internal wave range at present prevents a detailed theoretical analysis of these source terms. The relative importance of the two mechanisms may roughly be estimated as follows: The strongest small-scale wind fluctuations at the sea surface are associated with advected geostrophically balanced fronts. If the turbulence in the atmospheric boundary layer is modeled by an ensemble of such fronts, the ratio of the two source terms (48) becomes

$$\frac{S_\tau{}^\nu}{S_p{}^\nu} \sim \left(\frac{g\rho_a C_D U_a}{\rho}\right)^2 \frac{\omega_\nu{}^2 + f^2}{(\omega_\nu{}^2 - f^2)^4} k_h{}^4$$

where a linearized stress law $\tau = \rho_a C_D U_a \mathbf{u}$ [*Willebrand*, 1978] has been used. With $f = 7 \times 10^{-5}$ s^{-1}, $\rho_a = 1.2 \times 10^{-3}$ g/cm^3, $C_D = 1.5 \times 10^{-3}$, and $U_a = 16$ m/s the ratio becomes (2 m/s/phase/speed)^4 at $\omega_\nu \gg f$. Here phase speeds of internal waves generally are much less than 2 m/s, and the wind stress should be more effective than the pressure. Only first-mode waves of low frequency may attain phase speeds of about 1 m/s (see Figure 22), but at $\omega_\nu \sim f$ the singularity of the ratio again expresses the dominance of generation by wind stress.

The magnitude of the energy transfer by the wind has been estimated by *Käse* [1979]. Integration of (48*b*) over low wave numbers approximately yields a total transfer rate to near-inertial waves,

$$\phi_\tau = \int d^2k\, S_\tau^\nu(\mathbf{k}_h) \sim 2\pi F^\tau(f)/L_\nu \qquad (49)$$

where $F^\tau(f)$ is the density of the stress spectrum at low frequencies and L_ν is a measure of the vertical length scale of the normal mode ν. With typical oceanic parameters, transfer rates of about 10^{-3} W/m^2 are obtained, which also follows from a propagating wave model [*Käse and Olbers*, 1980]. This magnitude of the transfer determined by a dynamical theory agrees favorably with the experimental estimates of the low-frequency energy flux reported above, which are merely derived from kinematical properties of the wave field (basically the phase propagation).

Spectral treatments of the generation of internal waves by buoyancy flux have not yet been performed. In a deterministic forcing model, *Magaard* [1973] came to the conclusion that this mechanism cannot compete with the effect of strong winds.

Surface waves: By resonant interaction a pair of surface waves with wave vectors $\mathbf{k}_{h1}$ and $\mathbf{k}_{h2}$ and frequencies ω_1 and ω_2 can generate an internal wave with wave vector $\mathbf{k}_h$ and frequency ω satisfying

$$\omega = \omega_1 - \omega_2 \qquad \mathbf{k}_h = \mathbf{k}_{h1} - \mathbf{k}_{h2} \qquad (50)$$

where ω equals the eigenfrequency $\Omega_\nu(k_h)$ of a mode ν. This mechanism belongs to the 'classical' candidates of internal wave generation (first studied by *Ball* [1964]), though at first sight it appears highly unlikely because the energy transfer must bridge the large gap in the frequency and wave number domain between the two wave modes. This gap causes one of the prominent signatures of the interaction: since ω is much less than ω_i, one gets also $k_h \ll k_{hi}$, so that the surface wave components propagate almost parallel to each other and perpendicular to the generated internal wave.

The first spectral concept of the process was pursued by *Kenyon* [1968], who found only insignificant transfer from an observed swell spectrum to the first mode in shallow water. Models for open ocean conditions have been worked out by *Watson et al.* [1976] and *Olbers and Herterich* [1979] with drastically different results: whereas Watson et al. find that more than enough energy is available from the interaction to maintain the wave field in the deep ocean, Olbers and Herterich show that the process is completely unimportant for generating waves in the main thermocline. The contradiction is readily resolved by considering the statistical assumptions of the two models. Watson et al. use a discretized representation of the surface wave spectrum by a large but finite set of wave components which have perfectly deterministic phase relationships during the growth time (some hours) of the internal wave. Such a spectral model seems to require rather extreme situations. Olbers and Herterich use a continuous random-phase representation of the spectrum, which seems to be a more reasonable model of ocean waves.

While being insignificant for internal waves in the deep ocean, the resonance mechanism may very efficiently generate high-frequency internal waves in the upper ocean. The spectral transfer from a surface wave spectrum $F^g(\mathbf{k}_h)$ to the νth mode is given by [*Hasselmann*, 1966; *Kenyon*, 1968]

$$S_g^\nu(\mathbf{k}_h) = \int d^2k_{h1}\delta(\omega_1 - \omega_2 - \omega) T^g F^g(\mathbf{k}_{h1}) F^g(\mathbf{k}_{h1} - \mathbf{k}_h) \qquad (51)$$

The scattering cross section T^g depends on the overlapping of the surface and internal wave modes. *Olbers and Herterich* [1979] show that the transfer rate (51) is nearly independent of the shape of the frequency distribution of the surface waves. It may adequately be parameterized by the total energy $\varepsilon_g = \rho g \langle \zeta_g^2 \rangle$, the peak frequency $\omega_m = (gk_m)^{1/2}$, and width σ_ω of the frequency distribution and by the angular spreading function $A(\chi)$ of the spectrum in the form

$$S_g^\nu(k_h, \chi) = \pi |\varphi_\nu(0)|^2 \frac{8\varepsilon_g^2 \omega}{g\sigma_\omega} \left\{ A^2\left(\chi + \frac{\pi}{2}\right) + A^2\left(\chi - \frac{\pi}{2}\right) \right\} \qquad (52)$$

as density of the horizontal wave number k_h and directional angle χ. This expression reflects the generation of the waves at right angles to the surface wave components. The dependence on the waveguide properties (through the eigenmode) is the same as that of the atmospheric transfer rates (48). The response of these mechanisms should therefore have a similar structure in the wave number and mode number domain. Further analysis shows predominant generation of the first mode at high frequencies and horizontal wavelengths of the order of 1 km. The total transfer to the first mode

$$\phi_g = \omega_m \varepsilon_g \frac{k_m^2 \langle \zeta_g^2 \rangle}{2\sigma_\omega \sigma_\chi} \left(\frac{N_0}{\omega_m}\right)^4 \left(\frac{\Delta}{d}\right)^2 \qquad (53)$$

follows by integration of (52) for a three-layer model of the stability frequency: a mixed layer with depth d, a thermocline of thickness Δ and stability frequency N_0, and a much less stratified deep ocean. In extreme situations (a rough sea and a shallow strongly stratified thermocline) this rate may attain values comparable to the rate of generation by wind stress (with $\langle \zeta_g^2 \rangle = 2$ m^2, $N_0 = 3 \times 10^{-2}$ s^{-1}, $d = 25$ m, and $\Delta = 50$ m the the energy transfer becomes 10^{-3} W/m^2). A separation of the contributions from the stress and the surface wave field in field data might then be difficult. The pronounced directionality of the response to surface waves may be helpful as well as the strong parametric dependence on the local wind speed U in the case of wind sea: since then $\varepsilon_g \sim U^4$ and $k_m \sim U^{-2}$ [*Hasselmann et al.*, 1973], the transfer from surface waves is proportional to U^7, whereas the wind stress implies only a dependence U^4 in the linear coupling models. This should have some influence on the statistical properties of the generated waves.

Mixed layer turbulence: Extending the theory on radiation of internal waves from a turbulent boundary layer by *Townsend* [1968] and others to the ocean, *Bell* [1978] has recently identified another candidate which may compete with the previously discussed processes forcing waves at the surface. The turbulent motions within the wind-mixed layer, which is advected by near-surface inertial oscillations, may excite waves in the underlying thermocline. The energy transferred to the wave field is the direct result of the working of the turbulent motions against the buoyancy forces which arise because of the density stratification below the mixed layer. If the inertial current U_0 is

moderately large ($U_0 \geq 5$ cm/s), the total transfer may be parameterized in the form

$$\phi_{ml} = \frac{4}{3\pi} N_0 \tfrac{1}{2} \rho_0 l N_0 \langle \zeta_0^2 \rangle \left\{ 1 + O\left(\frac{N_0 l}{U_0} \right) \right\} \tag{54}$$

in terms of the integral scale l of the mixed layer turbulence, the rms turbulent displacement $\langle \zeta_0^2 \rangle^{1/2}$ at the base of the mixed layer, and the stability frequency N_0. Notice that $\frac{1}{2}\rho_0 l N_0 \langle \zeta_0^2 \rangle$ is a measure of the potential energy associated with the corrugation of the mixed layer base. This amount is converted to wave engery in a third of the buoyancy period. Representative values ($N_0 = 10^{-2}$ s^{-1}, $\zeta_0 \sim 0.1D$, $l = D/2$, where $D = 25$ m is the depth of the mixed layer) yield a flux ϕ_{ml} of the order of 10^{-3} W/m^2. Waves of high frequency (a significant fraction of N_0) and wavelength of the order of $2\pi U_0/N_0$ (some hundred meters) are excited. Bell shows that the energy comes predominantly from the inertial motion leaving the turbulent field quasi-steady. The process therefore is important as a generation mechanism of internal waves in the upper ocean as well as a dissipation mechanism of inertial oscillations in the mixed layer. Resulting decay times range from a day to a week or so, in agreement with observations [*Pollard and Millard*, 1970].

Passing reference is made to another mechanism which may generate internal waves near the surface. Instability of the stratified Ekman boundary layer may excite wave disturbances as shown by *Kaylor and Faller* [1972]. This process was investigated by *Stern* [1977] and *Mollo-Christensen* [1977] in an 'overreflection' model: upward propagating waves gain energy as the result of wave-current interaction in the mixed layer and are reflected downward. Estimates of spectral transfer rates have not been made.

Tides: The conversion of barotropic tidal energy to baroclinic tides and the coupling to the internal wave field have been proposed as a missing link in the global tidal energy budget by the tidal community [e.g., *Hendershott*, 1973; *Cartwright*, 1978]. The rate of loss of energy of the earth-moon system is known from observations of the moon's orbit to be about 5×10^{12} W [*Kaula and Harris*, 1975], and this must equal the total input into the tidal system. Bottom frictional dissipation in shallow seas accounts for about a third ($1.4–1.7 \times 10^{12}$ W) of the total required dissipation [*Miller*, 1966]. Bottom friction in the deep sea as well as dissipation in the earth's mantle and core are unimportant, so that generation of internal tides remains the most promising energy sink. Conversion of barotropic to baroclinic energy may proceed by different mechanisms. Scattering at the continental slope [*Wunsch and Hendry*, 1972; *Schott*, 1977] and at rough bottom topography [*Cox and Sandstrom*, 1962; *Munk*, 1966] cannot account for more than 1% of the total dissipation rate.

The generation of internal tides by the tidal current over bottom irregularities was analyzed by *Bell* [1975*a*]. Waves are generated at the tidal frequency, and all of its harmonics but the energy flux are primarily associated with the fundamental tide. For an isotropic bottom spectrum $\sim k_h^{-5/2}$, Bell obtains a total flux

$$\phi_t = 2\rho_0 f N_b U_t^2 \langle \delta h^2 \rangle \{ 1 + O(f^2/N_b^2) \} \tag{55}$$

where U_t is the tidal current, N_b the bottom stability frequency, and $\langle \delta h^2 \rangle$ the square height of the topography for scales smaller than U_t/f. With $\langle \delta h^2 \rangle = (20 \text{ m})^2$, $N_b = 7 \times 10^{-4}$ s^{-1}, and $U_t = 3$ cm/s, internal tides are generated at a rate of 10^{-3} W/m^2, amounting to about 3×10^{11} W globally. This value is an order of magnitude smaller than the required dissipation rate, but it is rather uncertain. At least it suggests that the mechanism may pump a significant fraction of the barotropic tidal energy to the internal tides in the deep ocean.

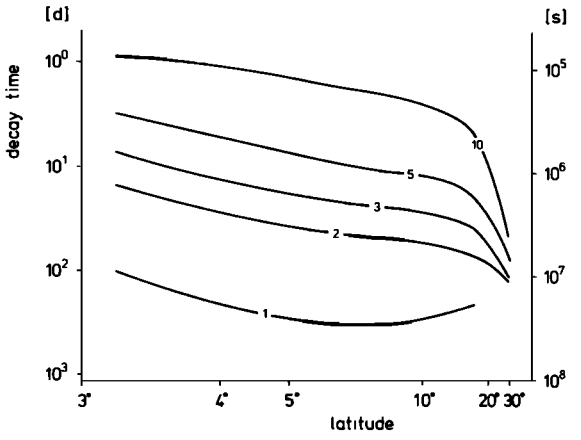

Fig. 33. The latitudinal and modal dependence of the decay time $1/\delta_D$ of the semidiurnal tide in an ambient Garrett and Munk spectrum.

It has been suggested that the energy of the internal tides may be spread over the internal wave spectrum by weak nonlinear interactions of the tidal wave components with waves in the continuum. The physics of weak wave-wave interactions will be reviewed below. The coupling of the tidal line to the continuum by this mechanism was investigated by *Olbers* [1974] and *Olbers and Pomphrey* [1981]. The rate of change of tidal energy E_t is given by

$$dE_t/dt = -\delta_D E_t \tag{56a}$$

where the 'decay' rate at wave vector $\mathbf{k}$,

$$\delta_D(\mathbf{k}) = \int d^3k_1 \int d^3k_2 \{ T^+ \delta(\mathbf{k} - \mathbf{k}_1 - \mathbf{k}_2) \cdot \delta(\omega - \omega_1 - \omega_2)(A_1 + A_2) + 2T^- \delta(\mathbf{k} + \mathbf{k}_1 - \mathbf{k}_2) \cdot \delta(\omega + \omega_1 - \omega_2)(A_1 - A_2) \} \tag{56b}$$

is an integral of the ambient wave action spectrum $A_i = A(\mathbf{k}_i)$ ($i = 1, 2$) weighted by positive cross sections T^+ and T^-. The first term of δ_D corresponding to sum interactions is always positive but contributes only if $\omega > 2f$. For the semidiurnal tide $\omega = M_2$ this is south of 28.7° latitude. The second term arising from difference interactions may attain negative values and contributes everywhere. The decay rate is therefore not necessarily positive; for negative δ_D the tidal line grows on account of the ambient wave field. The energy lost (or gained) by the tide must appear in (or be taken from) the internal wave continuum.

Pomphrey et al. [1980] evaluated the decay rate δ_D in a modal approach for the Garrett and Munk spectrum with high-wave number slope -2 and an exponential stability frequency. Their results apply to a latitude of 30° but can be scaled to lower latitudes [*Olbers and Pomphrey*, 1981]. Figure 33 displays the latitudinal dependence of the decay time $1/\delta_D$ at the frequency of the semidiurnal tide for modes in the range 1–10. The internal tidal energy is predominantly observed in the lowest few modes [*Wunsch*, 1975*b*], which appear to be rather passive on top of the ambient wave spectrum. Typical energy densities of 10^2 J/m^2 in the internal tides yield transfer rates of 10^{-5} W/m^2 at temperate latitudes with a slight increase

toward the equator. These values are far too low to be of any importance in the energetics of the wave field.

Mean flow: Two mechanisms by which internal waves may draw energy from the mesoscale mean flow have been investigated in a spectral concept. *Bell* [1975*a*] considered the generation of lee waves by the mean flow over abyssal hills, and *Müller* [1974, 1976, 1977] studied the interaction of waves with a mesoscale shear flow.

A steady bottom current U_b interacting with a Fourier component $\mathbf{k}_h$ of the bottom roughness generates a lee wave of frequency $\mathbf{k}_h \cdot \boldsymbol{U}_b$. Wave numbers of upward propagating waves are in the range $f/U_b < k_h < N_b/U_b$, corresponding to wavelengths between 400 m and 4000 m for a bottom current of 4 cm/s. The energy flux may be parameterized as the tidal flux (55) and also amounts to about 10^{-3} W/m^2 [*Bell*, 1975*a*]. However, Bell argues that this flux does not contribute to the wave energy in the ocean, since strong bottom currents occur only locally and are mostly associated with bottom trapped modes which decay away from the bottom. The waves thus are likely to encounter critical layers. Their momentum will be absorbed again by the mean flow in the bottom kilometer of the ocean, and their energy will partly be used for mixing, giving rise to eddy diffusivities as high as 10^{-3} m^2/s in this part of the water column.

The interaction of an internal wave with a mean shear flow is described by the ray equations (7) and conservation of action (13). The wave exchanges energy with the mean flow such that action $\varepsilon/[\omega - kU(z)]$ remains constant. However, the system is reversible: a wave that would gain energy on its way would lose the same amount reflected back to its initial level if other processes (e.g., critical layer effects) are disregarded. A symmetrical field of freely propagating waves would thus remain unaffected by a mean shear. This is not true in the presence of processes which try to relax local distortions of the spectrum by the shear to some shear-independent equilibrium shape. As shown by *Müller* [1974, 1976, 1977], the balance between the tendency of the shear to distort the spectrum and the internal relaxation tendency of the wave field leads to asymmetries in the wave field such that the field exerts a stress which opposes the mean shear. The effect may be parameterized by eddy viscosities which depend on the equilibrium wave spectrum. Using the Garrett and Munk model, Müller predicted the very large vertical wave-induced eddy viscosity of 0.4 m^2/s and a horizontal one of 7 m^2/s. Because of the large aspect ratio of the mean flow the vertical viscosity yields a much larger energy input into the wave field (a few milliwatts per square meter) than the horizontal one.

Müller's results suggested two important conclusions. The mechanism is an effective tool for dissipating mesoscale kinetic energy, and it allows the deep-ocean wave field to stay energized independent of boundary forcing (correlations of the spectrum with surface forcing could not convincingly be demonstrated). A local energy balance of the wave field was proposed [*Olbers*, 1974; *Müller and Olbers*, 1975] according to which the energy gain from the mean flow is transferred by wave-wave interactions down the spectrum and dissipated by wave breaking. So far, experimental tests of this model have failed to support it. Correlations between the spectral level and the squared mean shear could be detected [*Frankignoul*, 1976; *Frankignoul and Joyce*, 1979], as displayed in Figure 32, which suggest an energy exchange but allow no conclusions about the mechanism. But correlation analysis of the vertical flux of horizontal momentum in the internal wave band and the squared mean shear showed that the eddy viscosity cannot be as high as Müller's value. This was confirmed by *Ruddick and Joyce* [1979], who were able to estimate an upper bound of 0.02 m^2/s for the vertical viscosity from Polymode data. The data correlation was in fact so weak that in some cases even the sign of the viscosity could not be determined. With this value the energy input to the wave field is 2×10^{-4} W/m^2 or less, and the mean flow would represent only a minor energy source. Ruddick and Joyce also suggest a reason for the failure of Müller's theory. They demonstrate that solutions to the radiative transfer equation (47) exist in the presence of a shear flow and a particular relaxation process (the induced diffusion of *McComas and Bretherton* [1977]; see below) which have nondivergent momentum flux and thus are in equilibrium with the mean flow.

Whereas the conception of a vertical wave-induced viscosity could not be well established by experiments, *Brown and Owens* [1981] found marginally significant correlations between the horizontal shear and the horizontal wave-induced Reynolds stresses in the Local Dynamics Experiment of Polymode. The analysis yields a wave-induced horizontal viscosity of the order of 10^2 m^2/s at depths of 600–800 m, much larger than the value predicted by Müller. With the observed shear variance of the order of 10^{-11} s^{-2} one arrives at a local energy input of 10^{-6} W/m^3 and thus up to 10^{-3} W/m^2 as input per unit surface area.

In view of these observational results it remains unclear how to judge Müller's theory of wave-induced viscosities. The failure to substantiate a vertical viscosity could well be attributed to errors in determining the vertical velocity from a linearized heat equation. The estimation of the horizontal viscosity, on the other hand, hinges upon rather marginal correlations. Further investigations appear to be necessary.

5.2.2. *Dissipation.* A survey of the many mechanisms by which internal waves can dissipate has been given by *Thorpe* [1975]. As yet, it is still a matter of speculation which of these actually work in the ocean to limit the growth of the observed spectrum. Processes suggested in this respect are wave breaking by gravitational instability [*Orlanski and Bryan*, 1969] and shear instability [*Phillips*, 1966], and critical larger absorption [*Bretherton*, 1966].

Instabilities: Gravitational overturning of a wave occurs if the fluid particle velocity exceeds the phase velocity. Shear instability requires the local Richardson number to be less than $\frac{1}{4}$. Obviously, both criteria depend not only on the wave properties (slope and shear) of the wave which actually breaks but also on the ambient flow, including other waves which might be present. In tank experiments, *Thorpe* [1978*a*, *b*] has demonstrated how these mechanisms work separately, that is, overturning in the absence of ambient shear and shear instability in the absence of ambient wave disturbances, and how each may be enhanced if the constituents of the other mechanism are present. In these experiments the breaking can be attributed to a particular wave in the fluid. In the many-wave environment of the ocean, as pointed out by *Gregg and Briscoe* [1979], there may be no identifiable 'breaking internal wave,' only a breakdown in the fluid due to internal waves. Breaking is a more amorphous, unrecognizable process [*Holloway*, 1980] which occurs locally in the fluid and thus affects a broader band in the spectrum.

It does not appear obvious if wave breaking in the ocean prefers one of the two modes of instability. Experimental evidence for the occurrence of shear instability has been presented by in situ flow visualization by *Woods* [1968]. Time series of

the Richardson number have been computed by *Eriksen* [1978] using simultaneous current and temperature observations made at a vertical separation of 7 m (density was estimated from a mean T-S relationship). The Richardson number computed for this separation indicated a cutoff at about $\frac{1}{4}$. Low values are caused by increasing shear rather than decreasing stability frequency and tend to be associated with temperature inversions. This supports the observation of *Woods* [1968] that Kelvin-Helmholtz billows occur near the crests of the growing waves, where their shear is greatest.

Critical layers: The properties of wave propagation near critical layers has been discussed in section 2. The value of the ambient Richardson number controls whether an incident wave is absorbed, reflected, or even overreflected. Critical layers represent a sink of wave energy for large values of the ambient Richardson number. In the ocean, critical layers are likely to exist for internal waves with short vertical wavelengths. A wave with horizontal wave number k_h parallel to the mean current $U(z)$ and intrinsic frequency $\omega_0(z) = \omega - k_h U(z)$ at depth z will encounter a critical level at z_c if the mean shear is large enough to satisfy

$$\omega_0(z) - f = k_h\{U(z_c) - U(z)\} \tag{57}$$

Thus waves in the spectral domain $\omega_0(z) - f < k_h \Delta U$ at depth z will approach their critical layer in a depth range over which the mean flow changes by ΔU. Equivalently, for $N(z) \gg \omega_0(z) \gg f$ the vertical wave number must satisfy

$$\beta(z) > \beta_c(z) = N(z)/\Delta U \tag{58}$$

This vertical wave number may attain typical values of 10^{-3} cm^{-1} in the upper ocean ($N = 10^{-2}\ s^{-1}$ and $\Delta U = 10\ cm\ s^{-1}$) and the main thermocline ($N = 10^{-3}\ s^{-1}$ and $\Delta U = 1\ cm\ s^{-1}$). Thus waves with vertical wavelengths shorter than about 60 m are susceptible to critical layer effects. *Munk* [1980] pointed out that (as with the instability mechanism discussed above) a large fraction of the velocity difference ΔU may be ascribed to low-frequency and low-wave number waves. Then critical layer absorption (and likewise overreflection) would not be considered an external process for the wave field but rather would cause an internal transfer of energy.

Dissipation rates: Little is known about the rate at which wave breaking extracts energy from the spectrum. A direct estimate of the dissipation rate in observed Kelvin-Helmholtz billows in the Mediterranean seasonal thermocline was derived by J. D. Woods (personal communication, 1979). From the billow height L, overturning speed u, and intermittency factor I, Woods gets for the dissipation rate $\varepsilon \sim IU^3/L$ some 10^{-3} W/m^2 over 100 m depth. Some information can be obtained from indirect considerations. The kinetic energy released by breaking will partly be used to mix the fluid and thereby increase the mean potential energy. If this turbulent mixing is parameterized by an eddy diffusivity K, the local rate of increase is

$$\varepsilon_p = KN^2 \tag{59}$$

The remaining part of the energy is converted to smaller scales at a rate ε_{sc} where it will eventually be dissipated by molecular action. The ratio $\varepsilon_P/(\varepsilon_p + \varepsilon_{sc})$ gives the efficiency of converting kinetic wave energy to mean potential energy. Following *Thompson*'s [1980] arguments, this ratio should just be the critical Richardson number

$$\varepsilon_p/(\varepsilon_p + \varepsilon_{sc}) = Ri_c = \tfrac{1}{4} \tag{60}$$

which agrees well with estimates by *Thorpe* [1973], who studied breaking events in a tank. The relations (59) and (60) can be used to evaluate the total dissipation rate due to breaking. If internal waves were responsible for mixing the ocean with the 'classical' diffusivity 10^{-4} m^2/s [*Munk*, 1966], this would require a total local dissipation of 4×10^{-6} W/m^3 (using a main thermocline $N = 3 \times 10^{-3}\ s^{-1}$), which amounts to some 10^{-3} W/m^2 by vertical integration [*Garrett and Munk*, 1972*b*]. Recent measurements of temperature fine structure [e.g., *Gregg*, 1977] do not support a value as high as 10^{-4} m^2/s for the vertical diffusivity (see also *Garrett* [1979] and *Gregg and Briscoe* [1979]). Values of the order of 10^{-6} m^2/s were found, which reduces the dissipation rate in the main thermocline to some 10^{-8} W/m^3 locally or 10^{-5} W/m^2 as vertical integral. Estimates of ε_{sc} can be obtained from velocity microstructure measurement [e.g., *Osborn*, 1978; *Gargett et al.*, 1981] if one assumes that all of the variance in these scale (less than 1 m) derives from wave dissipation. Observed values for ε_{sc} range from 10^{-6} W/m^3 to 10^{-5} W/m^3 in the upper few hundred meters of ocean, which supports Woods' direct estimate mentioned above. Deeper values of ε_{sc} have not been reported.

The importance of critical layer absorption has been estimated by *Ruddick* [1980]. Taking the Garrett and Munk spectrum to be fully asymmetric so that all wave components propagate vertically in one direction in a shear flow $U(z)$, the momentum flux $(\overline{u_1 u_3})_{lost}$ associated with the spectral region $\omega - kU(z) \leq f$ subject to absorption is found to be less than 5×10^{-2} cm^2/s^2, arising mainly from low frequencies for current speeds $U \leq 20$ cm/s. If one assumes that all of this flux is lost in a shear layer of $\Delta U = 5$ cm/s, the energy loss of the wave field would amount to $\Delta z(\overline{u_1 u_3})_{lost}(\Delta U/\Delta z) = 2.5 \times 10^{-4}$ W/m^2. The observed asymmetry in the wave field is 10–20% at low frequencies [*Müller et al.*, 1978], so that this value must be considered as an upper bound for the loss due to critical layer effects. Still, the loss rate is comparable to the dissipation rates estimated for the instability mechanisms.

The relationship between wave dissipation and oceanic fine structure has been reviewed by *Gregg and Briscoe* [1979] and *Munk* [1981], and the aspects of mixing due to internal waves by *Garrett* [1979].

5.2.3. *Transfer*. There are processes which redistribute energy within the spectrum but conserve its total amount. These effect a cascade of energy through the spectrum and may play an important role in the interplay of generation and dissipation and the shaping of the spectrum. The most prominent transfer process is the weak resonant coupling among the spectral components. Another possible mechanism for transfer is resonant coupling of internal waves to external steady fields (Bragg scattering), for example, bottom inhomogeneities or stationary fine structure in the density field.

Resonant wave-wave interactions: Because of the nonlinear terms in the equations of motion a triad of internal waves with frequencies ω, ω_1, and ω_2 and wave vectors $\mathbf{k}$, $\mathbf{k}_1$, and $\mathbf{k}_2$ may interact resonantly and redistribute energy among themselves if

$$\begin{aligned} \omega \pm \omega_1 \pm \omega_2 &= 0 \\ \mathbf{k} \pm \mathbf{k}_1 \pm \mathbf{k}_2 &= 0 \end{aligned} \tag{61}$$

The form of the spectral transfer rate of this process,

$$\begin{aligned} S_{ww}(\mathbf{k}) = &\int d^3k_1 \int d^3k_2 \\ &\cdot \{T^+(A_1A_2 - AA_1 - AA_2)\delta(\mathbf{k} - \mathbf{k}_1 - \mathbf{k}_2)\delta(\omega - \omega_1 - \omega_2) \\ &+ 2T^-(A_1A_2 + AA_1 - AA_2)\delta(\mathbf{k} - \mathbf{k}_1 + \mathbf{k}_2)\delta(\omega - \omega_1 + \omega_2)\} \end{aligned} \tag{62}$$

has been worked out by *Hasselmann* [1966], who also pointed out its formal similarity to Boltzmann's collision integral for interacting particles, Intensive study and evaluation of the transfer integral began when *Garrett and Munk* [1972*a*] published their first version of the wave spectrum. This continued in intimate relation with the construction of the later spectral models described in section 3. The main changes in the spectrum concerned the wave number distribution, which was converted from a simple top hat in the 1972 version to the power law dependence with $t = 2.5$ in the 1974 version (32) and $t = 2$ in the 1979 version (37). These changes, even the apparently minor change in the wave number slope between the latter versions, had profound influence on the transfer rate (62).

Using the early version of the spectrum, *Olbers* [1974, 1976] found that wave energy is systematically transferred from the intermediate frequency range to $f < \omega < 2f$ and toward smaller vertical wavelengths at a rate of 3×10^{-3} W/m^2, implying a delivery time scale of the order of 10 days. The time scale of the transfer varies as the stability period, suggesting that the interactions are most intense in the main thermocline. The transfer to the high-wave number region would drain the whole spectrum in a few days, since the increasing shear will create turbulence and mixing. The later, 1975 model of the spectrum yields lower transfer rates. *McComas and Bretherton* [1977] have repeated the calculations with similar results, but they found a strong sensitivity of the spectral transfer to the wave number slope. This was confirmed by *Pomphrey et al.* [1980] by systematic variation of the spectral slope parameter. Following their analysis a spectrum with wave number slope $t = 2$ is closest to equilibrium in the high-wave number region, but the major flow of energy is still from low to high to high vertical wavelengths and low frequencies at a rate of 6×10^{-4} W/m^2.

McComas and Bretherton [1977] were able to identify three classes of resonant wave coupling which are responsible for much of the complex transfer in a spectrum with the form of the Garrett and Munk model where the energy is mainly in low frequencies and large vertical scales and the shear is mainly in small vertical scales [cf. *McComas and Müller*, 1981*b*]. A class may dominate the transfer in some region either because the cross section of the triad is large or because the triad has one small wave number and low-frequency component with a very large action. The resonant triads of the three classes are sketched in Figure 34. The Garrett and Munk models are in approximate equilibrium with two of these mechanisms (elastic scattering (ES) and induced diffusion (ID)), whereas the third process (parametric subharmonic instability (PSI) controls the energy flow to the low-frequency, high-wave number region with the transfer rates given above. The processes are also responsible for a rapid relaxation of spectral perturbations to the equilibrium form. This was demonstrated by *McComas* [1977], by numerical calculation of the transfer in perturbed spectra, and by *McComas and Müller* [1981*a*], who derived analytical approximations of the transfer rates. A brief survey of the properties of the triad classes follows. Their consequences for an overall spectral balance will be postponed to the next section.

In the induced diffusion mechanism (Figure 34*a*) a high-frequency, high-wave number component interacts with a wave component of much lower frequency and wave number to generate another high-frequency, high-wave number component. The process has some similarity with diffusion of particles in physical space, and, in fact, the transfer rate in the high-frequency, high-wave number region due to ID interactions takes the form of a diffusion of wave action (which is the particle density in wave number space); that is, the ID contribution to (62) becomes

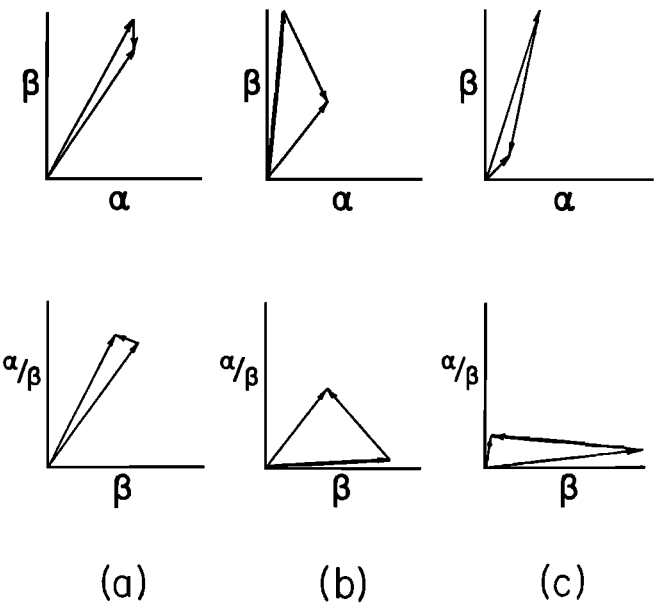

Fig. 34. Schematic representation of (*a*) induced diffusion, and (*b*) elastic scattering, and (*c*) parametric subharmonic instability triads, displayed in (top) wave number space of vertical wave number β versus horizontal wave number α and (bottom) a stretched frequency–vertical wave number space. The aspect ratio α/β is equivalent to a fixed frequency ω, as internal wave frequency depends only on the wave number slope α/β [*McComas*, 1977].

$$\left(\frac{\partial A(\mathbf{k})}{\partial t}\right)_{\mathrm{ID}} = \frac{\partial}{\partial k_3} D \frac{\partial}{\partial k_3} A(\mathbf{k}) \tag{63}$$

with a diffusion coefficient D determined by the shear spectrum of the low-frequency, low-wave number part of the wave field. It appears obvious from (63) that the diffusion term may become very large and the corresponding time scale very small (even smaller than the wave period) if the spectrum develops sharp gradients. As was pointed out by *Holloway* [1980, 1982], the assumption of weakness of the resonant interactions under which (62) was derived is then violated. For a smooth spectrum, such as the Garrett and Munk models, the ID time scale is larger than the wave period except at very high wave numbers. The wave fields thus will respond to a source or sink of energy in the spectrum with weak interactions if the sources and sinks are weak so that a slow ID diffusion can manage the redistribution. The observed low midocean dissipation rates (see section 5.2.2) are compatible with weak resonant interactions down to vertical scales of 1 m [*McComas and Müller*, 1981*a*, *b*].

The rate of change of the energy spectrum due to ID processes is

$$\left(\frac{\partial E(\mathbf{k})}{\partial t}\right)_{\mathrm{ID}} = \omega \frac{\partial}{\partial k_3} Q_A = \frac{\partial}{\partial k_3} \omega Q_A - Q_A \frac{\partial \omega}{\partial k_3} \tag{64}$$

where

$$Q_A(\mathbf{k}) = D \frac{\partial}{\partial k_3} A(\mathbf{k}) \tag{65}$$

is the flux of action in wave number space. Hence the rate of change of the energy spectrum is given by the divergence of the energy flux ωQ_A associated with the action flux and a local (in wave number space) source $-Q_A \partial\omega/\partial k_3$ describing the loss of high-frequency energy to the low-frequency, low-wave number

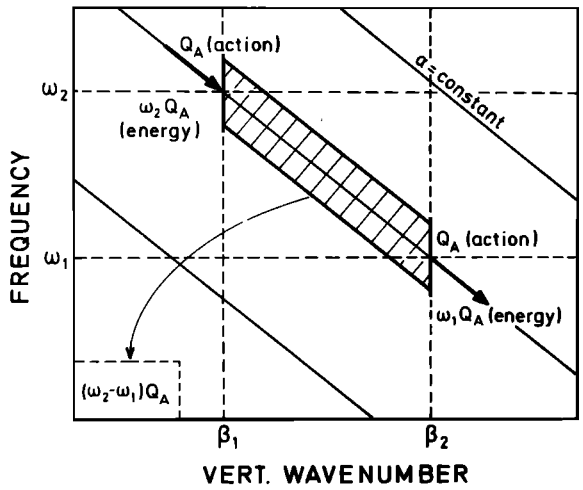

Fig. 35. Schematic representation of the induced diffusion transfer. If action is transferred with a uniform flux Q_A across the frequency range ω_1 to ω_2, the energy flux is nonuniform but accumulates in the low-frequency, low-wave number region.

component participating in the ID triad. Clearly, the action and the energy spectrum in the high-frequency, high-wave number region are in equilibrium with respect to the ID transfer if Q_A is independent of k_3. Whereas action then flows uniformly from large to small vertical scales, energy does not do so but accumulates in the low-frequency, low-wave number region unless $Q_A = 0$ (Figure 35). A nonflux solution (i.e., $Q_A = 0$) to (63) yields a slope $t = 2$ for the energy spectrum at high wave numbers; a constant-flux solution (i.e., $Q_A = Q_A(\mathbf{k}_h) \neq 0$) is compatible with $t = 2$ at high wave numbers if $D \sim \beta$, which requires a slope of $t = 2.5$ at low wave numbers, However, both solutions have their drawbacks. The nonflux solution implies no dissipation at high vertical wave numbers, which appears unlikely, since these waves contribute most of the shear of the wave field. The constant-flux solution implies that the low-frequency, low-wave number region is not in equilibrium.

In the elastic scattering mechanism (Figure 34*b*) a high-frequency wave is scattered into another one with approximately reversed vertical wave number by interaction with a low-frequency component of approximately twice the vertical wave number. This Bragg scattering thus tends to eliminate vertical asymmetries in the wave field. The process is very efficient (but still weak except in the dissipation range) with exclusion of the very low frequencies. The asymmetries of near-inertial waves do not relax, in agreement with the observations of the wave field asymmetry reported above.

The last mechanism, the parametric subharmonic instability (Figure 34*c*), describes the decay of a low-vertical wave number component into two high-vertical wave number components of about half the frequency. This process accounts for much of the transfer to the near-inertial band at high vertical wave numbers in the Garrett and Munk models. The growth time is about 100 inertial periods at 100 m vertical wavelength and decreases to about one-third the inertial period at 1 m (violating again the weakness assumption only at very high wave numbers).

Bragg scattering at fine structure: The scattering of internal waves at horizontally layered irreversible fine structure of the stratification was considered by *Mysak and Howe* [1976] by modeling the latter in the form of a randomly varying stability frequency $\delta N^2(z) = N^2(z) - \langle N^2(z)\rangle$. Waves with vertical wave number k_3 are scattered backwards at the Fourier component at $-2k_3$ of δN^2. The source term may be cast into the form [*Müller and Olbers*, 1975]

$$S_{fs}(\mathbf{k}) = \frac{\pi}{2}\,\omega^2\,\frac{F^{fs}(2\beta)}{|v_3(\mathbf{k})|}\,\{A(\mathbf{k}_h, -\beta) - A(\mathbf{k}_h, \beta)\} \qquad (66)$$

where $F^{fs}(\beta)$ is the one-sided spectrum of $\delta N^2(z)/\langle N^2(z)\rangle$. Thus the interaction affects only the asymmetric part of the spectrum, which would decay exponentially with a time scale

$$\tau = (4/\pi\omega)\beta F^{fs}(2\beta)^{-1} \qquad (67)$$

for frequencies $f \ll \omega \ll N$. The difficulty in separating the irreversible and reversible contributions in observed fine structure spectra has been eludicated in section 4. An evaluation of (66) therefore is not yet possible. The scattering of high-frequency internal waves at irreversible fine structure has its analogue in the elastic scattering mechanism, which describes the backscattering of high-frequency waves at the low-frequency wave shear which causes the reversible part of the observed fine structure.

Bottom scattering: The effect of random bottom inhomogeneities on internal wave modes was studied by *Cox and Sandstrom* [1962] in an attempt to explain the conversion of the surface tide into internal tides. The source term for a random wave field and a bottom spectrum $F^b(\mathbf{k}_n)$ is of the form [*Müller and Olbers*, 1975]

$$\phi_{bs}(\mathbf{k}) = \int d^2k_{h1} \int_0^\infty d\beta_1\; T^{bs}F^b(\mathbf{k}_h - \mathbf{k}_{h1}) \cdot \{v_3(\mathbf{k})A(\mathbf{k}_1) + v_3(\mathbf{k}_1)A(\mathbf{k})\} \qquad (68)$$

with a cross section T^{bs}. This flux has not yet been adequately evaluated. The first term represents the flux to the wave vector $\mathbf{k}$ arising from the scattering of the downward propagating spectral component; the second term describes the extraction of energy at $\mathbf{k}$ due to scattering of this component into other upward propagating waves. An order of magnitude of the source terms follows from (68):

$$\int d^3k|\phi_{bs}(\mathbf{k})| \Big/ \int d^3k v_3 A = \langle s^2\rangle/\pi^2 \qquad (69)$$

where s is the slope of the topography. Typical slope variances of abyssal hill topography are in the range 10^{-2}–10^{-1} [*Bell*, 1975*b*], so that roughly a fraction 10^{-3}–10^{-2} of the downward propagating wave flux will be redistributed in wave number space. In comparison to the redistribution by wave-wave interaction, the bottom scattering is thus negligible.

6. CONCLUSIONS: A PERSPECTIVE OF THE SPECTRAL BALANCE

The discussion of individual processes affecting the oceanic internal wave field is summarized in Figure 36 using the illustrative notation of *Thorpe*'s [1975] visualization of the sources and sinks of internal waves. A sign of progress since then is that values of the energy fluxes can now be assigned to many of the interactions, clarifying their relevance. A summary is given in Table 1. There are many interactions which have been left out because their effect on the wave spectrum could not be estimated or turned out to be small. Scattering at fine structure has been mentioned as causing symmetry of the wave field. Generation by atmospheric pressure and buoyancy flux fluctuation is presumably neligible. Shear instability of the mean flow might

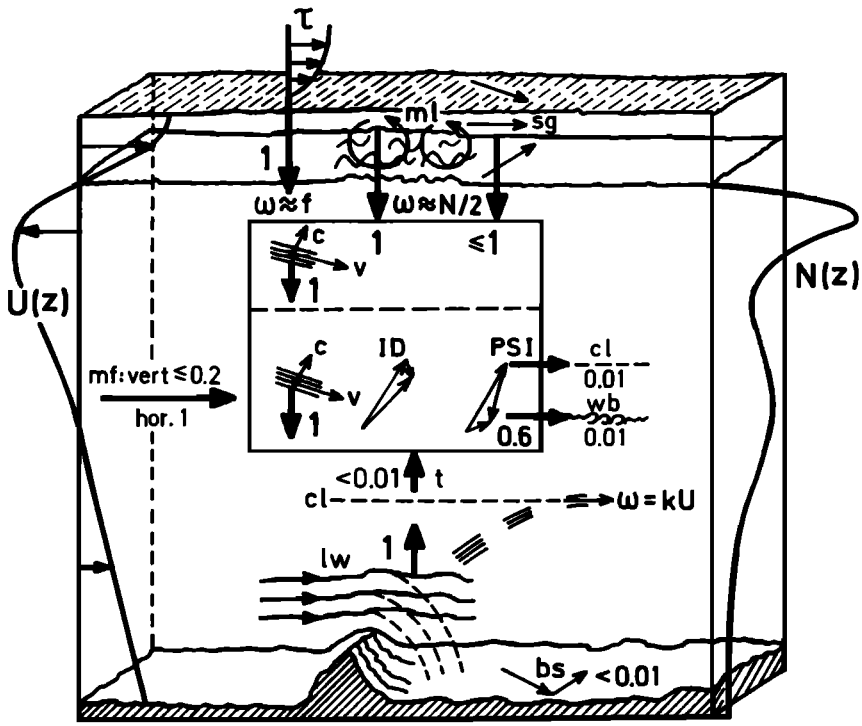

Fig. 36. Sketch of interaction processes affecting the internal wave field in the upper and the deep ocean. Energy fluxes are in units of 10^{-3} W/m^2. Abbreviations are as follows: τ, wind stress; ml, mixed layer turbulence; sg, surface gravity waves; cv, near-inertial waves; mf, large-scale mean flow; t, baroclinic tides; lw, lee waves; bs, bottom scattering; cl, critical layers; wb, wave breaking; ID, induced diffusion; and PSI, parametric subharmonic instability.

be important [see *Thorpe*, 1975] as well as scattering of internal waves at mesoscale fronts in the upper ocean [*Olbers*, 1981*a*].

Surprisingly, many of the energy fluxes associated with generation and transfer processes of internal waves turn out to be of the same order of magnitude, 10^{-3} W/m^2. Such a magnitude has been found to be typical for the energy input in other oceanic motions. *Gill et al.* [1974] estimate the energy input into the Sverdrup flow as 10^{-3} W/m^2. *Frankignoul and Müller* [1979] give a lower bound of 10^{-4} W/m^2 for the generation of baroclinic Rossby waves by stochastic atmospheric forcing. *Bryden* [1982] estimates the net local conversion of mean to eddy energy as 1.8×10^{-6} W/m^3. These examples demonstrate

TABLE 1. Summary of Energy Fluxes

Process	Authors	Energy Flux, 10^{-3} W/m^2 Upper Ocean	Energy Flux, 10^{-3} W/m^2 Main Thermocline	Spectral Domain
Wind stress (τ)	*Käse* [1979], *Käse and Olbers* [1980]	1		near inertial
Surface gravity waves (sg)	*Olbers and Herterich* [1979]	≤1		high frequencies (trapped)
Mixed layer turbulence (ml)	*Bell* [1978]	1		high frequencies (trapped)
Mean flow (mf)				
Vertical viscosity	*Ruddick and Joyce* [1979]		<0.2	
Horizontal viscosity	*Brown and Owens* [1981]		1	
Baroclinic tides (t)	*Olbers and Pomphrey* [1981]		<0.01	
Wave-wave interaction (PSI)	*Pomphrey et al.* [1980]		0.6	low-frequency, high-wave number domain
Lee waves (lw)	*Bell* [1975*a*]		(1)	dissipated close to bottom
Critical layers (cl)	*Ruddick* [1980]		<0.1	low frequencies
Dissipation (d)	*Osborn* [1978]	1		
	Woods [1968]	5		
	Garrett [1979]		0.01–0.1	
Flux in inertial waves (v)	*Käse and Olbers* [1980]	1		
	Perkins and Van Leer [1977]	0.7		near inertial
	Leaman [1976]		0.6	(downward flux)
	IWEX [*Müller et al.*, 1978]		3	
	Rossby and Sanford [1976]		1	

Energy fluxes are in units of 10^{-3} W/m^2. The references are not intended to be a complete listing.

that internal waves play an active dynamical role in the interplay of oceanic motion. A tentative picture of this interplay has recently been put forward by *Woods* [1980].

In view toward a spectral balance, the main statements in Table 1 are as follows:

1. The flux in near-inertial waves is downward, of the same magnitude in the upper ocean and the main thermocline, and consistent with fluxes estimated from inertial wave generation by wind stress.
2. Energy fluxes into the upper ocean wave field as well as dissipation rates appear to be larger than in the main thermocline.
3. The transfer by wave-wave interaction to small scales (in the main thermocline) is not entirely compatible with dissipation rates estimated from fine structure observations.
4. Generation rates are not entirely compatible with dissipation rates (in particular in the main thermocline).

This information is too meager to construct a well-founded spectral balance. Because of the uncertainties in all of the estimates of the fluxes a listing such as in Table 1 could only reveal a balance if there were one dominant source of energy. Apparently, such a source does not exist (it certainly would have been found experimentally), and simple models of the balance such as those proposed by *Müller and Olbers* [1975] and *Bell* [1975*a*] are no longer convincing.

Consideration of Table 1 suggests rather that the oceanic wave field may draw energy from many sources and that forcing as well as dissipation is weak. It may well be that characteristics of the forcing have only marginal control over the energy content and maybe even less over the shape of the spectrum. The wave field may be in such a state where any additional weak input of energy is taken by nonlinear transfer to the spectral domain where dissipation can handle it. A wave field with a saturated spectral form at dissipation scales is the result of a two-dimensional numerical simulation by *Orlanski and Cerasoli* [1981]. This two-dimensional model integrates the equations of motion and simulates dissipation according to an overturning criterion. The authors point out that dissipation in the saturated high wave numbers may occur simultaneously even without cross-spectral transfer if low–wave number energy is added: the low–wave number component may just increase the local slope (in physical space) of the wave superposition such that the overturning criterion is met. The simulated equilibrium spectra bear some resemblance to observations (one may object to the comparison of a three-dimensional spectrum with a rotationless two-dimensional simulation), but the model gives no indication of what kind of triad coupling is responsible for the transfer in the spectrum and how dissipation affects it. An advantage over the weak interaction approach is that the numerical simulation can handle strong wave coupling.

An intriguing, complementary approach toward the spectral balance was recently made by *McComas and Müller* [1981*a*]. This approach also assumes that forcing and dissipation are weak and that nonlinear wave coupling is the main key to the spectral balance. However, McComas and Müller's model is based on the weak interaction limit leading to the spectral transfer rate (62) and the dominant triad interactions in the Garrett and Munk model discussed above. The balance model is sketched in Figure 37. The forcing is assumed at low vertical wave numbers $\beta < \beta_*$. Dissipation is assumed weak and smooth in wave number space (a minimum of assumptions leads to a spectral dissipation which is proportional to the shear spectrum). Energy is transferred at low frequencies by the

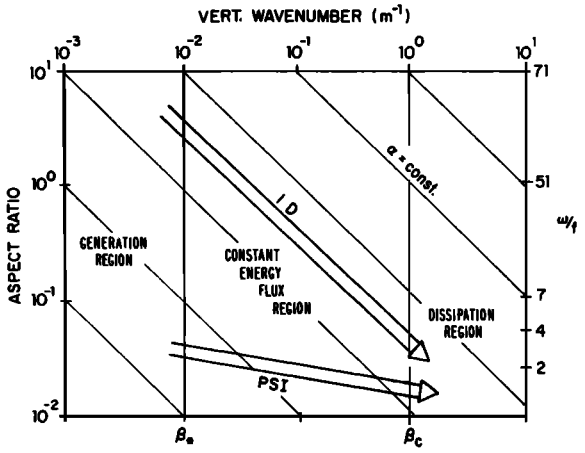

Fig. 37. Schematic view of the energy balance of the internal wave field. Energy is generated at low vertical wave numbers $\beta < \beta_*$. It is transferred at high frequencies by the ID mechanism and at low frequencies by the PSI mechanism to high wave numbers $\beta > \beta_c$. Here dissipation is dominant over the weak nonlinear transfer [*McComas and Müller*, 1981*b*].

PSI mechanism and at high frequencies by the ID mechanism. The break point β_c is determined as the wave number where the nonlinear transfer can no longer keep up with the dissipation. The balance, worked out by a detailed analytical treatment of the transfer expressions for the ID and the PSI processes, is based on a solution with constant energy flux (not action flux as considered above) for both mechanisms between β_* and β_c. Only the combination of ID and PSI yields equilibrium of the vertical wave number spectrum. The model predicts spectral slopes $p = 2$ and $t = 2$ of the Garrett and Munk model $E(\omega, \beta) \sim \omega^{-p}\beta^{-t}$ at high frequencies. At low frequencies the slope $t = 2$ of the vertical wave number spectrum $E(\beta) \sim \beta^{-t}$ is determined, but not the frequency dependence. The constant energy fluxes Q_E due to the ID and the PSI processes in the inertial range $\beta_* < \beta < \beta_c$ are proportional to the total energy E in the wave field and the shear $S_* = \beta_*^2 E$ of the energy-containing waves, that is,

$$Q_E \sim ES_* = \beta_*^2 E^2 \tag{70}$$

Only three of the four parameters E, β_*, β_c, and the total shear S, are independent: the cutoff scale β_c may be expressed as

$$\beta_c \sim \beta_* S/S_* = S/(\beta_* E) \tag{71}$$

The authors argue that the total shear $S = N^2/Ri$ should be fairly constant, so that effectively the model has only two parameters E and β_*. Thus these two rough measures E and β_* of the spectrum completely specify the rest of it. In the presumed slow evolution of the spectrum, E and β_* change slowly, on a time scale of the order of 100 days. The quadratic dependence of the flux Q_E on the dissipation range guarantees rapid relaxation of the spectrum in the energy-containing region. The relations (70) and (71) indicate that in response to growth of either the source region (i.e., β_*) or the total energy E (which in practice is the content of the energy-containing range $0 < \beta < \beta_*$) the flux to the dissipation region, and hence the dissipation rate, increases and the inertial range shrinks. For the scale parameters of the Garrett and Munk model the break point β_c between the inertial range and the dissipation range is at 1 m^{-1}, which is just where observed temperature (cf. Figure 24) and velocity spectra (cf. Figure 25) show a change in slope.

The essential features of this spectral balance were confirmed

by a numerical time-stepping solution of the radiative transfer equation which considers the complete nonlinear transfer term (62) and the spectral dissipation model. Apparently, the model of *McComas and Müller* [1981*a*] gives the most complete view of the spectral balance today. However, many important questions which did come up in the course of the recent internal wave research remain untouched. The model of McComas and Müller applies to the wave field in the main thermocline. The balance in the upper ocean will certainly be quite different, since the state of the wave field differs. A particular problem is whether it can be modeled separately from the deep-ocean wave field. Coupling of the superenergetic high frequencies in the seasonal thermocline to the lower frequencies in the main thermocline (via the PSI mechanism?) may be important. Another problem is the fate of the near-inertial flux. Complete transfer of the asymmetric low-frequency part to the wave continuum would represent a large and presumably steady energy input, which is hardly compatible with the low dissipation rates. Dissipation of near-inertial energy in the benthic boundary layer is weak [*Fu*, 1981; *D'Asaro*, 1982], so that the question arises of whether the near-inertial flux may be overestimated (of course, this question may also apply to other energy fluxes in Table 1). Most estimates of the near-inertial flux are obtained from the relation (10*b*) by computing the vertical group velocity $v_3 = 2(\omega - f)/\beta$ at near-inertial frequencies from the blue shift of the inertial peak. An accurate determination of the blue shift requires long records. Furthermore, *Fu*'s [1981] model of the global near-inertial wave field has revealed that the peak in the frequency spectrum does not necessarily derive from the asymmetric part of the spectrum which alone causes a vertical energy flux.

Aside from such particular items of the energy balance a concept must be put forward which explains the universality of the spectrum. The known sources of energy are not sufficiently steady and uniformly distributed to account for the universality. A simple but important idea was presented by C. S. Cox and C. L. Johnson (unpublished manuscript, 1979) and discussed by *Garrett and Munk* [1979]. If internal waves do not dissipate quickly, as suggested by the low dissipation rates in the deep ocean, they can travel large distances. The low-frequency, energy-containing waves with nonlinear relaxation times of the order of 100 days can propagate 1000 km within their relaxation time of some days. Beyond this mean free path of the wave groups, wave energy may diffuse and spread over even larger regions (in the same way as phonons propagate in a lattice and interact resonantly, leading to a diffusion of heat). This would make the energy level almost uniform. Universality of the spectral shape could then be understood from the balance model of *McComas and Müller* [1981*a*].

Acknowledgments. I thank the many internal wave addicts for all the joint seminars, discussions, and quarrels and for scientific and personal encouragement in recent years. Special thanks to Klaus Hasselmann, Jürgen Willebrand, and Peter Müller. Strong criticism on the weak interactions came from Gregg Holloway; he and Mel Briscoe were very helpful reviewers. Seven typists were possibly driven to despair due to the many versions of the manuscript. I am particularly indebted to Ulla Kircher.

REFERENCES

Ball, F. K., Energy transfer between external and internal gravity waves, *J. Fluid Mech.*, *19*, 465, 1964.

Banks, W. H. H., P. G. Drazin, and M. B. Zaturska, On the normal modes of parallel flow of inviscid stratified fluid, *J. Fluid Mech.*, *75*, 149–171, 1976.

Bell, T. H., Jr., Topographically generated internal waves in the open ocean, *J. Geophys. Res.*, *80*, 320–327, 1975*a*.

Bell, T. H., Jr., Statistical features of sea-floor topography, *Deep Sea Res.*, *22*, 883–892, 1975*b*.

Bell, T. H., Jr., The structure of internal wave spectra as determined from towed thermistor chain measurements, *J. Geophys. Res.*, *81*, 3709–3714, 1976.

Bell, T. H., Radiation damping of inertial oscillations in the upper ocean, *J. Fluid Mech.*, *88*, 289–308, 1978.

Booker, J. R., and F. P. Bretherton, The critical layer for internal gravity waves in a shear flow, *J. Fluid Mech.*, *27*, 513–539, 1967.

Brekhovskikh, L. M., K. V. Konjaev, K. D. Sabinin, and A. N. Serikov, Short-period internal waves in the sea, *J. Geophys. Res.*, *80*, 856–864, 1975.

Bretherton, F. P., The propagation of groups of internal gravity waves in a shear flow, *Q. J. R. Meteorol. Soc.*, *92*, 466–480, 1966.

Bretherton, F. P., and C. J. R. Garrett, Wave trains in inhomogeneous moving media, *Proc. R. Soc. London, Ser. A*, *302*, 529–554, 1968.

Briscoe, M. G., Internal waves in the ocean, *Rev. Geophys. Space Phys.*, *13*, 591–598, 636–645, 1975*a*.

Briscoe, M. G., Preliminary results from the tri-moored internal wave experiment (IWEX), *J. Geophys. Res.*, *80*, 3872–3884, 1975*b*.

Briscoe, M. G., Gaussianity of internal waves, *J. Geophys. Res.*, *82*, 2117–2126, 1977.

Briscoe, M. G., Observations on the energy balance of internal waves during JASIN, *Philos. Trans. R. Soc. London, Ser. A*, *308*, 427–444, 1983.

Brown, E. D., and W. B. Owens, Observations of the horizontal interactions between the internal wave field and the mesoscale flow, *J. Phys. Oceanogr.*, *11*, 1474–1480, 1981.

Bryden, H. L., Sources of eddy energy and effects of eddies in the Gulf Stream recirculation region, *J. Mar. Res.*, *40*, 1047–1068, 1982.

Cairns, J. L., Internal wave measurements from a midwater float, *J. Geophys. Res.*, *80*, 299–305, 1975.

Cairns, J. L., and G. O. Williams, Internal wave observations from a midwater float, 2, *J. Geophys. Res.*, *81*, 1943–1950, 1976.

Cartwright, D. E., Oceanic tides, *Int. Hydrogr. Rev. Monaco*, *2*, 35–84, 1978.

Charnock, H., A preliminary study on the directional spectrum of short period waves, *Proc. U.S. Navy Symp. Military Oceanogr. 2nd*, 175–178, 1965.

Cox, C., and H. Sandstrom, Coupling of internal and surface waves in water of variable depth, *J. Oceanogr. Soc. Jpn.*, 20th anniv. vol., 499–513, 1962.

D'Asaro, E., Absorption of internal waves by the benthic boundary layer, *J. Phys. Oceanogr.*, *12*, 323–336, 1982.

Day, C. G., and F. Webster, Some current measurements in the Sargasso Sea, *Deep Sea Res.*, *12*, 805–814, 1965.

Defant, A., *Physical Oceanography*, vol. 2, 598 pp., Pergamon, New York, 1961.

Desaubies, Y. J. F., Internal waves near the turning point, *Geophys. Fluid Dyn.*, *5*, 143–154, 1973.

Desaubies, Y. J. F., A linear theory of internal wave spectra and coherences near the Väisälä frequency, *J. Geophys. Res.*, *80*, 895–899, 1975.

Desaubies, Y. J. F., Analytical representation of internal wave spectra, *J. Phys. Oceanogr.*, *6*, 970–981, 1976.

Desaubies, Y. J. F., and M. G. Gregg, Reversible and irreversible finestructure, *J. Phys. Oceanogr.*, *11*, 541–566, 1981.

Eckart, C., Internal waves in the ocean, *Phys. Fluids*, *4*, 791–799, 1961.

Eriksen, C. C., Measurements and models of fine structure, internal gravity waves, and wave breaking in the deep ocean, *J. Geophys. Res.*, *83*, 2989–3009, 1978.

Eriksen, C. C., Observations of internal wave reflection off sloping bottoms, *J. Geophys. Res.*, *87*, 525–538, 1982.

Fofonoff, N. P., Spectral characteristics of internal waves in the ocean, *Deep Sea Res.*, *16*, suppl., 58–71, 1969.

Fofonoff, N. P., and F. Webster, Current measurements in the western Atlantic, *Philos. Trans. R. Soc. London, Ser. A*, *279*, 423–436, 1971.

Frankignoul, C. J., Preliminary observations of internal wave energy flux in frequency, depth space, *Deep Sea Res.*, *21*, 895–910, 1974*a*.

Frankignoul, C. J., Observed anisotropy of spectral characteristics of internal waves induced by low-frequency currents, *J. Phys. Oceanogr.*, *4*, 625–634, 1974*b*.

Frankignoul, C. J., Observed interaction between ocean internal waves and mesoscale eddies, *Deep Sea Res.*, *23*, 805–820, 1976.

Frankignoul, C. J., and T. M. Joyce, On the internal wave variability

during the internal wave experiment (IWEX), *J. Geophys. Res.*, *84*, 769–776, 1979.
Frankignoul, C. J., and P. Müller, Quasi-geostrophic response of an infinite β-plane ocean to stochastic forcing by the atmosphere, *J. Phys. Oceanogr.*, *9*, 194–227, 1979.
Fu, L.-L., Observations and models of inertial waves in the deep ocean, *Rev. Geophys. Space Phys.*, *19*, 141–170, 1981.
Gargett, A. E., P. J. Hendricks, T. B. Sanford, T. R. Osborn, and A. J. Williams III, A composite spectrum of vertical shear in the upper ocean, *J. Phys. Oceanogr.*, *11*, 1258–1271, 1981.
Garrett, C. J. R., The effect of internal wave strain on vertical spectra of finestructure, *J. Phys. Oceanogr.*, *3*, 83–85, 1973.
Garrett, C. J. R., Mixing in the ocean interior, *Dyn. Atmos. Oceans*, *3*, 239–265, 1979.
Garrett, C. J. R., and W. H. Munk, Internal wave spectra in the presence of finestructure, *J. Phys. Oceanogr.*, *1*, 196–202, 1971.
Garrett, C. J. R., and W. H. Munk, Space-time scales of internal waves, *Geophys. Fluid Dyn.*, *2*, 225–264, 1972*a*.
Garrett, C. J. R., and W. H. Munk, Oceanic mixing by breaking internal waves, *Deep Sea Res.*, *19*, 823–832, 1972*b*.
Garrett, C. J. R., and W. H. Munk, Space-time scales of internal waves: A progress report, *J. Geophys. Res.*, *80*, 291–297, 1975.
Garrett, C. J. R., and W. H. Munk, Internal waves in the ocean, *Annu. Rev. Fluid Mech.*, *11*, 339–369, 1979.
Gill, A. E., J. S. A. Green, and A. J. Simmons, Energy partition in the large-scale ocean circulation and the production of mid-ocean eddies, *Deep Sea Res.*, *21*, 499–528, 1974.
Gregg, M. C., Variations in the intensity of small-scale mixing in the main thermocline, *J. Phys. Oceanogr.*, *7*, 436–545, 1977.
Gregg, M. C., and M. G. Briscoe, Internal waves, finestructure, microstructure, and mixing in the ocean, *Rev. Geophys. Space Phys.*, *17*, 1524–1548, 1979.
Hasselmann, K., Feynman diagrams and interaction rules of wave-wave scattering processes, *Rev. Geophys. Space Phys.*, *4*, 1–32, 1966.
Hasselmann, K., et al., Measurements of wind-wave growth and swell decay during the Joint North Sea Wave Project (JONSWAP), *Dtsch. Hydrogr. Z.*, Suppl. A(8°), no. 12, 95 pp., 1973.
Hayes, S. P., Preliminary measurements of the time-lagged coherence of vertical temperature profiles, *J. Geophys. Res.*, *80*, 307–311, 1975.
Hayes, S. P., T. M. Joyce, and R. C. Millard, Measurements of vertical fine structure in the Sargasso Sea, *J. Geophys. Res.*, *80*, 314–319, 1975.
Hendershott, M. C., Ocean tides, *Eos Trans. AGU*, *54*, 76–86, 1973.
Hogg, N. G., E. J. Katz, and T. B. Sandford, Eddies, islands, and mixing, *J. Geophys. Res.*, *83*, 2921–2938, 1978.
Holloway, G., Oceanic internal waves are not weak waves, *J. Phys. Oceanogr.*, *10*, 906–914, 1980.
Holloway, G., Theoretical approaches to interactions among internal waves, in *Nonlinear Properties of Internal Waves: Conference Proceedings*, edited by B. West, pp. 47–77, American Institute of Physics, New York, 1981.
Holloway, G., On interaction time scales of oceanic internal waves, *J. Phys. Oceanogr.*, *12*, 293–296, 1982.
Johnson, C. L., C. S. Cox, and B. Gallagher, The separation of wave-induced and intrusive oceanic finestructure, *J. Phys. Oceanogr.*, *8*, 846–860, 1978.
Jones, W. L., Reflexion and stability of waves in stably stratified fluids with shear flow: A numerical study, *J. Fluid Mech.*, *34*, 609–624, 1968.
Jones, W. L., Ray tracing for internal gravity waves, *J. Geophys. Res.*, *74*, 2028–2033, 1969.
Joyce, T. M., and Y. J. F. Desaubies, Discrimination between internal waves and temperature finestructure, *J. Phys. Oceanogr.*, *7*, 22–32, 1977.
Käse, R. H., Calculations of the energy transfer by the wind to near-inertial internal waves, *Deep Sea Res.*, *26*, 227–232, 1979.
Käse, R. H., and R. A. Clarke, High frequency internal waves in the upper thermocline during GATE, *Deep Sea Res.*, *25*, 1978.
Käse, R. H., and D. J. Olbers, Wind-driven inertial waves observed during phase III of GATE, *Deep Sea Res.*, *26*, *suppl.*, 191–216, 1980.
Käse, R. H., and G. Siedler, Internal wave kinematics in the upper tropical Atlantic, *Deep Sea Res.*, *26*, Suppl. I, 161–189, 1980.
Käse, R. H., and C. L. Tang, Spectra and coherence of wind-generated internal waves, *J. Fish. Res. Board Can.*, *33*, 2323–2328, 1976.
Katz, E. J., Tow spectra from MODE, *J. Geophys. Res.*, *80*, 1163–1167, 1975.
Katz, E. J., and M. G. Briscoe, Vertical coherence of the internal wave field from towed sensors, *J. Phys. Oceanogr.*, *9*, 518–530, 1979.
Kaula, W. M., and A. W. Harris, Dynamics of lunar origin and orbital evolution, *Rev. Geophys. Space Phys.*, *13*, 363–371, 1975.
Kaylor, R., and A. J. Faller, Instability of the stratified Ekman boundary layer and generation of internal waves, *J. Atmos. Sci.*, *29* (3), 497–509, 1972.
Kenyon, K. E., Wave-wave interactions of surface and internal waves, *J. Mar. Res.*, *26*, 208–231, 1968.
Kroll, J., The propagation of wind-generated inertial oscillations from the surface into the deep ocean, *J. Mar. Res.*, *33*, 15–51, 1975.
Kundu, P. K., An analysis of inertial oscillations observed near Oregon coast, *J. Phys. Oceanogr.*, *6*, 879–893, 1976.
LaFond, E. C., Internal waves, in *The Sea*, edited by M. N. Hill, vol. 1, part 1, pp. 731–751, Interscience, New York, 1962.
Landau, L. D., and E. M. Lifschitz, *Mechanik*, Akademie, Berlin, 1970.
Leaman, K. D., Observations on the vertical polarization and energy flux of near-inertial waves, *J. Phys. Oceanogr.*, *6*, 894–908, 1976.
LeBlond, P. H., and L. A. Mysak, *Waves in the Ocean*, 560 pp., Elsevier, New York, 1978.
Leonov, A. I., and Yu. Z. Miropol'skiy, Resonant excitation of internal gravity waves in the ocean by atmospheric pressure fluctuations, *Izv. Acad. Sci. Atmos. USSR Oceanic Phys.*, Engl. Transl., *9*, 480–485, 1973.
Levine, M. D., R. A. de Szoeke, and P. P. Niiler, Internal waves in the upper ocean during MILE, *J. Phys. Oceanogr.*, *13*, 240–257, 1983.
Lighthill, J., *Waves in Fluids*, 504 pp., Cambridge University Press, New York, 1978.
Lindzen, R. S., and A. J. Rosenthal, On the instability of Helmholtz velocity profiles in stably stratified fluids when a lower boundary is present, *J. Geophys. Res.*, *81*, 1561–1571, 1976.
Magaard, L., Ein Beitrag zur Theorie der internen Wellen als Störungen geostrophischer Strömungen, *Dtsch. Hydrogr. Z.*, *21*, 241–278, 1968.
Magaard, L., On the generation of internal gravity waves by a fluctuating buoyancy flux at the sea surface, *Geophys. Fluid Dyn.*, *5*, 101–111, 1973.
McComas, C. H., Equilibrium mechanism within the oceanic internal wave field, *J. Phys. Oceanogr.*, *7*, 836–845, 1977.
McComas, C. H., and F. P. Bretherton, Resonant interactions of oceanic internal waves, *J. Geophys. Res.*, *82*, 1397–1412, 1977.
McComas, C. H., and P. Müller, Time scales of resonant interactions among oceanic internal waves, *J. Phys. Oceanogr.*, *11*, 139–147, 1981*a*.
McComas, C. H., and P. Müller, The dynamic balance of internal waves, *J. Phys. Oceanogr.*, *11*, 970–986, 1981*b*.
McKean, R. S., Interpretation of internal wave measurements in the presence of finestructure, *J. Phys. Oceanogr.*, *4*, 200–213, 1974.
Miller, G. R., The flux of tidal energy out of the deep oceans, *J. Geophys. Res.*, *71*, 2485–2489, 1966.
Miropol'skiy, Yu. Z., Propagation of internal waves in an ocean with horizontal inhomogeneities of the density field, *Izv. Acad. Sci. USSR Atmos. Oceanic Phys.*, Engl. Transl., *10*, 312–318, 1974.
Miropol'skiy, Yu. Z., N. I. Solntseva, and B. N. Filyuskin, On horizontal variability of Brunt-Vaisala frequency in the ocean, *Oceanology*, Engl. Transl., *15*, 15–20, 1976.
Mollo-Christensen, E., Impingement of internal waves from below onto a moving mixed surface layer, *J. Phys. Oceanogr.*, *7*, 684–690, 1977.
Mooers, C. N. K., Several effects of a baroclinic current on the cross-stream propagation of inertial-internal waves, *Geophys. Fluid Dyn.*, *6*, 245–275, 1975*a*.
Mooers, C. N. K., Several effects of baroclinic currents on the three-dimensional propagation of inertial-internal waves, *Geophys. Fluid Dyn.*, *6*, 277–284, 1975*b*.
Mowbray, D., and B. S. H. Rarity, A theoretical and experimental investigation of the phase configuration of internal waves of small amplitude in a density stratified fluid, *J. Fluid Mech.*, *28*, 1–16, 1967.
Müller, P., On the interaction between short internal waves and larger scale motion in the ocean, *Hamb. Geophys. Einzelschr.*, *23*, 98 pp., 1974.
Müller, P., On the diffusion of momentum and mass by internal gravity waves, *J. Fluid Mech.*, *77*, 789–823, 1976.
Müller, P., Spectral features of the energy transfer between internal waves and larger-scale shear flow, *Dyn. Atmos. Oceans*, *2*, 49–72, 1977.

Müller, P., and D. J. Olbers, On the dynamics of internal waves in the deep ocean, *J. Geophys. Res.*, *80*, 3848–3860, 1975.
Müller, P., and G. Siedler, Consistency relations for internal waves, *Deep Sea Res.*, *23*, 613–628, 1976.
Müller, P., D. J. Olbers, and J. Willebrand, The IWEX spectrum, *J. Geophys. Res.*, *83*, 479–500, 1978.
Munk, W. H., Abyssal recipes, *Deep Sea Res.*, *13*, 707–730, 1966.
Munk, W. H., Internal wave spectra at the buoyancy and inertial frequencies, *J. Phys. Oceanogr.*, *10*, 1718–1728, 1980.
Munk, W. H., Internal waves and small-scale processes, in *Evolution of Physical Oceanography Scientific Surveys in Honor of Henry Stommel*, edited by B. A. Warren and C. Wunsch, pp. 264–291, MIT Press, Cambridge, Mass., 1981.
Munk, W. H., and N. Phillips, Coherence and band structure of inertial motion in the sea, *Rev. Geophys. Space Phys.*, *6*, 447–472, 1968.
Mysak, L. A., and M. S. Howe, A kinetic theory for internal waves in a randomly stratified fluid, *Dyn. Atmos. Oceans*, *1*, 3–31, 1976.
Olbers, D. J., On the energy balance of small-scale internal waves in the deep sea, *Hamb. Geophys. Einzelschr.*, *24*, 91 pp., 1974.
Olbers, D. J., Nonlinear energy transfer and the energy balance of the internal wave field in the deep ocean, *J. Fluid Mech.*, *74*, 375–399, 1976.
Olbers, D. J., Weak coupling in statistical geophysical systems, *Z. Angew. Math. Mech.*, *59*, 10–15, 1979.
Olbers, D. J., A formal theory of internal wave scattering with application to ocean fronts, *J. Phys. Oceanogr.*, *11*, 1078–1099, 1981*a*.
Olbers, D. J., The propagation of internal waves in a geostrophic current, *J. Phys. Oceanogr.*, *11*, 1224–1233, 1981*b*.
Olbers, D. J., and K. Herterich, The spectral energy transfer from surface waves to internal waves in the ocean, *J. Fluid Mech.*, *92*, 349–379, 1979.
Olbers, D. J., and N. Pomphrey, Disqualifying two candidates for the energy balance of oceanic internal waves, *J. Phys. Oceanogr.*, *11*, 1423–1425, 1981.
Olbers, D. J., P. Müller, and J. Willebrand, Inverse technique analysis of a large data set, *Phys. Earth Planet. Inter.*, *12*, 248–252, 1976.
Orlanski, I., and K. Bryan, Formation of the thermocline step structure by large-amplitude internal gravity waves, *J. Geophys. Res.*, *74*, 6975–6983, 1969.
Orlanski, I., and C. P. Cerasoli, Energy transfer among internal gravity modes: Weak and strong interactions, *J. Geophys. Res.*, *86*, 4103–4124, 1981.
Osborn, T. R., Measurements of energy dissipation adjacent to an island, *J. Geophys. Res.*, *83*, 2939–2958, 1978.
Perkins, H., and J. Van Leer, Simultaneous current-temperature profiles in the equatorial counter current, *J. Phys. Oceanogr.*, *7*, 264–271, 1977.
Peters, H., Dispersion curves and modes of high frequency internal waves during JASIN '78, *Jasin News*, *18*, 1–3, 1980.
Peters, H., Zur Kinematik eines stochastischen Feldes interner Wellen in einer Scherströmung, *Ber. Inst. Meereskd. Christian Albrechts Univ. Kiel*, *82*, 117 pp., 1981.
Peters, H., The kinematics of a stochastic field of internal waves modified by a mean shear current, *Deep Sea Res.*, *30*, 119–148, 1983.
Phillips, O. M., *The Dynamics of the Upper Ocean*, 261 pp., Cambridge University Press, New York, 1966.
Phillips, O. M., On spectra measured in an undulating layered medium, *J. Phys. Oceanogr.*, *1*, 1–6, 1971.
Phillips, O. M., *The Dynamics of the Upper Ocean*, 2nd ed., 336 pp., Cambridge University Press, New York, 1977.
Pinkel, R., Upper ocean internal wave observations from Flip, *J. Geophys. Res.*, *80*, 3892–3910, 1975.
Pinkel, R., Observations of strongly non-linear internal motion in the open sea using a range-gated Doppler sonar, *J. Phys. Oceanogr.*, *9*, 675–686, 1979.
Pinkel, R., On the use of Doppler sonar for internal wave measurements, *Deep Sea Res.*, *28*, 269–289, 1981.
Pollard, R. T., Properties of near-surface inertial oscillations, *J. Phys. Oceanogr.*, *10*, 385–398, 1980.
Pollard, R. T., and R. C. Millard, Comparisons between observed and simulated wind-generated inertial oscillations, *Deep Sea Res.*, *17*, 813–821, 1970.
Pomphrey, N., J. D. Meiss, and K. M. Watson, Description of nonlinear internal wave interactions using Langevin methods, *J. Geophys. Res.*, *85*, 1085–1094, 1980.
Prigogine, I., *Non Equilibrium Statistical Mechanics*, Interscience, New York, 1962.
Rayleigh (J. W. Strutt), Investigation of the character of the equilibrium of an incompressible heavy fluid of variable density, *Proc. London Math. Soc.*, *14*, 170–178, 1883.
Rossby, T. H., and T. B. Sanford, A study of velocity profiles through the main thermocline, *J. Phys. Oceanogr.*, *6*, 766–774, 1976.
Roth, M. W., M. G. Briscoe, and C. H. McComas III, Internal waves in the upper ocean, *J. Phys. Oceanogr.*, *11*, 1234–1247, 1981.
Ruddick, B. R., Critical layers and the Garrett-Munk spectrum, *J. Mar. Res.*, *38*, 135–145, 1980.
Ruddick, B. R., and T. M. Joyce, Observations of interaction between the internal wavefield and low frequency flows in the North Atlantic, *J. Phys. Oceanogr.*, *9*, 498–517, 1979.
Sabinin, N. D., Certain features of short-period internal waves in the ocean, *Izv. Acad. Sci. USSR Atmos. Oceanic Phys.*, Engl. Transl., *9*, 32–36, 1973.
Samodurov, A. S., Internal waves in a medium with a horizontally-varying Väisälä frequency, *Izv. Acad. Sci. USSR Atmos. Oceanic Phys.*, Engl. Transl., *10*, 185–191, 1974.
Sanford, T. B., Observations of the vertical structure of internal waves, *J. Geophys. Res.*, *80*, 3861–3871, 1975.
Schott, F., Spatial structure of inertial-period motions in a two-layered sea, based on observations, *J. Mar. Res.*, *29*, 85–102, 1971.
Schott, F., On the energetics of baroclinic internal tides in the North Atlantic, *Ann. Geophys.*, *33*, 41–61, 1977.
Siedler, G., Vertical coherence of short periodic current variations, *Deep Sea Res.*, *18*, 179–191, 1971.
Siedler, G., Observations of internal wave coherence in the deep ocean, *Deep Sea Res.*, *21*, 597–610, 1974.
Stegen, G. R., K. Bryan, J. L. Held, and F. Ostapoff, Dropped horizontal coherence based on temperature profiles in the upper thermocline, *J. Geophys. Res.*, *80*, 3841–3847, 1975.
Stern, M. E., Interaction of inertia-gravity waves with the wind, *J. Mar. Res.*, *35*, 479–498, 1977.
Stokes, G. G., On the theory of oscillating waves, *Trans. Cambridge Philos. Soc.*, *8*, 441–455, 1847.
Thompson, R. O. R. Y., Efficiency of conversion of kinetic energy to potential energy by a breaking internal gravity wave, *J. Geophys. Res.*, *85*, 6631–6635, 1980.
Thorpe, S. A., Turbulence in stably stratified fluids: A review of laboratory experiments, *Boundary Layer Meteorol.*, *5*, 95–119, 1973.
Thorpe, S. A., The excitation, dissipation, and interaction of internal waves in the deep ocean, *J. Geophys. Res.*, *80*, 328–338, 1975.
Thorpe, S. A., On the shape and breaking of finite amplitude internal gravity waves in a shear flow, *J. Fluid Mech.*, *85*, 7–31, 1978*a*.
Thorpe, S. A., On internal gravity waves in an accelerating shear flow, *J. Fluid Mech.*, *88*, 623–639, 1978*b*.
Townsend, A. A., Excitation of internal waves in a stably-stratified atmosphere with considerable wind-shear, *J. Fluid Mech.*, *32*, 145–171, 1968.
U.S. Polymode Organizing Committee, U.S. Polymode program and plan, Mass. Inst. of Technol., Cambridge, 1976.
Watson, K. M., B. J. West, and B. L. Cohen, Coupling of surface and internal gravity waves: A mode coupling model. *J. Fluid Mech.*, *77*, 185–208, 1976.
Webster, F., Estimates of the coherence of ocean currents over vertical distances, *Deep Sea Res.*, *19*, 35–44, 1972.
Weller, R. A., Observations of the velocity response to wind forcing in the upper ocean, *J. Geophys. Res.*, *86*, 1969–1977, 1981.
West, B. (Ed.), *Nonlinear Properties of Internal Waves: Conference Proceedings*, American Institute of Physics, New York, 1981.
Whitham, G. B., Two-timing, variational principles and waves, *J. Fluid Mech.*, *44*, 373–395, 1970.
Willebrand, J., Temporal and spatial scales of the wind field over the North Pacific and North Atlantic, *J. Phys. Oceanogr.*, *8*, 1080–1094, 1978.
Willebrand, J., P. Müller, and D. J. Olbers, Inverse analysis of the trimoored internal wave experiment (IWEX), *Ber. Inst. Meereskd. Christian Albrechts Univ. Kiel*, *20a, b*, 224 pp., 1977.
Woods, J. D., Wave induced shear instability in the summer thermocline, *J. Fluid Mech.*, *32*, 791–800, 1968.
Woods, J. D., Do waves limit turbulent diffusion in the ocean?, *Nature*, *288*, 219–224, 1980.
Woods, J. D., and P. J. Minnett, Analysis of mesoscale thermoclinicity

with an example from the tropical thermocline during GATE, *Deep Sea Res., 26A*, 85–96, 1979.
Wunsch, C., Deep ocean internal waves: What do we really know?, *J. Geophys. Res., 80*, 339–343, 1975*a*.
Wunsch, C., Internal tides in the ocean, *Rev. Geophys. Space Phys., 13*, 167–182, 1975*b*.
Wunsch, C., Geographical variability of the internal wave field: A search for sources and sinks, *J. Phys. Oceanogr., 6*, 471–485, 1976.
Wunsch, C., and R. Hendry, Array measurements of the bottom boundary layer and the internal wave field in the continental slope, *Geophys. Fluid Dyn., 4*, 101–145, 1972.
Wunsch, C., and S. Webb, The climatology of deep ocean internal waves, *J. Phys. Oceanogr., 9*, 235–243, 1979.

(Received November 5, 1982;
accepted February 17, 1983.)